JPRS L/10079

28 October 1981

Translation

FINESTRUCTURE AND SYNOPTIC VARIABILITY OF THE SEAS

Ed. by

A.M. Aytsam

FBIS FOREIGN BROADCAST INFORMATION SERVICE

NOTE

JPRS publications contain information primarily from foreign newspapers, periodicals and books, but also from news agency transmissions and broadcasts. Materials from foreign-language sources are translated; those from English-language sources are transcribed or reprinted, with the original phrasing and other characteristics retained.

Headlines, editorial reports, and material enclosed in brackets [] are supplied by JPRS. Processing indicators such as [Text] or [Excerpt] in the first line of each item, or following the last line of a brief, indicate how the original information was processed. Where no processing indicator is given, the information was summarized or extracted.

Unfamiliar names rendered phonetically or transliterated are enclosed in parentheses. Words or names preceded by a question mark and enclosed in parentheses were not clear in the original but have been supplied as appropriate in context. Other unattributed parenthetical notes within the body of an item originate with the source. Times within items are as given by source.

The contents of this publication in no way represent the policies, views or attitudes of the U.S. Government.

APPROVED FOR RELEASE: 2007/02/09: CIA-RDP82-00850R000400060056-0

JPRS L/10079

28 October 1981

FINESTRUCTURE AND SYNOPTIC VARIABILITY OF THE SEAS

Tallinn TONKAYA STRUKTURA I SINOPTICHESKAYA IZMENCHIVOST' MOREY in Russian 1977 (signed to press 23 Oct 80) pp 1-200

[Text of book edited by A.M. Aytsam, Eesti NSV Teaduste Akadeemia, 1980, 200 copies, 200 pages]

CONTENTS

FOREWORD

In recent decades oceanologists have established presence of significant variability in ocean waters, embracing from several seconds to several years in time, and from millimeters to thousands of kilometers in space. Variability of ocean waters is elicited by various physical processes; however, the laws of these processes are not always sufficiently well known.

Scientists of the Baltic Sea Division of the Institute of Thermophysics and Electrophysics began intense research on variability of the Baltic Sea in 1976. Expeditionary research conducted aboard the scientific research vessel "Ayu-Dag" also established significant variability in waters of the Baltic Sea. In 20 trips made in 4 years, many typical traits of the variability of Baltic waters were determined, especially in regard to finestructure and synoptic variability. The necessity for extracting optimum information from the accumulated experimental material, and for critically discussing the obtained results, led to the idea of holding a seminar-symposium on the finestructure and synoptic variability of the seas and oceans.

The idea of conducting such a seminar-symposium was approved by the scientific society of oceanologists, as is evidenced by the present collection of report summaries.

Discussion of the latest results of research on variability of the World Ocean at different scales, and comparative analysis of these results and information on the variability of the Baltic Sea will probably promote further development of research on variability of the seas and oceans.

The report summaries were placed in this collection in the form in which they were submitted by the authors. Therefore the editor of this collection claims no responsibility for misprints and mistakes in the text.

Finestructure of Deep Waters of the Open Part of the Baltic Sea

A. Aytsam, Ya. Laanemets, M.-Ya. Lilover

Introduction

The open part of the Baltic Sea may be divided into four layers in relation to vertical temperature distribution: an upper mixed layer, the thermocline, an intermediate cold winter-convection layer and an abyssal layer (halocline). The average structure of water in the abyssal layer is governed by intrusion processes through the Danish straits (saltier and warmer water enters the sea) and by vertical exchange processes. Research on processes occurring in the marine environment and assessments of vertical exchange of scalar magnitudes make broad use of the results of vertical sounding of temperature and salinity fields with salinity-temperature-density probes. Vertical structure may be interpreted as the result of the interaction of different processes, ones which often overlap in scale. These problems are reviewed in (1,2,3,4).

Measurements and Analysis Procedure

Several series of vertical soundings were made with a Mark III Neil Brown probe at the central station of the BOSEX traverse in 1979 and 1980 in order to study vertical structure formation in the abyssal layer of the Baltic Sea. In spring 1979 six series of 30 soundings each, in an interval of depths from 70 to 95 meters, were made from aboard a drifting vessel in still weather. Following each series the vessel returned to its starting point. The vessel drifted 1-2 km. The time interval between soundings was 3 minutes.

In spring 1980 two series of 20 soundings each were made in the BOSEX transverse in an interval of depths from 60 to 90 meters and a time interval of 3.5 minutes. The first series was completed before a storm, and the second series was completed 3-4 days following the end of an 8-9 point storm.

The probe was lowered at a rate of 25 cm/sec, and the recording rate was 30 times per second, which made a depth resolution of about 1 cm possible. During initial treatment, all readings were interpolated to a constant interval of 2 cm. The measured series was divided into an average and a pulsating component with the help of a cosine filter.

The BPF [not further identified] method was used to compute spectral densities following preliminary smoothing with a four-point Kaiser-Bessel filter (5).

Discussion of Results

The influence exerted by shores and the Danish straits may be assumed to be low within the area of the BOSEX traverse. The vertical temperature, salinity and density profiles varied monotonously with depth in the interval from 60 to 95 meters. It was hypothesized that wave-generated vortical turbulence, laminar convection (because temperature and salinity increase with depth in the Baltic Sea's abyssal layer) and the kinematic effect of internal waves are the principal processes forming the vertical structure of scalar magnitudes at the finestructural and microstructural levels. Moreover when the first two processes occur, they are accompanied by vertical transport of scalar magnitudes.

To determine the conditions under which laminar convection occurs, we calculated the function $R_\rho(Z_i) = \frac{\beta(Z_i)\Delta S_i}{\alpha(Z_i)\Delta T_i}$ with the vertical interval being $\Delta Z = 10$ cm. Analysis of the function $R_\rho(Z_i)$ showed that $R_\rho(Z_i) < 15$ only at some specific points of the vertical profile, and that for the most part $R_\rho(Z_i) > 15$, which implies purely molecular diffusion. Of course, a final conclusion as to the importance of laminar convection to vertical transport in the abyssal layer of the open part of the Baltic Sea would require analysis of greater detail. One more thing we should note here is that in double-diffusion processes, the mass flow is directed downward, which requires additional upward turbulent flow or vertical transport.

The BPF method was used to calculate the spectral densities of vertical discontinuities in temperature, salinity and specific gravity. The maximum wave number is $K\mu = 1/2\Delta Z = 25\mu^{-1}$. A transition zone bounded by wave numbers $3 < K < 6\mu^{-1}$ exists in individual spectral curves. The spectral densities of temperature $S_T(K)$, salinity $S_S(K)$ and specific gravity $S_{\sigma_t}(K)$ are approximated well by an exponential law in the interval $6 < K < 25$:

$$S_T(K) \sim S_S(K) \sim S_{\sigma_t}(K) \sim K^{-3}.$$

This indicates that internal gravity waves have an influence. In the range $K < 3$, the slopes of the spectral curves are steeper. Figure 1 shows set-averaged spectral curves for temperature, salinity and specific gravity. The transition zone is less noticeable on the averaged spectral curves. A subinterval of fine-scale turbulence was not noted in any of the spectrums. Nor was a zone with significant negative gradients observed on the profiles of the vertical specific gravity gradients.

All of this indicates that fluctuations in temperature, salinity and density in the interval from several meters to 4 cm were generated by internal gravity waves. In the case where the average gradient changes little with depth,

$$S_\xi(K) = \frac{S_T(K)}{(\delta\bar{T}/\delta z)^2} = \frac{S_S(K)}{(\delta\bar{S}/\delta z)^2} = \frac{S_{\sigma_t}(K)}{(\delta\bar{\sigma}_t/\delta z)^2}$$

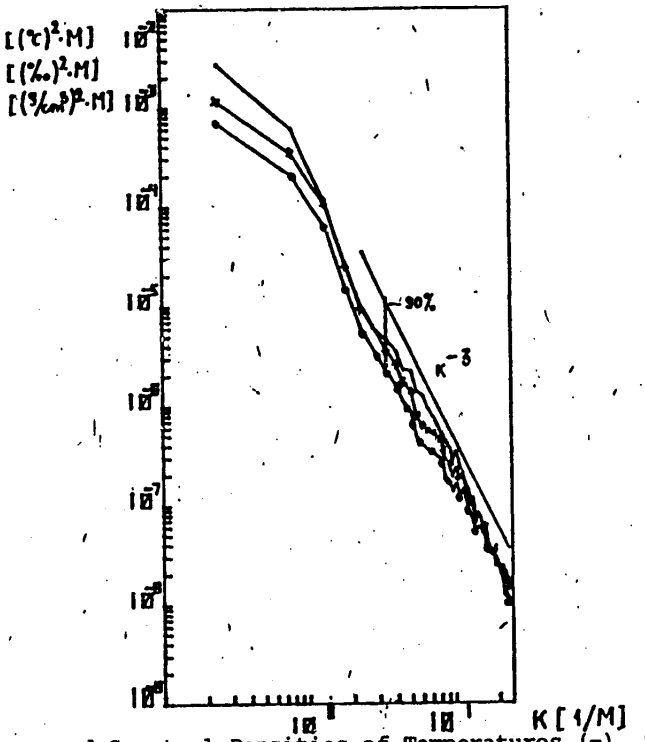

Figure 1. Set-Averaged Spectral Densities of Temperatures (-), Salinity (**) and Specific Gravity (oo) in the Abyssal Layer

where ξ is vertical displacement. Using the spectral densities of temperature, salinity and specific gravity, we determined the mean square value of vertical displacements, which was approximately equal to 0.2 meters.

BIBLIOGRAPHY

1. Fedorov, K. N., "Tonkaya termokhalinnaya struktura vod okeana" [The Fine Thermohaline Structure of Ocean Waters], Gidrometeoizdat, Leningrad, 1976.

2. Ozmidov, R. V., "Turbulentnost' v verkhnem sloye okeana. Mekhanika zhidkosti i gaza" [Turbulence in the Upper Layer of the Ocean. Fluid and Gas Mechanics], Vol 12, 1976.

3. Garrett, C., "Mixing in the Ocean Interior," DYNAMICS OF ATMOSPHERES AND OCEANS, No 3. 1979.

4. Gregg, M. C., "Microstructure: Signature of Mixing in the Ocean," NAVAL RESEARCH, 1976.

5. Harris, Fr. J., "On the Use of Windows for Harmonic Analysis With the Discrete Fourier Transform," PROCEEDINGS OF THE IEEE, Vol 66, No 1, 1978.

Spatial Variability in the Temperature of the Surface Layer of the Baltic Sea

A. M. Ayatsam, Yu. Kh. Pavel'son

A relatively large number of works have been devoted in recent years to measurement and analysis of the temperature of the surface layer of the oceans (see the review in (2)). However, similar research on inland seas, including the Baltic, has been clearly lacking. Various factors form the thermohaline structure of waters of the Baltic Sea. We can arbitrarily divide them into three categories: meteorological, geographic and vortical.

The first category includes the following factors: variable winds, which determine the mixing time of the surface layer;

irregular cloudiness, resulting in irregular heat absorption by the surface layer;

the diurnal air temperature trend;

precipitation, which basically influences the salinity field;

changes in atmospheric pressure, as a dynamic factor in evolution of thermohaline fields.

The second, so-called geographic group includes water exchange through the Danish straits, river runoff and dynamic effects associated with the shore line (upwelling, Kelvin waves). Synoptic vortices recently discovered in the Baltic Sea (3,6) make a significant contribution to the variability of physical fields; these vortices are explained by baroclinicity phenomena in the presence of an irregular bottom.

Considering the above, the horizontal distribution of temperature in the surface layer of the Baltic Sea may turn out to be relatively complex. This is confirmed by our measurements, started in 1979, with a towed thermistor. The analysis was performed on cross sections measured in different seasons and in different parts of the Baltic Sea, having a total length of about 6,000 km. It should be noted that the cross sections measured by a towed thermistor are not instantaneous. However, considering the scale of the studied phenomena (1-50 km or more than 1 day), we may assume the cross sections to be quasistatic. Moreover inasmuch as the cross sections were measured without prior information on the temperature field, the extreme values of perturbation characteristics (amplitude, horizontal dimensions) may

be distorted. Following conversion of analog temperature recordings into digital form, the resulting series were subjected to computer processing. The average dimensions of perturbations, their amplitudes and their gradients were determined. In order to reveal the contribution of different processes and the most preferable scale, the series were subjected to spectral analysis. For this purpose we evaluated the maximum entropy spectrum (4). The choice of this method was predicated upon the frequency of the processed series, since it was impossible to penetrate into the domain of small wave numbers by traditional methods. The principal results of the analysis are summarized below.

1. In open areas of the Baltic Sea, during spring warming (May, June) and fall cooling (September, October), the temperature of the surface layer exhibits a complex structure, with the perturbation amplitude averaging 0.7°C (Figure 1). In some cases the amplitude could reach 2-3°C. The horizontal scale of perturbations is within the 10-50 km range, with most falling in the 15-25 km range--that is, one to two Rossby deformation radii.

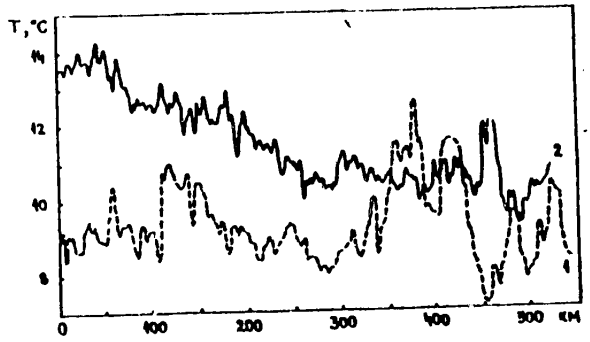

Figure 1. Typical Horizontal Temperature Profiles for the Surface Layer of the Baltic Sea

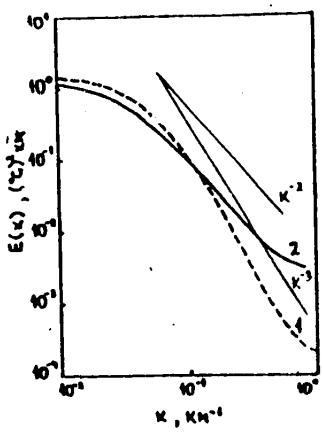

Figure 2. Spectral Densities of the Temperature of the Baltic Sea's Surface Layer

2. In summer (July, August) the temperature distribution is uniform in these same areas of the sea. Smooth temperature changes of up to 0.3°C can be noted. These changes were not dependent on the diurnal water temperature trend or the meridian temperature trend along the towing route.

3. Irrespective of the season, well-pronounced fronts were discovered in shore areas, and especially near the Danish straits. Fronts with a temperature difference of 2.3°C in 200 meters can be noted. Additional measurements indicated a salinity gradient of $0.3^0/_{00}$, though without a noticeable jump in density. One unique feature is the existence of a small temperature decrease (0.2°C) on the cold side directly before the front. A similar phenomenon is described in (8).

4. According to our data, fronts are rarely encountered in the open sea. Gradient analysis, performed in keeping with the criteria that the simultaneous temperature gradient had to exceed 0.2°C/km and the temperature difference had to be not less than 1°C, resulted in 31 km as the average distance between fronts. This estimate is significantly higher than that given in (1), in which the strictness of the chosen criteria was lower. On the other hand numerous sharp temperature gradients not associated with fronts could be found on some curves. For example 51 cases with a temperature difference between neighboring points greater than 0.2°C are encountered in curve 2 of Figure 1; when conversion to digital form is considered, this means a gradient estimate greater than 0.8°C/km.

5. In the 0.05-1 km^{-1} wave number range, the found spectrums are basically characterized by a k^{-3} dependence, which is in keeping with Charney's geostrophic turbulence hypothesis (5). Curve 2 on Figure 1, discussed earlier, is an exception. Its spectrum is approximated by a k^{-2} dependence, which, considering the sharp gradients present, permits the use of Saffman's model (7). Maximums which could define the most preferable and "energy-carrying" scales are entirely absent from these spectrums.

As we can see, the complex distribution of temperatures in the surface layer of the Baltic Sea agrees well with the intricate complex of forming factors. The objective of this paper was to demonstrate the variability of the temperature field in the meso- and synoptic scales, as well as the need for expanding the research to the entire quasiuniform layer, taking salinity and density fields into account as well.

BIBLIOGRAPHY

1. Karabasheva, E. I., Paka, V. T., and Fedorov, K. N., "Are Thermal Fronts Frequently Encountered in the Ocean?" OKEANOLOGIYA, Vol 18, No 6, 1978, pp 1004-1013.

2. Krasnopevtsev, A. Yu., Vinogradova, K. G., and Kuz'mina, N. P., "Spatial Variability of the Temperature Field in the Surface Layer of the Ocean," in "Mezomasshtabnaya izmenchivost' polya temperatury v okeane" [Mesoscale Variability of the Temperature Field in the Ocean], Moscow, 1977, pp 6-32.

3. Aitsam, A., Elken, J., Pavelson, J., and Talpsepp, L., "Preliminary Results of the Investigation of Spatial-Temporal Characteristics of the Baltic Sea Synoptic Variability," in "Investigation and Modelling of the Baltic Sea," Tallinn (in press).

4. Andersen, N., "On the Calculation of Filter Coefficients for Maximum Entropy Spectral Analysis," GEOPHYSICS, Vol 39, No 1, 1974, pp 69-72.

5. Charney, J. G., "Geostrophic Turbulence," J. ATMOS. SCI., Vol 28, No 6, 1971, pp 1087-1095.

6. Keunecke, K. H., and Magaard, L., "Measurements by Means of Towed Thermistor Cables and Problems of Their Interpretation With Respect to Mesoscale Processes," MEM. SOC. ROY DE SCI. DE LIEGE. Vol 7, No 6. 1974, pp 147-160.

7. Saffman, P. G., "On the Spectrum and Decay of Random Two-Dimensional Vorticity Distribution," STUDIES IN APPLIED MATH, Vol 50, No 3-4, 1971, pp 377-383.

8. Simpson, J. H., Allen, C. M., and Morris, N. C. G., "Fronts on the Continental Shelf," J. GEOPHYS. RES., Vol 83, No C9, 1978, pp 4607-4614.

Investigation of the Variability of Currents on a Synoptic Scale in the Central Part of the Baltic Sea in 1977-1980

A. Aytsam, L. Talpsepp

Current and temperature measurements obtained by expeditions of the Estonian SSR Academy of Sciences Institute of Thermophysics and Electrophysics on the Baltic Sea in 1977-1980 show that there are different forms of variability in the Baltic Sea, playing a significant role in the control of the spread of pollutants and in research on the distribution of the phyto- and zooplankton in the sea. All of these measurements imply that oscillations with an inertial frequency having a period of 13.9-14.2 hours in the region of investigation possess a noticeable part of the sea's kinetic energy. It was found that a significant amount of kinetic energy is contained in, besides inertial oscillations, variations on a synoptic scale. Experimental studies using Aanderaa RCM-4 and VASM flow rate and temperature gauges were conducted in 1977, 1979 and 1980.

In fall 1977 we dropped two buoy stations 20 nautical miles apart for a period of 20 days. Gauges were suspended from these buoys at five horizons. It was established that at one of the stations (station N) synoptic-scale kinetic energy grew with depth in the layers close to the bottom. It was found that the time series of flow rates and temperatures in the bottom layers were typified by the same periods (over 40 hours), shifted in phase. A more-noticeable correlation between temperature and the current component directed upward along the slope exists in the interval from 1.3 to 4 days. The facts agreed well with the theory of topographic waves entrained by the bottom, suggested by Rhines (2,3), when the stratification, bottom slope and water depth were typical of the given region. It was found by the least squares method that the dominant periods for the bottom layers of station N were 68 and 44 hours, which exceeded the theoretical lower limit for the periods of topographic waves. Basing ourselves on the theory of topographic bottom-entrained waves, we found the theoretical wavelengths (employing the measured vertical distribution of kinetic energy), which exhibited little dependence upon frequency and were within 12-14 kilometers. In order to find the direction of the wave vector, we found the orientation of the new coordinates in such a way that the coherence between the flow rate components in the new coordinate system was minimal. Minimization of coherence, accounting for invariants relative to rotation of the coordinate system (1), results in the formula

$$\tan 2\varphi = \frac{2 P_{uv}}{S_{uu} - S_{vv}} \qquad (I)$$

where S_{uu}, S_{vv} are the spectral densities of the rate component, P_{uv} is the synphasal component of mutual spectral density, and ψ is the angle between the new and initial coordinate systems. Wave orientation and energy are described by energy ellipses (Figure 1), where orientation was found with formula (1) and from an eilipse as eigenvalues of the correlation matrix.

$$\begin{pmatrix} S_{uu} & P_{uv} \\ P_{uv} & S_{vv} \end{pmatrix}.$$

The axis of the ellipse represents the energy of the rate component in the new coordinate system, where coherence between the rate components is minimal (where orientation is a function of frequency). We can see from Figure 1 that there is more energy in the frequency range of the proposed topographic waves. Topographic waves were not discovered at the other stations. There, the bottom was more even and the station was too far away from a region with a sloped bottom (more than 30 km away).

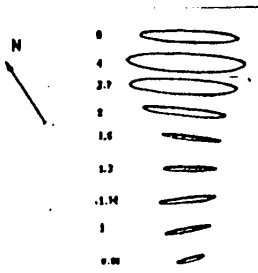

Figure 1. Energy Ellipses at the 118-Meter Horizon of Station N in 1977

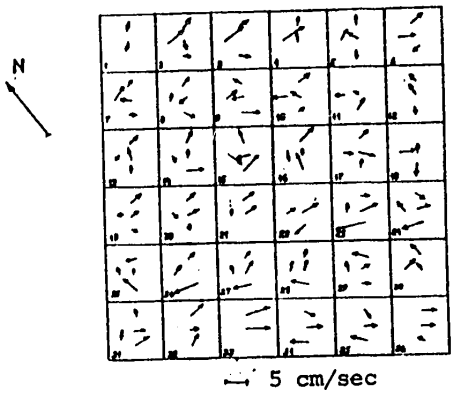

Figure 2. Temporal Sequence of Mean Daily Currents in the 1979 Traverse

A cross-shaped traverse consisting of five buoy stations with one gauge for surface layers and one for bottom layers was placed in the same region in May-June 1979. The stations were spaced 10 nautical miles apart. Additional recorders were set up at the central station to study vertical distribution of synoptic-scale kinetic energy. This year, growth in kinetic energy with depth and other clear indications of topographic waves were not observed. This period was dominated by still weather, and this perhaps explains the relatively lower energy in the synoptic range. The pattern of currents observed is generally complex, with typical flow rates of 5-7 cm/sec in the bottom layer. The temporal sequence of mean daily currents is shown in Figure 2 for a horizon located 15 meters above the bottom, beginning on 12 May. Vortical currents may be observed at the end of the measurement period. The appearance of the mean daily current vector diagrams and the appearance of the current vectors are correlated. The appearance of the current vector diagram for the surface layer at station SW is the same as that observed following the passage of a vortex with a scale on the order of 30 km, in a northwesterly direction at a speed of 2-3 cm/sec. The diagram for the bottom layer differs from that for the surface.

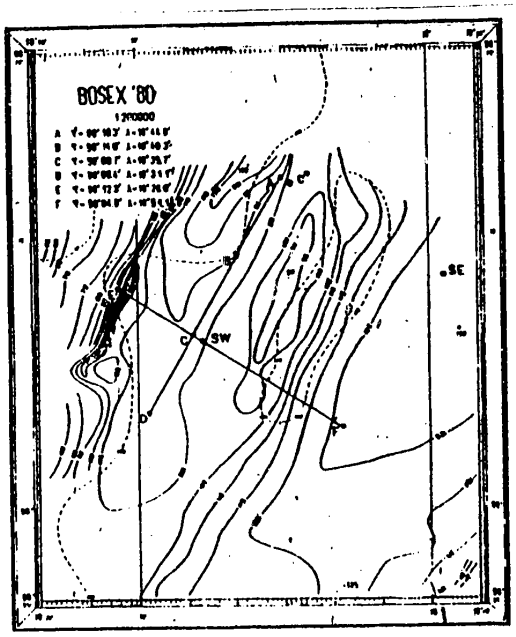

Figure 3. Bottom Topography of the 1980 Traverse

A cross-shaped traverse (Figure 3) was laid out in 1980, consisting of stations A-F for May-August and temporary (2-weeks) station G between stations C and F. Figure 3 also shows the location of part of the 1979 traverse (stations C*, SW, SE) and the bottom topography.

It is concluded that the current flowmeters indicate the existence of vortical current and that strongly pronounced bottom-entrained topographic waves may exist under favorable conditions.

BIBLIOGRAPHY

1. Fofonoff, N. P., "Spectral Characteristics of Internal Waves in the Ocean," DEEP-SEA RES., Supplement to Vol 16, 1969, pp 59-71.

2. Rhines, P., "Edge-, Bottom- and Rossby Waves in a Rotating Stratified Fluid," GEOPHYS. FLUID DYN., Vol 1, 1970, pp 273-302.

3. Rhines, P., "The Dynamics of Unsteady Currents," Vol 6, "The Sea," 1978.

Results of STD Mapping in the BOSEX Traverse on the Baltic Sea

A. Aytsam, Yu. El'ken

A series of STD [salinity-temperature-density] maps were plotted with the assistance of a Neil Brown probe in 1979-1980 during cruises of the scientific research vessel "Ayu-Dag" in the BOSEX traverse located in the central part of the Baltic Sea. The spacing of the square network of measuring points was 5 nautical miles, the y and x axes were oriented 30° left of north and east respectively, and the dimensions of the traverse were 20 or 25 nautical miles on the x and y axes. The time of one mapping session was about a day and a half.

The main object of interest was synoptic variability and its manifestation in the distribution of thermohaline fields. While the mapping was going on, buoy stations carrying current flow meters were dropped off in the traverse in order to obtain an integrated picture of the dynamics of synoptic processes in this portion of the sea. The 1980 materials had not been subjected to comparison yet.

One unique feature in the stratification of the BOSEX traverse is presence of a halocline with its upper boundary located at an average depth of 70 meters. In summer a very steep thermocline appears at 15-30 meters. Analysis of the correlation functions would show that some characteristics of internal waves that are less-perturbed by the presence of noise are sufficiently well correlated ($K > 0.2$-0.3) at a Rossby radius of approximately 10 km. This means that such waves can be mapped with the assistance of optimum interpolation. Relative dynamic topography (RDT) maps and isopycn depth maps offer greater interest. At given depths, the distributions of temperature and salinity are disturbed by considerable noise, while at given densities, their distributions are uniform.

Using maps plotted sufficiently close together in time, we can distinguish two "scenarios" for the evolution of perturbations on a synoptic scale:

1) vortical perturbations resembling the topographic wave with the horizontal dimension $L \approx 2R_d$ discovered in August 1979. Deformation of the thermocline and the halocline was of the same sign, both being raised above their "average position." Geostrophic shifts relative to the rotation rate were greater in the halocline than in the thermocline. The perturbation moved along the isobath at a rate of about 2 cm/sec. In 10 days the relative rate of rotation doubled. Concurrently the axis of the perturbation was tilted, such that the perturbation spread faster in the thermocline. This "scenario" may be explained by the theory of topographic waves (1);

2) the "large" decomposing vortical perturbation with dimension $L \approx 4R_d$ discovered in May-June 1980. At this time a developed thermocline was absent, such that the perturbation revealed itself in the halocline. The amplitude of the isopycn depth attained 22 meters, and the geostrophic shift in rotation attained 15-20 cm/sec between the 60-meter and 90-meter strata. Figure 1 shows the evolution of this main perturbation in successive RDT maps (the difference in dynamic depths was 70 and 30 decibars). In 9 days the center of the main perturbation moved 5-10 nautical miles transverse to a submarine channel from one edge of an even portion of the bottom to the other edge. In the periphery of the vortex the field was deformed in comparison with the previous map. In map No 4 (plotted 10-11 June 1980) the traverse was shifted, and the initial phase of decomposition of the "large" perturbation into two "small" ones with dimension $L \approx 2R_d$ could be seen on the RTD map.

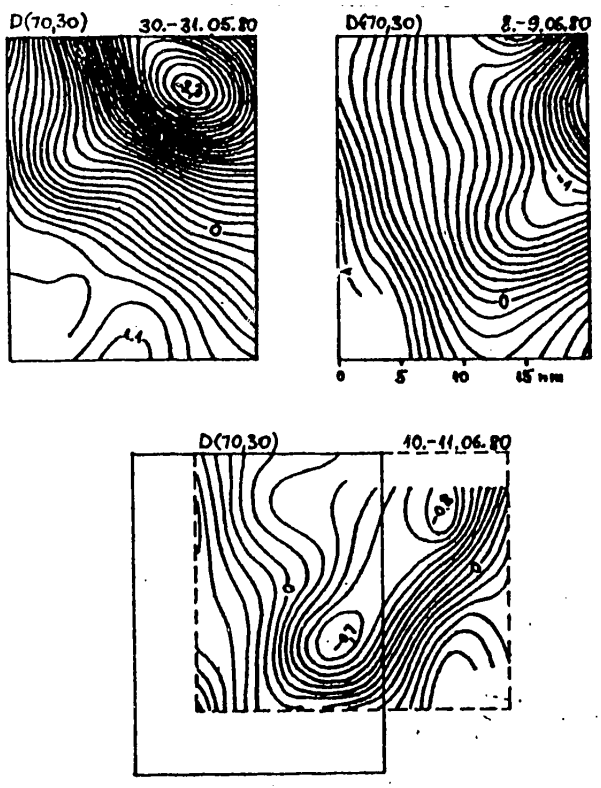

Figure 1. Decomposition of a Vortex on RTD Maps

In addition to these two time-dependent "scenarios", we discovered the following perturbation structures on single maps:

3) an open perturbation (the maximum of the anomaly intersected the bottom slope) in late May 1979 with dimension $L \approx 4\text{-}5R_d$;

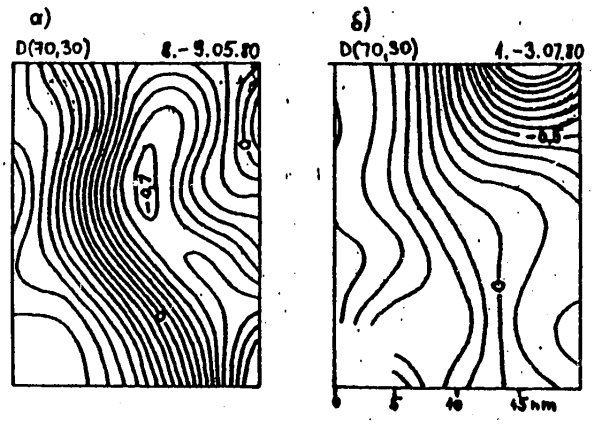

Figure 2. RTD Maps for D (70,30)

4) a tongue-shaped perturbation (a meander) in early May 1980 with dimension $L \approx 4\text{-}6R_d$ (Figure 2*a*);

5) the periphery of a perturbation with dimension $L \approx 4\text{-}6R_d$ in early June 1980 (Figure 2*b*). The structure of the thermocline was distorted by a storm, which began toward the end of the mapping session (according to (4), erosion of the thermocline begins 6 hours after the start of a storm). It appears as if deformation of the thermocline and of the halocline is of the same sign;

6) two vortical perturbations in mid-August 1980 with dimension $L \approx 2R_d$. The thermoclines of both perturbations were low, while the halocline of one perturbation was raised higher while that of the other was lower.

According to Kielmann (personal communication) synoptic baroclinic perturbations may arise owing to fluctuating atmospheric influences. To demonstrate this, he used a linear digital barocline model for which the initial and boundary conditions were similar to those in (3). A pattern similar to that in the first "scenario" was observed in the BOSEX region following interruption of the effects of wind fluctuations.

However, the second "scenario" permits suggestion of another hypothesis concerning generation of synoptic variability and various vortices. According to calculations made by M. Payuste using Tang's model (5) for baroclinic instability, supplemented by a bottom slope factor (this model contains both a particular case of Tang's two-layer model, Idi's model and the Blumsack-Gierasch model (2)), in different conditions perturbations with dimensions within $L \approx 3\text{-}4R_d$ exhibit maximum instability. Therefore it may be suggested that owing to baroclinic instability, first "large" vortices arise owing to the available potential energy of large-scale motion, and then these vortices, after growing to a certain maximum amplitude, decompose into smaller-scale vortices in view of nonlinearity.

BIBLIOGRAPHY

1. Aitsam, A., Elken, J., Pavelson, J., and Talpsepp, L., "Preliminary Results of the Investigation of Spatial-Temporal Characteristics of the Baltic Sea Synoptic Variability," in "The Investigation and Modelling of Processes in the Baltic," Tallinn (in press).

2. Blumsack, S. L., and Gierasch, P. G., "Mars: The Effects of Topography on Baroclinic Instability," J. ATM. SCI., Vol 29, 1972, pp 1081-1089.

3. Kielmann, J., "Mesoscale Eddies in the Baltic," in "Proc. of XI Conf. of Baltic Oceanographers," Vol 2, Rostock, 1978.

4. Krauss, W., "Inertial Waves and Mixing in the Thermocline (BOSEX Results)," in "Proc. of XI Conf. of Baltic Oceanographers," Vol 2, Rostock, 1978.

5. Tang, C. M., "Baroclinic Instability of Stratified Shear Flows in the Ocean and Atmosphere," J. GEOPHYS. RES., Vol 80, 1975, pp 1168-1175.

Finestructure of the Thermocline in the Ocean

V. S. Belyayev

1. Continuous growth in the volume of research on the finestructure of oceanological fields has been observed in recent years (2). The ocean's interstratification, which is typified by quasiuniform strata alternating with interlayers of significantly lesser thickness, and by sharp changes in medium properties, has a typical vertical scale on the order of 1-10 meters. This finestructure of the ocean was modeled by a stepped distribution of properties in relation to depth (3,4). However, few measurements have yet been made of parameters characterizing interstratification of oceanic water, especially in the upper part of the thermocline (in the layer exhibiting a temperature gradient). The distribution of interlayers in relation to depth in the main thermocline was described in (4) by a stochastic Poisson process. These measurements of the finestructure of the electroconductivity field in the upper thermocline, obtained during the 22d cruise of the scientific research vessel "Dmitriy Mendeleyev" (1979) in the western equatorial region of the Pacific, also attested to a possibility for modeling the vertical distribution of interlayers exhibiting high electroconductivity (temperature) gradients by a Poisson process. The empirical distributions of the thicknesses of quasiuniform layers h were approximated by an exponential law with a probability density of

$$p(h) = \mu \exp(-\mu h). \qquad (I)$$

the values of parameter μ (where μ^{-1} is the average thickness of a quasi-isothermic layer) for the main and upper thermoclines are 0.92 and 0.29 m^{-1} respectively. The distribution of the amplitudes of temperature gradients in the interlayers, as determined from measurements in the upper thermocline, were also approximated by an exponential law with a parameter of 41 $(°C)^{-1}$.

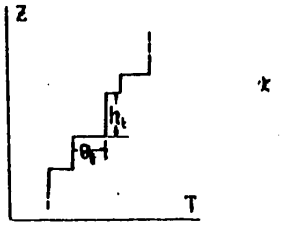

Figure 1. Modeled Vertical Temperature Profile

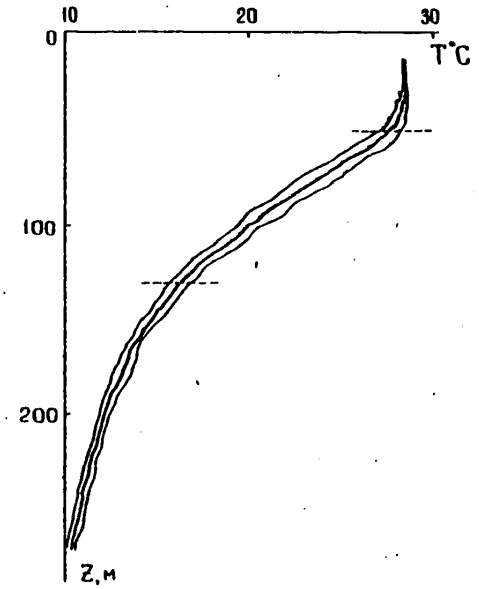

Figure 2. Mean Temperature Profile for the Traverse (Thick Curve): The thin curves indicate the standard deviation of temperatures from the mean value at individual sounding points

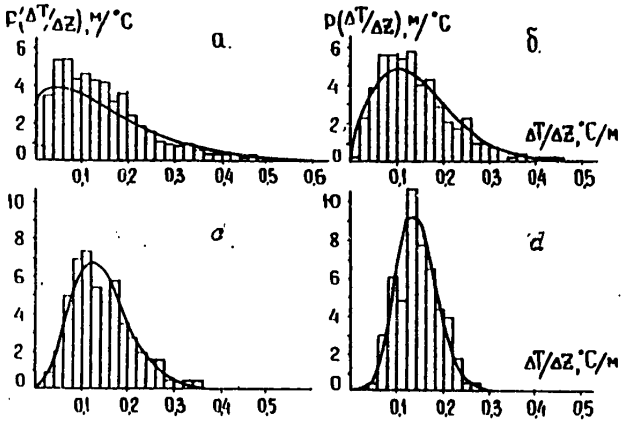

Figure 3. Histograms of Temperature Gradient Estimates Based on Finite Differences at $\Delta Z = 2$ (*a*), 4 (*b*), 8 (*c*) and 16 meters (*d*): Continuous curves represent the model law (2)

Figure 4. Fragment of Depth (1) and Temperature (2) Signal Recordings at a Fixed Horizon in the Thermocline

2. A model representing stepped distribution of temperature in relation to depth is examined (Figure 1); in this case the temperature difference in the depth interval ΔZ is

$$\Delta T = \sum_{i=1}^{n} \Theta_i$$

where Θ_i and n are random. If we assume that the distribution of temperature gradient amplitudes is exponential (1) with parameter β^{-1}, then for a Poisson distribution of temperature gradients in relation to depth, the probability density for estimates of the temperature gradient, $\xi = \Delta T/\Delta Z$ (where the Z axis is oriented upward), has the form

$$P_{\xi}(\xi) = \sqrt{\frac{\mu}{\beta\xi}} \exp\left[-\left(\xi/\beta + \sqrt{\mu}\right)\Delta z\right] I_1\left(2\sqrt{\frac{\mu\xi}{\beta}}\Delta z\right)\Delta z \quad (2)$$

after the values of the principal parameters μ and β are chosen on the basis of one consideration or another, function (2) would depend only on ΔZ.

3. Information on vertical temperature distribution obtained during the 22d cruise of the research vessel "Dmitriy Mendeleyev" in a traverse in the Indian Ocean south of the island of Sumatra (stations 1819-1830, 1032) was used to experimentally test the validity of relationship (2). In an interval of depths from 50 to 130 meters the vertical gradient of the mean temperature varies little, being $0.15°C \cdot m^{-1}$ (Figure 2). The histograms of temperature gradient estimates for different ΔZ, obtained in this layer, are shown in Figure 3.

The estimates of the principal parameters in law (2) were obtained as the first two moments of random variable ξ at $\Delta Z = 16$ meters, assuming the values $\mu = 1.3\ m^{-1}$ and $\beta^{-1} = 9.1\ (°C)^{-1}$. Probability density curves computed with formula (2) for ΔZ values of 2, 4, 8 and 16 meters are shown in Figure 3. The model of distribution law (2) for the temperature gradient estimates reflects the basic features of the histograms obtained for ξ. Good agreement between the empirical data and the modeled distribution of temperature gradient estimates indicates that the finestructure of an upper thermocline with a thickness less than 16 meters may be adquately described by a stepped function with certain probability characteristics.

4. Existence of individual quasi-isothermic layers in the upper thermocline is demonstrated by measurements made during the 50th cruise of the research vessel "Vityaz'" (1976) in the central part of the northern Pacific. Figure 4 shows a fragment of a recording of temperature T and depth Z signals (the measurement horizon was located in the thermocline). Fluctuations with periods of 7-10 sec elicited by rolling of the ship can be distinctly seen in the T and Z signals. Information on synchronous changes in depth ΔZ and temperature ΔT can be used to determine local values of the vertical temperature gradient $\Delta T/\Delta Z$. Small local values for $\Delta T/\Delta Z$ in individual time intervals indicate that the sensors entered quasi-isothermic layers.

5. It would be suitable to perform further experimental research with the objective of finding the dependence of parameters of the finestructure of the upper oceanic thermocline on the background hydrometeorological conditions.

BIBLIOGRAPHY

1. Ozmidov, R. V., "The 22d Cruise of the Scientific Research Vessel 'Dmitriy Mendeleyev'," OKEANOLOGIYA, Vol 19, No 5, 1979, pp 948-954.

2. Gregg, M. C., and Briscoe, M. G., "Internal Waves, Finestructure, Microstructure, and Mixing in the Ocean," REVIEWS OF GEOPHYSICS AND SPACE PHYSICS, Vol 17, No 7, 1979, pp 1524-1548.

3. Hayes, S. P., Joyce, T. N., and Millard, R. C. Jr., "Measurements of Vertical Finestructure in the Sargasso Sea," J. OF GEOPHYSICAL RESEARCH., Vol 80, No 3, 1975, pp 314-319.

4. Joyce, T. M., and Desaublies, Y. J. P., "Discrimination Between Internal Waves and Temperature Finestructure," J. PHYS. OCEANOGR., Vol 7, No 1, 1977, pp 22-32.

A Model of Interstratified Turbulence in the Ocean

V. S. Belyayev, R. V. Ozmidov

Extensive observations made in recent years on small-scale turbulence in different regions of the ocean showed that oceanic turbulence is typified by intense interstratification: Zones of highly turbulent liquid alternate with layers in which water flow is close to laminar (2). These data fundamentally alter the existing idea that turbulence is continuous in the ocean, typified by some coefficient of vertical turbulent exchange, K (1). In the first approximation this coefficient was thought to be constant in relation to depth, while in more-sophisticated models of vertical turbulent exchange in the ocean, K was given as some function of depth z. Examples of using different types of functions $K(z)$ in a model for a completely turbulent ocean are shown in Figure 1*a* (*1*--K is constant in relation to depth, *2*--the exchange coefficient decreases smoothly with depth).

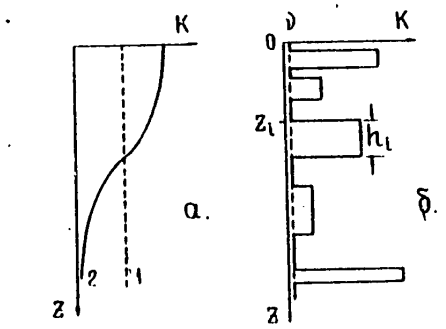

Figure 1. Schematic Distribution of the Coefficient of Vertical Turbulent Exchange in Relation to Depth: *a*--models of a continuously turbulent ocean; *b*--a model of interstratified turbulence

The interstratified nature of oceanic turbulence implies the following pattern for vertical turbulence distribution. At certain horizons Z_i, there exist turbulent fluid layers with thickness h_i. The levels of turbulence in these layers (the mean square values of turbulent pulsations in velocity) are correspondingly equal to σ_i at a certain fixed moment in time. Variables Z_i, h_i and σ_i are random. With time,

the turbulence in these layers would decrease, and in the end these layers would disappear, but concurrently new turbulent zones would appear at other points in space, which in turn evolve and then disappear. The mechanisms responsible for generation of new turbulent zones of liquid may include inversion of internal waves, the shear instability of oceanic currents and other processes. According to the available measurements the movement of liquid between turbulent zones may be assumed to be close to laminar, with a molecular kinematic exchange coefficient ν.

Generally speaking K_i, the effective value of the coefficient of vertical turbulent exchange in each of the turbulent layers of liquid, depends on both the intensity of turbulence in the layer σ_i and the vertical dimension of the layer h_i--that is, $K_i = f(\sigma_i, h_i)$. A possible form of function $f(\sigma_i, h_i)$ will be indicated below.

The instantaneous distribution of values for the coefficient of vertical turbulent exchange in relation to depth may be described as a first approximation by a random impulse function (Figure 1*b*):

$$K(z) = \sum_{i=1}^{n} f(\sigma_i, h_i) F\left(\frac{z - z_i}{h_i}\right), \quad \text{where } F(x) = \begin{cases} 1 & 0 \le x < 1 \\ 0 & \text{for all other } x \end{cases}$$

If we make the natural supposition that σ_i and h_i do not depend statistically on z_i and that the distribution densities of these variables do not depend on i, then the conditional mean value of function $K(z)$ for n turbulent spots in the ocean layer under analysis, H, would take the form

$$\langle K|n\rangle = \sum_{i=1}^{n} \int_{\sigma_i} \int_{h_i} \left\{ f(\sigma_i, h_i) P_{\sigma h}(\sigma_i, h_i) d\sigma_i dh_i \int_{z_i} F\left(\frac{z - z_i}{h_i}\right) P_z(z_i) dz_i \right\},$$

where P_z is the distribution density for z_i and $P_{\sigma h}$ is the joint distribution density for σ_i and h_i. Given a uniform distribution density for the location of an individual impulse in the depth interval H--that is, when $P_z(z_i) dz_i = \frac{dz_i}{H}$,

$$I = \int_{z_i} F\left(\frac{z - z_i}{h_i}\right) P_z(z_i) dz_i = \frac{1}{H} \int_{-h_i}^{H} F\left(\frac{z - z_i}{h_i}\right) dz_i$$

If the thickness of turbulent layers is significantly less than the total thickness of the column of ocean water under examination, then $I \approx h_i/H$ and

$$\langle K|n\rangle = \sum_{i=1}^{n} \int_{\sigma_i} \int_{h_i} \frac{h_i}{H} f(\sigma_i, h_i) P_{\sigma h}(\sigma_i, h_i) d\sigma_i dh_i = \frac{n}{H} \langle hf \rangle.$$

Averaging in relation to n, we get the unconditional mean $\langle K\rangle = \frac{\langle n\rangle}{H}\langle hf\rangle$.

For a Poisson distribution of the number of impulses in interval, $P_H(n) = \frac{(n_1 H)^n}{n!}\exp(-n_1 H)$, where $n_1 = \langle n\rangle / H$ is the mean number of turbulent layers in a unit interval of depths, we get $\langle K\rangle = h_1\langle hf\rangle$.

It would be natural to assume from considerations of scale that $K_i = f(\sigma_i, h_i) = c\sigma_i h_i$, where c is a certain dimensionless universal constant. Then

$$\langle K\rangle = cn_1 \int_0^\infty \int_0^\infty h^2 \sigma\, p_{\sigma h}(\sigma, h)\, d\sigma\, dh. \qquad (1)$$

If σ and h are statistically independent, then $p_{\sigma h}(\sigma, h) = p_\sigma(\sigma)\, p_h(h)$ and

$$\langle K\rangle = cn_1 \int_0^\infty \sigma p_\sigma(\sigma)\, d\sigma \int_0^\infty h^2 p_h(h)\, dh. \qquad (2)$$

When σ and h are statistically dependent, $p_{\sigma h}(\sigma, h) = p_h(h)\,\psi_1(\sigma|h) = p_\sigma(\sigma)\,\psi_2(h|\sigma)$, (3)

where ψ_1 and ψ_2 are the corresponding conditional probability densities.

Extremely few empirical estimates of the distribution laws in formulas (1)-(3) have been obtained thus far. The distribution of the thicknesses of turbulent layers in the Gulf of Tunis was approximated in (5) by a logarithmically normal law:

$$p_h(h) = \frac{1}{h\sqrt{2\pi}\Delta}\exp\left[-\frac{(\ln h - \mu_0)^2}{2\Delta^2}\right],$$

where μ_0 and Δ are, correspondingly, the mean and standard deviation of $\ln h$. In this case $\langle h^2\rangle = \exp[2(\mu_0 + \Delta^2)]$. The values for the parameters arrived at in (5) are: $\mu_0 = 2.3$, $\Delta = 0.60$, $\langle\sigma\rangle = 0.6$ cm/sec and $n_1 = 0.081$.

At the Second International Colloquium on Geophysical Hydrodynamics in Liege (4), M. Gregg presented data on the thicknesses of turbulent layers in the main thermocline of the central part of the Pacific Ocean's northern subtropical circulation. The distribution of values for these thicknesses may be approximated by an exponential law:

$$p_h(h) = \mu_1 \exp(-\mu_1 h)$$

where $\mu_1 = 0.46$ m^{-1}, such that $\langle h^2\rangle = 2/\mu_1^2 = 9.4^2$ m, and the value for parameter n_1, given a Poisson distribution, was found equal to 0.21 m^{-1} for a 200-400 meter layer and 0.14 m^{-1} for an 800-1,200 meter layer.

Numerous measurements were made of the vertical profiles of the microstructure of the current velocity field during the 22d cruise of the research vessel "Dmitriy Mendeleyev" in the Indian Ocean within a traverse south of the island of Sumatra (3). For the upper 250-meter layer of the ocean, the value of n_1 arrived at on the basis of these data is 0.021 m^{-1}, while the values of the other parameters are: $\langle\sigma\rangle = 1.0$ cm/sec and $\langle h^2\rangle = 21$ m^2.

The values of the coefficient of vertical turbulent exchange, computed with formula (2) at $c = 0.1$ and $n_1 = 0.175$ m^{-1} for typical values $\langle\sigma\rangle = 0.1$-1 cm/sec, lie within 1.6 and 16 cm^2/sec (for the central part of the northern subtropical circulation of the Pacific Ocean). The corresponding value of $\langle K\rangle$ for the Gulf of Tunis attained 97 cm^2/sec, while according to measurements made in the traverse in the Indian Ocean, $\langle K\rangle = 4.4$ cm^2/sec.

Two-dimensional density distributions for probabilities $P_{\sigma h}(\sigma,h)$ are given in (6). The values of $\langle K\rangle$ obtained with formula (1) on the basis of these data are 40 and 16 cm^2/sec correspondingly for the western and eastern parts of the Gulf of Tunis. The corresonding value of the coefficient of vertical turbulent exchange based on measurements made in the Indian Ocean traverse is 6.8 cm^2/sec. The scatter of $\langle K\rangle$ values obtained above for different regions of the World Ocean may be the product of differences in the average hydrometeorological conditions of these regions.

The proposed statistical model, which accounts for interstratification of oceanic turbulence, permits computation of the effective coefficient of vertical turbulent exchange on the basis of information on the distribution laws for the thicknesses of turbulent spots and the intensity of turbulence within them. Such representation of turbulent exchange processes in the ocean by parameters also permits us to adequately account for the specific features of turbulence in different regions of the ocean and in different hydrometeorological conditions.

BIBLIOGRAPHY

1. Ozmidov, R. V., "Horizontal Turbulence and Turbulent Exchange in the Ocean," Moscow, "Nauka", 1967.

2. Ozmidov, R. V., "Turbulence in the Upper Layer of the Ocean," ITOGI NAUKI I TEKHNIKI. MEKHANIKA ZHIDKOSTI I GAZA, VINITI, Vol 12, 1978, pp 52-143.

3. Ozmidov, R. V., "The 22d Cruise of the Scientific Research Vessel 'Dmitriy Mendeleyev'," OKEANOLOGIYA, Vol 19, No 5, 1979, pp 948-954.

4. Ozmidov, R. V., and Fedorov, K. N., "Turbulence in the Ocean (Second International Liege Colloquium on Geophysical Hydrodynamics and the Second International Symposium on Turbulence in the Ocean, Liege, Belgium, 17-May 1979)," IZV. AN SSSR. FIZIKA ATMOSFERI I OKEANA, Vol 15, No 12, 1979, pp 1330-1333.

5. Pozdynin, V. D., "Statistical Characteristics of Turbulence Stratification and of Fluctuations in the Vertical Flow Rate Gradients in the Gulf of Tunis," OKEANOLOGIYA, Vol 18, No 2, 1978, pp 226-231.

6. Pozdynin, V. D., "The Vertical Structure of the Small-Scale Turbulence Field in the Gulf of Tunis," OKEANOLOGIYA, Vol 19, No 5, 1979, pp 776-781.

Synoptic Variability of Equatorial Currents in the Pacific Ocean

V. A. Bubnov, V. D. Yegorikhin

In February-March 1980, during the 24th cruise of the scientific research vessel "Dmitriy Mendeleyev," measurements were made in a special traverse with the purpose of studying the average structure and synoptic variability of equatorial currents in the Central Pacific. The traverse contained ten autonomous buoy stations (ABS) carrying current flowmeters. Those stations were located on two meridional sections through the equator at 167° W. Long. and 163°15' W. Long. near mapping points 1°30' N. Lat., 0°45' N. Lat., 0° Lat., 0°45' S. Lat. and 1°30' S. Lat. The obtained series of observations covered 28-39 days, and the time of synchronous observations along both cross sections of the traverse was about 27 days.

The vertical dynamic structure in a water layer down to 600 meters in the traverse is formed by three flows occurring in different directions: the South Tradewind Current, the Equatorial Subsurface Countercurrent (Cromwell's Current), and the Equatorial Intermediate Current.

The South Tradewind Current embraces the upper layer, and its thickness varies from 70-100 meters near the equator to 120-150 meters at 1°30' N. and S. Lat. The velocity of this current varies within broad limits (from 30 to 100 cm/sec), averaging about 60 cm/sec (at a 15-meter horizon).

Cromwell's Current is an eastward flow embracing a layer about 200 meters thick. Its lower boundary is usually at a depth of 260-280 meters, and the center of maximum velocities is within the center of the pycnocline, at a depth of 140-170 meters. The average velocity in the center of the current is 75-80 cm/sec, while in certain periods it exceeds 100 cm/sec. Below Cromwell's Current the water flow once again acquires a westerly direction, and it is called the Equatorial Intermediate Current. In the vicinity of the traverse this current has a vertical dimension of up to 180 meters, and it is typified by a maximum velocity of up to 30 cm/sec at a depth of 300-400 meters.

Combining quantitative (computation of energy spectrums) and qualitative (examination of different sorts of time and latitude-time graphs of flow velocities) analysis of the observation data from the traverse, we determined the variability of the velocity field in the equatorial zone within a range of periods from half a day to 2 weeks.

Half-day and daily fluctuations in velocity associated with tidal forces of the moon and sun were revealed by spectrum analysis in both the surface layer, embraced by the South Tradewind Current, and in the deeper reaches of Cromwell's Current (Figure 1).

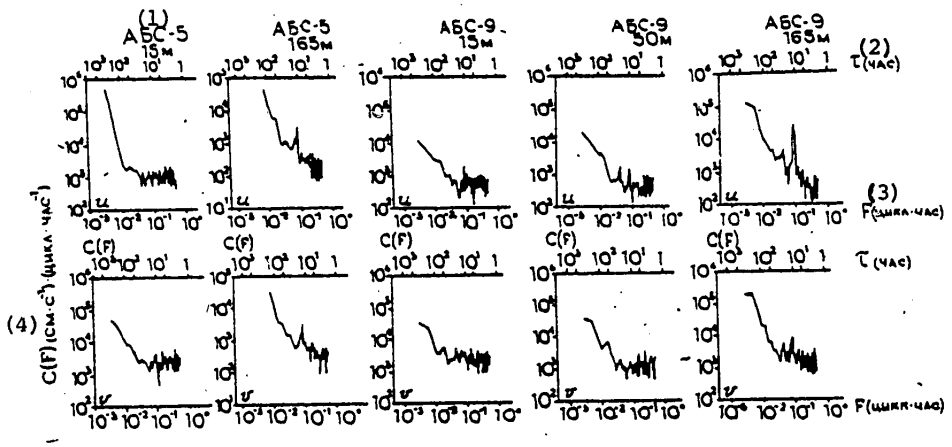

Figure 1. Examples of Kinetic Energy Spectrums for the Zonal (u) and Meridional (v) Components of the Current Velocity in the Equatorial Traverse

Key:

1. ABS
2. Hours
3. Cycles·hour
4. Cm·sec

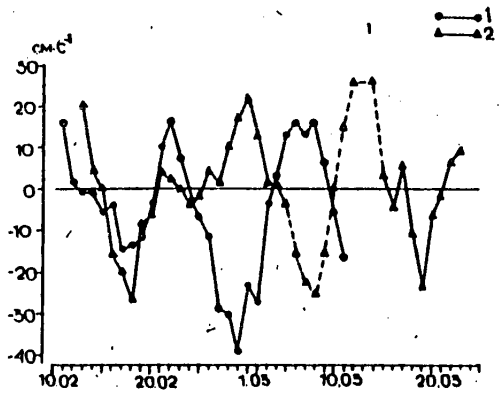

Figure 2. Change in Mean Daily Values of the Meridional Component of the Current Velocity at the 15 Meter Horizon: *1*--167° W. Long. meridian, *2*--163°15' W. Long. meridian. Data are averaged for the interval from 1°30' N. Lat. to 1°30' S. Lat.

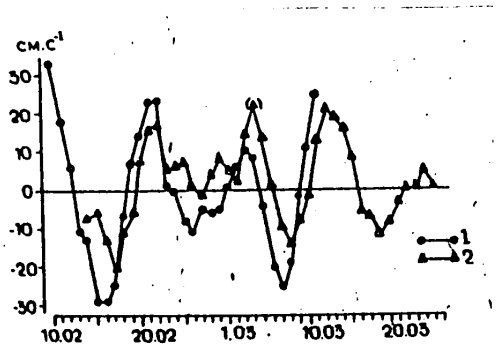

Figure 3. Change in Mean Daily Values of the Meridional Component of the Current Velocity at the 165 Meter Horizon: *1*--167° W. Long. meridian, *2*--163°15' W. Long. merdian. Data are averaged in the interval from 0° Lat. to 1°30' S. Lat.

Within the limits of the South Tradewind Current and Cromwell's Current, we also observe fluctuations with a 3-4 day period (Figure 1), which are also typical of the atmospheric pressure and wind fields in the equatorial region. It may be suggested that at this frequency, the ocean receives energy from the atmosphere by means of direct wind effects.

The energy-richest fluctuations in flow rate of the South Tradewind Current are those with a period of 12-14 days (Figure 2). Observations did not reveal a direct connection between these fluctuations and changes in local winds in the area of the traverse.

The main feature of synoptic variability in Cromwell's Current is the meandering of its axis relative to the equatorial plane. Meandering is a complex unstable phenomenon, a product of the polymodal nature of the fluctuations, which cause superimposition of waves varying in physical nature. The amplitude of meanders is 30-40' of latitude. Fluctuations with a 10-day period are the most regular (Figure 3). The directions and velocity of propagation, and consequently the length of these waves cannot be determined uniquely from observations made in the traverse due to our ignorance of the number of whole waves falling within the distance between the eastern and western cross sections of the traverse. Three possible interpretations of the data in Figure 3 deserve attention:

a) very long waves propagating quickly eastward (length about 400 km, phasal velocity about 5 m/sec)--possibly Kelvin waves, having their origin on the eastern shores of Australia and being entrained in the equatorial zone;

b) eastern waves of moderate length and propagation velocity (length about 380 km, phasal velocity about 0.4 m/sec);

c) western waves of moderate length and propagation velocity (length about 460 km, phasal velocity about 0.5 m/sec).

Waves of the last two types may be interpreted as Rossby waves entrained by an equatorial waveguide; according to Zaytsev et al. (1), such waves may propagate both eastward and westward in eastward currents.

BIBLIOGRAPHY

1. Zaytsev, A. A., Zubin, A. B., and Monin, A. S., "Meandering of Lomonosov's Current," DOKLADY AN SSSR, Vol 248, No 5, 1979, pp 1229-1232.

Vertical Structure of Current Velocities and Internal Waves in the Ocean

Ye. P. Varlatyy, V. V. Navrotskiy, I. D. Rostov

The fine vertical structure of current velocities in the ocean has not been studied adequately due to difficulties in measuring continuous velocity distributions in the vertical plane (1,3,4). It is usually explained by the sliding, in different directions, of water layers having different densities, especially near straits and frontal zones. In the open ocean, such structures may be the consequence of internal waves with almost-inertial periods (2). This paper analyzes observations that rather clearly reveal the effect of inertial-gravity waves with small periods on the vertical distribution of horizontal current velocities.

Let us write the equation for inertial-gravity waves shifted $\{,\eta,\}=\rho^{1/2}\psi$ on axes x, y, z relative to the steady state, using Bussinesk's approximation:

$$\psi'' + n^2\psi = 0, \qquad (1)$$

$$n^2 = l^2\frac{N^2-\omega^2}{\omega^2-\Omega^2}, \qquad (2)$$

where n,l--vertical and horizontal components of wave vector $\vec{K}(l,m,n)$, which for simplicity of notation is assumed to lie in plane xz; ω--wave frequency; Ω--vertical component of the Coriolis vector (inertial frequency); $N=\left(\frac{g}{\rho}\frac{\partial\rho}{\partial z}\right)^{1/2}$ --Vyaysyal'-Brent frequency.

The dispersion ratio for these waves may be written in the form

$$\omega^2 = N^2\sin^2\theta + \Omega^2\cos^2\theta, \qquad (3)$$

where Θ is the angle between wave vector $\vec{K}$ and the vertical axis.

It would be interesting to note that $\omega^2 = N^2\sin^2\Theta$ is the dispersion ratio for internal waves of a nonrotating stratified liquid, while $\omega^2 = \Omega^2\cos^2\Theta$ is the dispersion ratio for inertial waves in an unstratified rotating liquid.

Displacements ξ,η are expressed by the derivatives of vertical displacements ζ_z from the motion equations. Given a constant Vyaysyal' frequency $N(z) = \text{const}$, we get:

$$\xi = \frac{i}{\ell}\zeta_z = -\frac{n}{\ell}\zeta, \quad \eta = \frac{1}{\ell}\frac{\Omega}{\omega}\zeta_z = \frac{in}{\ell}\frac{\Omega}{\omega}\zeta. \quad (4)$$

The projection of the particle projectory onto plane [coordinates omitted in the original] is the same ellipse seen in relation to internal waves in the absence of rotation, while the projection onto plane xy results in the same ellipse seen with inertial waves in a uniform liquid. The trajectory in space is an ellipse intersecting plane xy on axis x and tilted at an angle d_1 to the vertical:

$$tg\,d_1 = \frac{|\eta|}{\zeta} = \frac{n}{\omega}\left(\frac{N^2 - \omega^2}{\omega^2 - \Omega^2}\right)^{1/2} = \frac{\Omega}{\omega}\cdot\frac{n}{\ell}. \quad (5)$$

Using (3), we can easily obtain angles d_2 and d_3 for phasal and group velocities $\vec{v}$ and $\vec{u}$, and the known orthogonality relationship for them:

$$tg\,d_2 = \frac{\ell}{n}\cdot tg\,d_3 = -\frac{n}{\ell}, \quad tg\,d_2 \cdot tg\,d_3 = -1. \quad (6)$$

It follows from these relationships that when movement occurs from the top downward (the positive direction of axis z), we would observe the same law applicable to purely gravitational inertial waves in a nonrotating liquid: clockwise rotation of the horizontal velocity vector in the presence of a positive z-component of the phasal velocity (the vertical component of the wave number is directed downward), and counter-clockwise rotation in the presence of the opposite z-component of phasal velocity. The difference from the case of inertial waves in a nonrotating liquid would lie in the size of the horizontal component of orbital velocity--in our case, given identical phasal velocities and tilt angles of $\vec{K}$ in relation to the vertical, the velocities in rotating and nonrotating systems would be associated by the relationship

$$u_{rot} = u_{nonrot} \cdot \sin d_1. \quad (7)$$

In principle, these relationships yield to experimental testing, but this could not be done with sufficient reliability in the ocean due to the complex vertical structure of the average currents and of the inertial wave field. Visual observations in the upper thermocline that can confirm the spiral behavior of the velocity vector on the vertical axis are very rare, they encompass too small a layer, and therefore they may apply only to very short waves. Confirmation of the relationships is important to choosing the means for modeling inertial waves in the ocean, inasmuch as the most popular method of normal modes physically presupposes reflection from boundaries to form standing vertical modes--that is, it presupposes predominantly horizontal waveguide propagation of energy without its noticeable vertical flow. Doubts as to the physical reality of this approach in relation to the open ocean have already been stated by some authors.

In June 1980 observations doubtlessly demonstrating the presence of vertical flows of wave energy and asymmetry of internal waves were made in the Pacific Ocean in a traverse with coordinates 35°53' N. Lat., 154°57' E. Long. A region was found in which a layer 300-400 meters thick at depths of 300-700 meters had a temperature gradient that was almost constant in relation to depth, and was separated from the upper thermocline by a quasi-uniform layer at depths of 100-300 meters, with an almost constant current direction.

The observations consisted of repeated soundings of current velocity, temperature and electroconductivity (AIK and "Istok-4" probes) at 30-minute intervals for periods of not less than a day, and of continuous recordings of fluctuations in scattering layers by means of echo sounders. The principal observation results are as follows:

1. In a layer with a non-zero average density gradient, beginning at a depth of 300-400 meters there appear quasiperiodic velocity fluctuations on the vertical axis, with a vertical scale varying from 20 to 100 meters. The maximum amplitude of the velocity fluctuations, 5-8 cm/sec, corresponds to a vertical scale of about 100 meters. The fluctuations deteriorate as the density gradient decreases at depths below 700-800 meters.

2. The current, which remains almost constant in direction and velocity to a depth of about 400 meters, begins to change direction rather abruptly below 400 meters. When the shift in current direction in the layer below 600-700 meters relative to the upper layer is greater than 120°, spiral clockwise rotation of the current arises in the intermediate layer; the spacing between spirals is 30-100 meters, and the rotation rate is nearly constant: $d\phi/dz \approx 2\pi/\lambda_z = n \approx \text{const}$. In this case the direction of the lower current establishes itself opposite to that of the upper current. After a set of spirals passes through (up to three or four 360° revolutions), the directions of the upper and lower currents converge to 90°, the number of spiral coils decreases or they disappear altogether, and the amplitudes of the oscillations decrease as well.

3. The mean density profile changes little, but the finestructure undergoes noticeable intensification when spiral coils appear.

4. The dominant periods of oscillations in the scattering layers at depths of 400-600 meters are 20-30 minutes, with periods of 90-120 minutes arising significantly less frequently. The vertical shifts in the layers are 10-20 meters.

We interpret the observed processes as propagation as trains of inertial waves. A number of good conclusions and numerical estimates of the wave parameters can be made on the basis of the relationships given above. According to theory, clockwise rotation of the velocity vectory corresponds to propagation of dominant internal waves from the top downward. Inasmuch as a complete revolution of a spiral occurs within the wave period, if we assume the vertical scale to be $\lambda_z = 100$ meters and a time scale of about 30 minutes, we get approximately 5 cm/sec as the estimate for the vertical component of phasal velocity. The vertical shifting velocity for the scattering layers is significantly smaller.

On the basis of relationships (4), at the observed horizontal velocity amplitudes of about 5 cm/sec, we get an estimate of $\lambda_x = 600$ meters for the horizontal wave scale and $V_x = 30$ cm/sec for the horizontal phasal velocity. Using (5), at

$N/\omega \approx 2$, we get $d_1 \approx 12°$ for the orbital ellipse and $d_2 \approx 78°$ for phasal velocity. Angles d_3 and d_1 are very close. The orbital velocities are about 1 cm/sec greater than the observed horizontal velocity amplitudes.

The question as to the origin of the observed waves is most interesting. There were practically no correlations with internal waves in the upper 100-meter layer. Considering the high correlation between appearance of spirals with significant amplitudes and growth in the difference between the directions of the current in the upper and lower layers, it would be natural to suggest that we are observing a shift in velocity in countercurrents serving as the main factor responsible for generation of trains of short-period internal waves propagating nonhorizontally. Waveguide properties were practically absent from the layer. Growth in impulse transfer under the influence of internal waves significantly changes the deep current, and the difference in directions and the corresponding velocity shift decrease. In this case the internal waves attenuate, resulting in recovery (amplification) of the displacements, and generation of a new set of waves. The vertical component of the Coriolos force may be a significant factor in the large and fast oscillations of horizontal velocity. When we take it into account, frequency in the dispersion relationship becomes asymmetrical, and the phasal velocities of waves propagating in different directions may differ noticeably. In correspondence with (5) and (7), the orbital velocities, which make a noticeable contribution to the measured currents, will differ significantly as well.

The objective of this report was to demonstrate, on the basis of visual data, the influence internal waves have on the observed vertical structure of the velocity field. It obviously follows from the observations that the finestructure of the velocity field may usually be the consequence of kinematic or irreversible effects produced by passage of internal waves. A more-formal statistical analysis of the measurements will be presented in a separate paper.

BIBLIOGRAPHY

1. Monin, A. S., "The Vertical Meso- and Microstructure of Ocean Currents," DAN SSSR, Vol 208, No 4, 1973.

2. Leaman, K. D., and Sanford, T. B., "Vertical Energy Propagation of Inertial Waves: A Vector Spectral Analysis of Velocity Profiles," J. GEOPHYS. RES., Vol 80, No 15.

3. Perkins, H., and Van Leer, J., "Simultaneous Current Temperature Profiles in the Equatorial Countercurrent," J. PHYS. OC., Vol 7, No 2, 1977.

4. Rossby, H. Th., and Sanford, Th. B., "A Study of Velocity Profiles Through the Main Thermocline," J. PHYS. OC., Vol 6, No 5, 1976.

Some Results of Synchronous Measurements of the Vertical Structure of Temperature, Salinity, Speed of Sound and the Current Vector Velocity

Ye. P. Varlatyy, I. D. Rostov

There are certain methodological difficulties in simultaneously measuring the vertical profiles of a current velocity vector and the basic thermodynamic parameters in the ocean; consequently such measurements are few in number today. The thermohaline and dynamic structure of waters in a 0-1000 meter layer in a water area including the Kamchatka and Kuril' currents and the subarctic front of the Northwest Pacific were subjected to detailed investigation during the eighth cruise of the scientific research vessel "Professor Bogorov" with assistance of an acoustic measuring complex (AIK) and "Istok-4" probe. Synchronously with these observations, we recorded the parameters of internal waves in a layer reaching from the surface down to several hundred meters. An analysis of the results permitted us to refine existing ideas concerning the unique features of the stratification and the meso- and small-scale variability of the fields.

The observations showed that the Kuril' current, the area of the northern subarctic front and the interfrontal zone can be classified as regions having a finestructure of clearly greater intensity. Typical features of stratification are propagation of inversional structures in these areas and a high degree of spatial-temporal variability in its characteristics. In waters of the Kuril' modification of the subarctic structure, the finestructure is well developed in summer within the limits of the cold subsurface reduced-salinity layer and the intermediate layer, where the conditions for double diffusion are present. The temperature field is dominated here by nonuniformities with a vertical scale on the order of meters. In the zone of the subarctic front, where warm and saline waters brought in by the Kurosio current interact and mix with cold and less-saline subarctic waters, the conditions are created for development of various mechanisms generating fine-scale structures, which leads to greater diversity in the forms, parameters and variability of the finestructure in the entire analyzed range of depths.

Analysis of the amplitude-frequency component of profile perturbations with a vertical scale of 2-50 meters in the 0-1000 meter layer, performed for stations along a meridional cross section from Kamchatka to 35° N. Lat., showed that the standard deviations of fluctuations in temperature, salinity and density for the region of the frontal zone exceed, by an average of 1-2 orders of magnitude, the analogous estimates of the finestructure of subarctic and subtropic waters. Moreover, far from coastal regions in a 400-1000 meter layer, finestructure makes practically no

contribution to the total dispersion of temperature gradients in subarctic waters. The averages and standard deviations of layer thicknesses and of the vertical gradients of temperature, salinity and density were relatively stable in time within a period of around a day, and in space within tens of nautical miles; however, they did differ significantly for traverses lying in different structural zones, or in individual sections of the profiles.

Measurements made with the AIK along a cross section within the frontal zone at 155° E. Long. confirmed the presence of northeasterly (northern front) and southeasterly (southern front) average currents with velocities from 40 to 80 cm/sec. The Kuril' current is a water flow moving southwest at a velocity of up to 30-50 cm/sec, and it is relatively stable in its direction. The principal contribution to total dispersion of vertical variations in current velocity is made here by perturbations with a vertical scale of 10-100 meters, in the region of the Kamchatka current by perturbations with a scale of 3-10 meters, and in the region of the north branch of the subarctic front by perturbations with a scale of up to 100-200 meters. Selective analysis of the profiles showed that the empirical distributions of the thicknesses of layers with approximately constant gradients for the current velocity and sound velocity fields are described reasonably well by a log-normal law, and that the gradient distributions are close to a normal law, with a positive excess dominating.

A comparison of curves describing vertical distribution of Vyaysyal' frequency and the shear modulus of the current velocity established that the nature of changes in these parameters was described in most cases by the following:

1. Changes in current velocity and direction at some stations reflected the basic structural features of the density profile. As a rule in this case, the values for the velocity shear modulus increased as the vertical scale of nonuniformities decreased.

2. The extremes of the curve $N(z)$ are well correlated with the extremes of the velocity shear modulus averaged at a vertical increment of 5-10 meters. This stratification feature was usually observed in the thermocline, in portions of the profiles having a significant density gradient and at the boundaries of layers exhibiting quasistationary temperature inversions. In the region of the Kuril' current the changes in velocity direction in inversions from 5 to 50 meters thick occurred at the boundaries of the layer with an increment of 10-30°.

3. Sawtooth changes in the profile of current velocity and direction with respect to depth appear on a background of a smooth temperature profile. Given a value of 10-30 meters for vertical isotherm fluctuations within the field of internal waves, the amplitude of velocity changes in layers 50-100 meters thick is about 10 cm/sec, while direction changes total up to 30-60°.

4. Sharp growth in the amplitude of fluctuations in current velocity and direction at different horizons in the shelf and coastal zones, indicating an influence by bottom relief and water exchange through straits. In this case the correlation between current density and velocity gradients was low, and conditions favoring propagation of thermohaline intrusions transverse to isopycnic surfaces evolved.

5. Abnormally large changes in current direction in layers on the order of tens of meters thick, going as far as its three-fold 360° rotation, without noticeable deformations in density structure.

The last case was observed several times in soundings made at 24-hour stations, and it can apparently be explained by unique features in the interaction between the average current and fluctuations in the inertial and tidal periods. Cyclic fluctuations in the dispersion of the velocity shear modulus that correlated with tidal phases were revealed at some stations in the Kuril' current. The contribution of fluctuations created by vertical shifts in current velocity and direction in response to waves occurring in the tidal period and waves of higher frequencies represented itself as velocity changes of 10-12 cm/sec. An analysis of the distribution of Richardson number values and the coefficient of vertical turbulent exchange showed that these fluctuations episodically intensify the critical velocity shifts in the average current, creating the conditions for development of hydrodynamic instability and for local mixing. Similar assessments were made for the subsurface layer on the basis of observations made during passage of a storm. In conclusion, the results are used as a basis for examining the causes and mechanisms of formation of inversion layers in the studied region.

An Acoustic Measuring Complex for Research on the Microstructure of Hydrophysical Fields in the Ocean

Ye. P. Varlatyy, V. P. Tikhomirov

An acoustic measuring complex (AIK) was developed by the Pacific Ocean Oceanological Institute of the USSR Academy of Sciences Far Eastern Scientific Center for research on the finestructure of hydrophysical fields. The AIK is capable of parallel measurements of current velocity and direction, speed of sound and the sound velocity gradient.

The apparatus consists of a sounding and an onboard system. Figure 1*a* shows a block diagram of the AIK. The sounding system contains an acoustic current velocity measuring device based on a single-channel frequency-impulse circuit. The measuring unit includes acoustic base *1*, measuring device *2*, square pulse delay oscillator *3*, band filter *4*, amplifier *5*, and converter *6*. The measurement process involves the following. Assume that at some moment in time the measuring unit emits a pulse in the direction of current flow. The next pulse would be emitted after time $t_1 = l/c + v$. Propagating against the current, this pulse reaches the converter of the acoustic base after time $t_2 = l/c - v$. Next, the entire process is repeated with a period of $T = t_1 + t_2$, the length of which, at a known base length l, is determined by the speed of sound c in a motionless medium:

$$f = f_0 = \frac{c}{2l}. \qquad (1)$$

Two identical trains of pulses with period T, shifted relative to one another by a time interval Δt, are fed to delay oscillator *3* from measuring unit *2* (Figure 1*b*):

$$\Delta t = \frac{T}{2} + \Delta T, \qquad (2)$$

where $\Delta T = \left|\frac{lV}{c^2}\right|$ --difference in time of propagation of the acoustic signal in the presence of a current and in a motionless medium; V--projection of the current velocity vector in the direction of the acoustic beam. A train of pulses (Figure 1*b*--*D*) passes from the square pulse oscillator to band filter *4* and amplifier *5*. A sinusoidal electric signal is picked off from the amplifier output; the frequency of this signal depends on the speed of sound in a motionless medium while its amplitude is determined by the current velocity. The signal at the amplifier output has the form:

$$u(t) = K \cdot V \cdot \cos\left(2\pi \frac{c}{2l} t\right), \quad (3)$$

where $K = \frac{2U_0 K_1}{c} \cdot \sin\left(\pi \frac{c}{2l} \tau\right)$ --a coefficient defining the instrument's sensitivity in relation to current velocity; U_0--square pulse amplitude; k_1--filter and amplifier transmission factor; τ--pulse length; c--speed of sound; l--measurement base length.

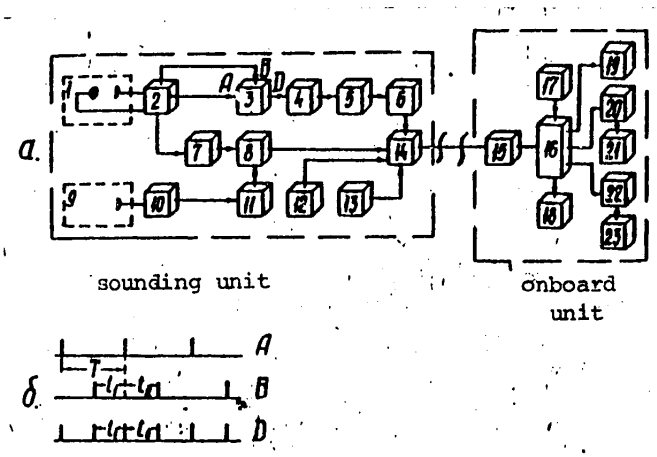

Figure 1. Block Diagram of the Acoustic Measuring Complex (a) and the Signal Time Diagram (b): *1,9*--acoustic base; *2*--measuring unit; *3*--delay oscillator; *4*--band filter; *5*--amplifier; *6,8,16*--converter; *7,11*--multiplier; *10*--speed of sound measuring block; *12*--direction sensor; *13*--pressure sensor; *14*--mixer; *15*--matching unit; *17-19*--two-coordinate recorder; *20*--digital recording system; *21*--period meter; *21,23*--perforator

The size of k depends on the speed of sound, which is undesirable because change in it may distort instrument readings during measurements of current velocity. In this case the relative error would be:

$$\left(\frac{\Delta V}{V}\right)_c = \frac{\Delta c}{c_0}\left(1 - \pi \tau f_0 \operatorname{ctg} \pi \tau f_0\right), \quad (4)$$

where $(\Delta v/v)_c$--relative current velocity measurement error due to change in speed of sound; c_0--average speed of sound; Δc--deviation of the real speed of sound in the ocean from its average; f_0--pulse repetition rate in the measuring unit's synchro-ring at the average speed of sound c_0; τ--length of square pulses at the output of oscillator *3*.

It follows from equation (4) that depending on τ, this error may take values from zero to a maximum value equal to relative change in the speed of sound in the ocean.

To reduce this error, it would be advantageous to use pulses of low duration, while to increase measurement sensitivity, the reverse would be required. The optimum τ can be found from the condition of ensuring a given measurement accuracy. Let us assume that the maximum permissible error is δ. Then, expanding the cotangent into a series and retaining the first two terms, we get the following from equation (4):

$$\tau = \frac{T_0}{\pi}\sqrt{3\delta\frac{c}{\Delta c}}, \qquad (5)$$

where $T_0 = 1/f_0$ is the pulse repetition period.

Substituting typical values for the ocean in equation (5)--$c_0 = 1{,}500$ m/sec and $\Delta c = \pm 50$ m/sec, we find that the relative error, equal to 0.5 percent, may be ensured by using pulses with a duration $\tau = T_0/5$. Another way is also possible for reducing the influence of the speed of sound, one not imposing limitations on pulse duration: The instrument readings are automatically corrected by adding a feedback to the current velocity channel's amplification tract. In this case the control signal is picked off from the output of the speed of sound channel.

According to the results of tests with the hydrochannel, the intensity of signals at the output of the current velocity measuring unit depends on current velocity within a broad range of change in the latter. This sensor measures current velocity on the basis of the speed of sound; therefore the magnitude of the latter is measured simultaneously with current velocity using the same acoustic base.

Two acoustic bases separated by a certain vertical distance and two identical measuring circuits feeding signals to multipliers 7, 11 (Figure 1*a*) with a multiplication factor of 100 are used to measure the speed of sound gradient. Multiplied signals are subsequently fed to a subtraction unit.

The size of the speed of sound gradient is determined by the equation:

$$G = \frac{1}{L}\left(\frac{2l_1}{N}\Delta f - \frac{\Delta l}{l_1}c_0 - \frac{\Delta l}{l_1}\Delta c\right), \qquad (6)$$

where G--speed of sound gradient; l--vertical distance between sensors; N--frequency multiplication factor; $\Delta l = l_2 - l_1$; $l_1 - l_2$--distance between converter and reflector in the acoustic base; Δf--signal frequency; c_0--average speed of sound in sea water; $\Delta c = c_1 - c_0$--deviation of the real speed from its average.

The first factor in the parentheses reflects the relationship between the frequency of the electric signal and the speed gradient. The other terms are additional correction factors depending on Δl. One of the correction factors is constant and has practically no influence on metrological characteristics while the other defines the dependence between the gradient measurement and the relative change in speed of sound in the medium under consideration and is completely a part of the total error. To decrease it, it would be sufficient to reduce the difference in lengths of the acoustic bases.

The sounding unit also contains a sensor that determines the instrument's azimuth orientation relative to the earth's magnetic meridian, and a standard DDV-200 pressure gage.

The sounding part of the AIK is connected via a current collector to the onboard unit by means of a winch cable. Signals received aboard are filtered and fed to the appropriate recorders. Two-coordinate recorders and a digital recording system are employed.

The measuring part of the probe is contained within a deepsea cylindrical container made from nonmagnetic material. It is equipped with control vanes used to orient the probe in line with the current, and it is supplied with a linking unit that keeps the acoustic bases horizontal irrespective of the tilt imparted to the housing by the oncoming current. The measuring complex possesses the following characteristics: current velocity measurement range--up to 2 meters/sec; directions--0-360°; speed of sound--1,430-1,540 meters/sec; range of measurement of speed of sound gradient--from +2 sec^{-1} to -30 sec^{-1}; vertical resolution--0.1-1 meters; measurement accuracy for current velocity--0.5 cm/sec, for speed of sound--0.3 meters/sec, for direction--3°, for the speed of sound gradient--0.01 sec^{-1}; maximum sensitivity in relation to speed of sound--1 cm/sec; maximum depth--2,000 meters.

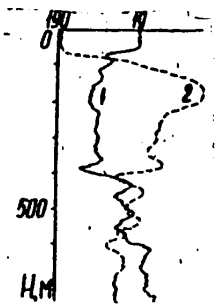

Figure 2. Recordings of Current Velocity and Direction Profiles Obtained in the Pacific Ocean: *1*--current velocity; *2*--direction

The AIK was used in a number of expeditions aboard the scientific research vessels "Dmitriy Mendeleyev" and "Professor Bogorov." The measurements were made by taking soundings from a drifting vessel. This instrument was used in a cycle of research projects having the objective of studying the finestructure of the dynamic characteristics of the water environment, and its relationship to microstratification of temperature, salinity and speed of sound. In particular, the obtained data indicated that the finestructure of current was often the product of high-mode internal waves.

Possibilities for Studying Finestructure and Turbulent Pulsations of the Ocean's Density Field With a Laser Photoelectric Interferometer

V. D. Vlasov

The Institute of Oceanology imeni P. P. Shirshov has developed a unique instrument--a submersible laser photoelectric interferometer that can simultaneously measure and record, with high spatial resolution and accuracy, the average and pulsational densities of the ocean (1).

This interferometer is based on an interference-resistant method, protected by several author's certificates (2,3), of dynamic measurement of the optical difference in the path traveled by light beams through the medium under analysis. The method is based on phasal photoelectric registration of the relative displacement of two systems of sawtooth-scanning interference bands, and on an instrument optical system designed in such a way that destabilizing factors elicit their identical drift and fluctuation, and their relative displacement α is associated only with change in the optical difference in the path Δz resulting from change in the medium's refraction index Δn:

where

$$\Delta z = \tfrac{1}{2} \lambda \alpha \qquad (I)$$

$$\Delta z = \Delta n \cdot l \qquad (I')$$

l--length of measurement base (Figure 1a);
λ--length of a light wave produced by a helium-neon laser, equal to 6,328 Å. In turn, change in density of sea water, $\Delta\rho$, is associated by a linear relationship with change in the refraction index (1):

$$\Delta\rho = 2{,}68\, \Delta n \qquad (2)$$

Although the present measurement accuracy for relative displacement of the two systems of interference bands is five one-thousandths of a band (4,5) and although the interferometer itself is practically noninertial, because of imperfections in the digital and analog recorders (Figure 1) the instrument accuracy is, respectively, ±0.05 and ±0.025 of a band (which at $l = 0.5$ cm is equal, for Δn and $\Delta\rho$, to $\pm 3.1 \cdot 10^{-6}$, $\pm 1.55 \cdot 10^{-6}$ and $\pm 8.3 \cdot 10^{-6}$ gm/cm^3, $\pm 4.15 \cdot 10^{-6}$ gm/cm^3 respectively), while its drift is about 0.01 sec.

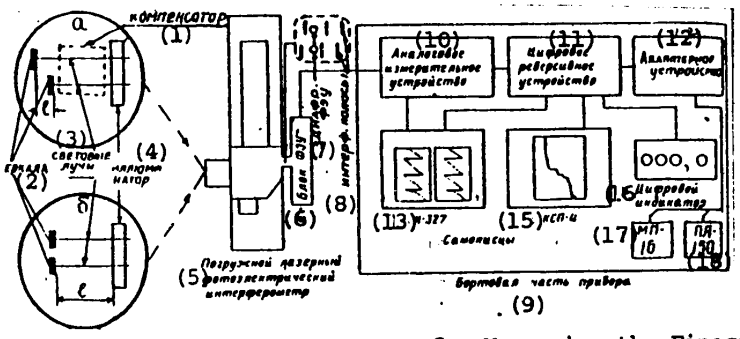

Figure 1. Block Diagram of Apparatus for Measuring the Finestructure of the Ocean's Density Field by the Optical Interference Method

Key:

1. Compensator
2. Mirrors
3. Light beams
4. Porthole
5. Submersible laser photelectric interferometer
6. Photomultiplier block
7. Photomultiplier aperture
8. Interference bands
9. Onboard part of the instrument
10. Analog measuring unit
11. Digital reversing unit
12. Adapter unit
13. N-327
14. Recorders
15. KSP-Ts
16. Digital display
17. MP-16
18. PL-150

Figure 2 (*1*) shows a portion of the vertical density profile $\Delta\rho(z)$ obtained by the described instrument in the Philippine Sea during the 19th cruise of the scientific research vessel "Dmitriy Mendeleyev" (1). It is clear from the results of spectral statistical treatment of a series of six similar profiles (extending to a depth of 120 meters with a sampling interval of 0.48 meters) that their variability at scales greater than 8 meters is associated with internal waves, while variability at scales less than 8 meters is apparently the result of the mixing action of microturbulence (1). The inset in Figure 2 (*1*) shows an intrastratification 1 meter thick, recorded with an N-327 high-speed recorder in profile (*1*), in which finestructural inversions of the density field with vertical scales of 10-5 cm and less are observed.

To reveal their nature and origin, similar profiles were recorded during the 22d cruise of the "Dmitriy Mendeleyev" using, besides the standard technique (Figure 1 (*a*) and Figure 2 (*2*)), a method requiring installation of a glass compensator in the path of both beams (Figure 1 (*a*) and Figure 2 (*3*)) and a zero measurement base (Figure 1 (*b*) and Figure 2 (*4*)).

The beam path was 7 cm, the distance between beams was 1.2 cm, and the length of the measurement base was $l = 0.58$ cm. Given such relationships, our analysis showed,

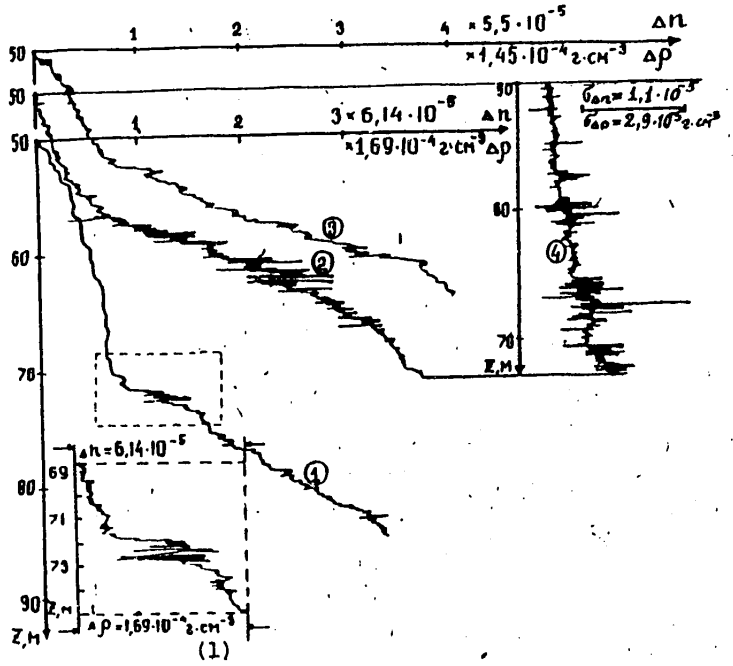

Figure 2. Vertical Profiles of Changes in Sea Water's Refraction Index (*1*) at Station 1611 (28 September 1977, 10°40' N., 126°45' E.), (*2*) at Station 1807 (7 February 1979, 0°8.5' S., 139°48.5' E.), (*3*) at the Same Station With a Compensator, (*4*) at the Same Station With a Zero Measurement Base

Key:
1. gm·cm

disappearance of small-scale pulsations in the presence of the compensator and their appearance without the compensator is possible, even with a zero measurement base, only if fluctuations of the refraction index are random and uncorrelated at a spatial scale of about 1 cm (6). This is an indication that these fluctuations arise in response to active small-scale turbulence in the stratified medium. In this case, similarly as in (6), the dispersions (mean squares) of fluctuations in Δz and Δn are associated with each other by the following formula:

$$\sigma^2_{\Delta z} = L_1 \cdot \mathcal{V} \sigma^2_{\Delta n} \qquad (3)$$

where $L = \frac{1}{\sigma^2_{\Delta n}} \int_0^\infty R(\xi) d\xi$ --unidimensional integral scale of fluctuations, equal in our case to 1.2 cm; $R(\xi)$--spatial autocorrelation function (given statistical

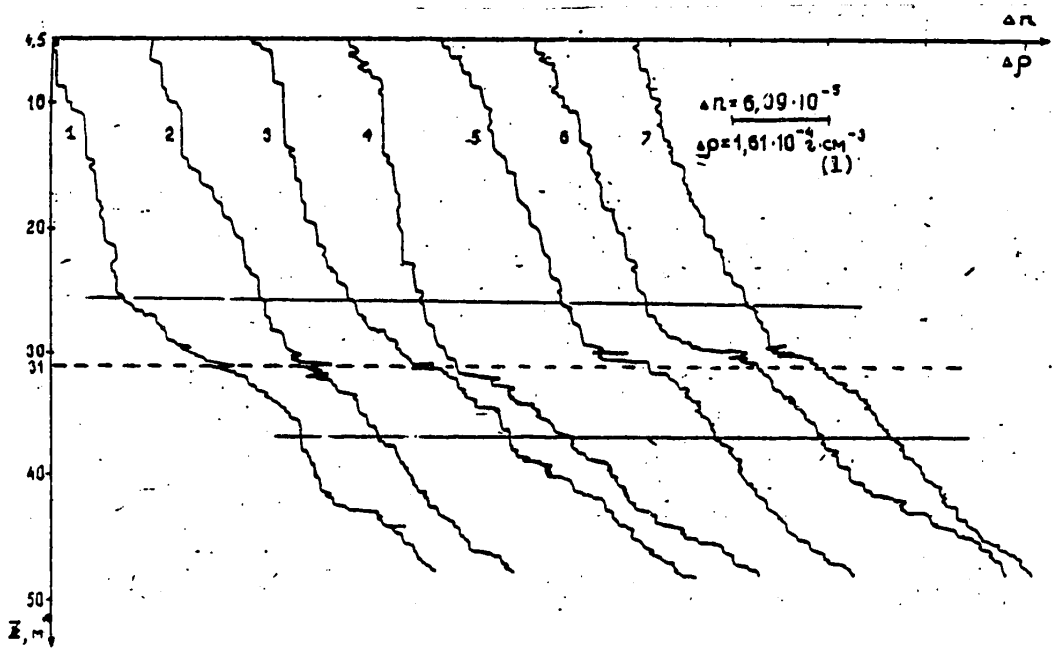

Figure 3. Evolution of Portions of the Vertical Profile for the Index of Refraction and Density of Sea Water in Response to Fine-Scale Turbulence (*1-5*) and Internal Waves (*6-7*) at Station 1843 (31 March 1979, 9°43.5' N., 127°12' E.): Time between soundings--25 minutes.

Key:
1. gm·cm

isotropicity of fluctuations). As we can see from a comparison of formulas (1') and (3), as well as from the scales of Figure 2 (*3*) and 2 (4), the instrument's sensitivity to small-scale random pulsations (at $L \ll l'$) is five times greater than it is in regard to measurements of the average for the $\Delta\rho(z)$ profile. This is a direct consequence of the fact that the mean square of fluctuations is proportional not to l but to l'--that is, to the number of uncorrelated nonuniformities in the path of the light beam (6).

Using this instrument during the 22d cruise of the scientific research vessel "Dmitriy Mendeleyev" in the Timor Sea, we were able to reveal formation of a jump in density that grew with time (Figure 3 (*3,4,5*)) in a portion of the profile where it experienced a discontinuity in response to small-scale turbulence (Figure 3 (*1,2*)), which had been predicted theoretically by Long as one of the mechanisms of formation of the ocean's finestructure (7); we also observed erosion of this jump (Figure 3 (*6,7*)) in response to the action of internal waves (7), which is readily apparent from Figure 3.

BIBLIOGRAPHY

1. Belyayev, V. S., Vlasov, V. L., and Ozmidov, R. V., "Investigation of the Fine Vertical Structure of Water Density in the Ocean by the Optical Interference Method," IZV. AN SSSR, FAO, Vol 15, No 8, 1979, pp 855-863.

2. Vlasov, V. L., "A Method for Measuring Fractional Shifts in Two Systems of Interference Bands in Interferometers, and the Device for this Method's Application," Author's Certificate No 124676, BYULL. IZOBR., No 23, 1959.

3. Vlasov, V. L., and Medvedev, A. N., "A Device for Measuring Fractional Shifts in Two Systems of Interference Bands," Author's Certificate No 509767, BYULL. IZOBR., No 13, 1971.

4. Vlasov, V. L., and Medvedev, A. N., "Precision Measurement of a Fractional Relative Shift in Two Systems of Interference Bands," PRIBORY I TEKHNIKA EKSPERIMENTA, No 4, 1972, pp 198-206.

5. Vlasov, V. L., and Medvedev, A. N., "A Photoelectric Method of Precision Measurement of Small Relative Shifts in Two Systems of Interference Bands," IZM. TEKHNIKA, No 8, 1975, pp 47-49.

6. Tatarskiy, V. I., "Rasprostraneniye voln v turbulentnoy atmosfere" [Propagation of Waves in a Turbulent Atmosphere], "Nauka", 1967, pp 233-237.

7. "Okeanologiya. Fizika okeana" [Oceanology. Ocean Physics], Vol 1, "Nauka", 1978, p 257.

The Diversity of Physical Cycles in the Upper Layer of the Ocean

A. I. Ginzburg, K. N. Fedorov

In oceanology, it has become a universally accepted practice to refer to the ocean's upper layer as "quasi-uniform" and to describe it with unidimensional models. Research conducted in recent years, motivated mainly by fast development of remote ocean sounding resources, revealed higher variability in hydrophysical characteristics in a layer near the surface a few meters thick. It was established that the greatest variability in horizontal and vertical thermostructure is observed during the time of intense solar heating in still weather and in the presence of light winds, and that it is basically associated with volume absorption of the sun's radiant energy, with convection, with modulation of the surface layer by internal waves and with unique features in salt stratification near the surface in response to precipitation and evaporation. Variability of salinity is mainly the product of freshening of the surface layer by rainwater. In this case differences in salinity of about 1 $^0/_{00}$ at distances on the order of a kilometer may be observed in the upper meter of ocean water in the absence of intense mixing (1).

Variability in thermal structure of the surface layer exhibits a clearly pronounced daily trend associated with the daily trend of solar heating and with the thickness of the layer in which convective mixing occurs. Maximum heating of the surface layer is observed at about 1500 hours local sun time. The thickness of the convective layer is, in the absence of salt stratification, within 10 cm in the hours around mid-day, it attains 1 meter by 1600 hours (3), and then it quickly grows, exceeding 10 meters at night, according to our observations. Given intense solar heating, low thickness of the convective layer means that the greatest increase in heat content occurs in a surface layer 0.5-1 meter thick. In this case the difference between its temperature and that at a depth of 7-10 meters may attain 3°C (5). As the thickness of the layer affected by convection grows, the profile of $T(z)$ gradually smoothes out, and at night we observe practically complete homothermy in a layer about 10 meters thick.

Arisal of persistent salt stratification near the surface as a result of rains additionally complicates the picture. During the day, a sudden change in salinity at the lower border of a freshened area, which prevents heat exchange and convective mixing with lower layers, leads to extreme heating of the surface layer. As an example in summer 1978, in the region of the POLYMODE experiment, in still weather the water temperature near the surface in freshened areas attained 29-32°C, while in neighboring points where rain had not fallen, it did not exceed 27.5-28.5°C (1). In this case a

a more-abrupt vertical salinity gradient corresponds to more-intensive heating, as is readily apparent from Figure 1, which shows three profiles of deviations in temperature $\Delta T(z)$ and salinity $\Delta S(z)$ from the corresponding values of T and S at the 10-meter horizon, recorded in summer 1978 in the Sargasso Sea with an AIST. At night, meanwhile, freshened areas cool more intensively owing to the small thickness of the freshened layer subjected to convection (1). Thus torrential rains cause arisal of horizontal kilometer-scale nonuniformities in the surface layer.

The most universal mechanism of formation of horizontal kilometer-scale nonuniformities is modulation of the thickness of the heated surface layer of the ocean by internal waves of the seasonal thermocline, appearing in still weather and in the presence of light winds during intensive solar heating (4). The amplitudes of such nonuniformities may attain 1-2°C. In this case very sharp horizontal temperature gradients (up to 2°C and more per km) are observed at the margins of warm and cold areas. An example of typical recordings of "still weather temperature nonuniformities," obtained with a temperature gage towed at a horizon $z = 0.15$ meters in summer 1978 in the Sargasso Sea, is shown in Figure 2*a*.

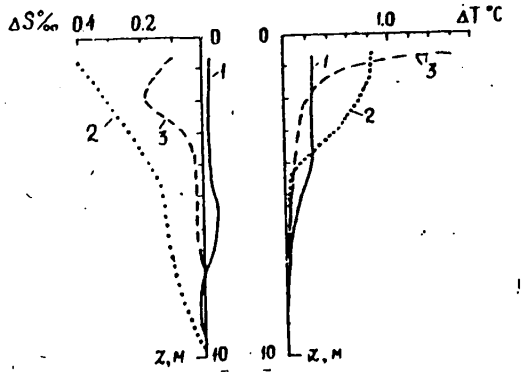

Figure 1

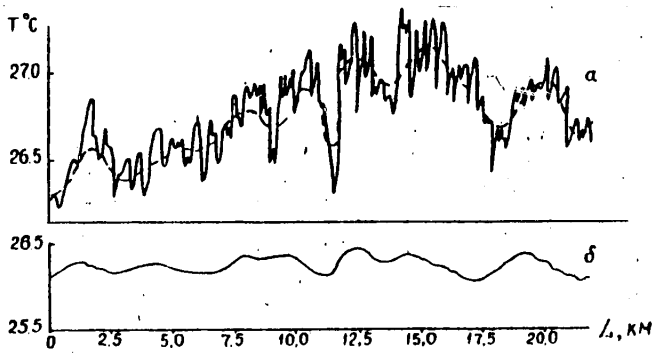

Figure 2

Such nonuniformities arise at about 1000-1100 hours local sun time, they reach their maximum amplitude at 1400-1500 hours--that is, by the moment of maximum heating of the surface layer, and for practical purposes they disappear by 2100 hours. When intense heating occurs, kilometer-scale nonuniformities (Figure 2*a*, broken curve) are recorded at 3-4 meter horizon as well (Figure 2*b*), while uniformities with a scale on the order of 100 meters and an amplitude of several tens of degrees are observed only near the surface (Figure 2*a*), disappearing after about 15 hours.

An appraisal of the typical horizontal scale L of areas containing a temperature nonuniformity, made in (4) in accordance with the results (2) of analyzing modulation of motion fields and passive perturbation in the surface layer by a random internal wave field, produced the value $L \approx 1{,}200$ meters for the region of observations, which agrees well with the measurement results (Figure 2*a*,*b*).

In addition to cycles associated with surface freshening and with modulation of the heated layer by internal waves--cycles typical of windless or light-wind weather, we see the widespread occurrence of "Langmuir circulations (or cells)," establishing themselves at winds from 3 to 10 meters/sec. Langmuir circulations are the result of interaction of drifting currents and wave action, and they manifest themselves on the ocean surface in the form of numerous parallel bands of convergence, stretched out along the wind direction or at a slight angle to it. The distance between convergence bands is approximately equal to the thickness of the upper quasi-uniform layer, and it may vary from 5-10 to 100 meters. Areas of divergence are situated between the convergence bands, above ascending branches of vertical circulations. In transverse vertical section, Langmuir circulations appear as closed cells penetrating downward usually (but not always) to the lower boundary of the mixed layer. In light winds and intensive solar heating, the water temperature in the convergenc bands is higher than in the intermediate bands. Heat carried downward by descending currents creates a banded thermal structure within a layer several meters thick. Inasmuch as wave and wind mixing operates in this case as well, the amplitudes of horizontal temperature changes in these banded structures are not so high as in still-weather nonuniformities, and they apparently do not exceed 0.2-0.4°C. Langmuir circulations are an extremely effective mechanism of heat transfer into deep water, and given intensive development, they may predetermine the position of the daily thermocline, which under various conditions may locate itself at horizons from 3-5 to 30-40 meters by the end of the light part of the day. Modulation by internal waves may elicit local deviations in the position of the daily thermocline within ±5 meters of the mean. Intense freshening by precipitation may cause formation of a very shallow (3-5 meter) daily thermocline.

Internal waves and currents modulate not only the thermal pattern but also the characteristics of surface wave action. Such effects occur with practically all wind velocities. The modulation patterns of the surface in the presence of intense winds are revealed best of all by observations from airplanes and from outer space. However, sharp disturbances in the state of the ocean surface, connected with fronts and large internal waves ((solitony) for example), usually are readily visible from a ship.

BIBLIOGRAPHY

1. Ginzburg, A. I., Zatsepin, A. G., Sklyarov, V. Ye., and Fedorov, K. N., "Effects of Precipitation in the Surface Layer of the Ocean," OKEANOLOGIYA, Vol 20, No 5, 1980, pp 828-836.

2. Monin, A. S., and Piterbarg, L. I., "Statistical Description of Internal Waves," DAN SSSR, Vol 234, No 3, 1977, pp 564-567.

3. Solov'yev, A. V., "Fine Thermal Structure of the Ocean's Surface Layer in the Vicinity of the 'POLYMODE-77' Traverse," IZV. AN SSSR, FIZIKA ATMOSFERY I OKEANA, Vol 15, No 7, pp 750-757, 1979.

4. Fedorov, K. N., Ginzburg, A. I., and Piterbarg, L. I., "The Physical Nature of 'Still Weather Nonuniformities' in the Ocean's Temperature Field," OKEANOLOGIYA, 1980 (in press).

5. Bruce, J. G., and Firing, E., "Temperature Measurements in the Upper 10 m With Modified Expendable Bathythermograph Probes," J. GEOPHYS., RES., Vol 79, No 2, pp 4110-4111, 1974.

Internal Waves and Turbulence in Synoptic Eddies According to Data on Vertical Finestructure

V. Z. Dykman, O. I. Yefremov, O. A. Kioyeleva, N. A. Pantaleyev

The study of internal waves has a direct relationship both to the main source of variability and, in all probability, to the main contributor to mixing processes in deep ocean layers in the absence of shearing currents. The influence of synoptic-scale eddy formations on small-scale motion and on internal waves was studied within the framework of an integrated experiment performed in the "Polymode" program with the purpose of investigating these formations. Information on vertical finestructure and microstructure of the temperature field was used with this goal in mind. Obviously there are grounds for doing so in the open ocean, outside water mixing zones of various origins. The research was performed in the Sargasso Sea at a depth of 1,000 meters. It may be hypothesized that under these conditions, the finestructure is "reversible"--that is, it is a consequence of deformation of the density field by internal waves; on the other hand its "irreversible structure"--a product of different mixing processes--makes a relatively small contribution (3,4). Thus information on finestructure and microstructure was used to appraise the dependence of the energy characteristics of small-scale turbulence and internal waves on local hydrological conditions within a zone of eddy formations and in so-called background conditions (the average hydrological conditions of the "Polymode" traverse).

Average hydrological characteristics were obtained from information contained in density maps of microtraverses sounded at a spacing of 15 nautical miles with ISTOK-4 and ISTOK-5 hydrological probes. In order to reveal the influence of eddy formations on small-scale processes, we analyzed data for a layer extending from 280 to 405 meters, exhibiting the greatest deformation of the density field in cyclonic eddies, and a layer extending from 550 to 800 meters, in which this deformation was minimal. For the purposes of comparison, data obtained in background conditions within these same layers were analyzed.

The small-scale structure of the temperature field was investigated with the help of cable-drawn probes which, in terms of their spatial resolution (3 cm) and sensitivity ($\sim 10^{-3}$°C), permitted analysis of the finestructure range (100-1 meters) and a portion of the microstructure range (100-7 cm) (1).

Using the formula $P_\xi = P_T / \left(\frac{\partial T}{\partial z}\right)^2$, we computed the spectrums of internal wave prominences in quasi-uniform portions of temperature profiles (exhibiting constancy of

temperature gradients dT/dz). It may be noted that the P_ξ spectrums are approximated well by the power of the dependence $P_\xi(k) \sim k^n$, where $n = -3$, within a wave number range of 0.1-1.0 cycles/meter. The shortwave portion of the spectrum, 1.0-14 cycles/meter, is approximated by an exponential dependence with power $n = 1.0$-1.8.

The variance of internal wave prominences, computed from the $P_\xi(k)$ spectrums in a fixed spectral range, 0.1-1.0 cycles/meter, is distinguished by significant variability in relation to both depth in background conditions (approximately 50-fold variability) and the area occupied by the eddy formation. In general, we can note that within a zone of eddy formations of the cyclonic and anticyclonic type, the potential energy density $E = \sigma_\xi^2 \cdot \overline{N}^2$ of the internal wave field exceeds background values by a factor of 5-10. E does not exhibit any sort of law in its distribution over the area occupied by the eddy. Normalization of the prominence spectrums, performed on the basis of VKB [not further identified] considerations with the approximation $\overset{\circ}{P}_\xi = \overline{N}/N_0 \cdot P_\xi(\gamma)$, where $\gamma = K/\overline{N}$ and $N_0 = 1$ cycle/hour, permits us to appraise the potential energy density of internal waves "of identical origin." The essence of such normalization entails acquisition of internal wave characteristics with a consideration for changes in vertical scale during propagation in a nonuniformly stratified medium. In keeping with this notion, the normalized prominence variance was computed on the basis of normalized spectrums, $\overset{\circ}{P}_\xi$. It can be noted that following normalization, the prominence spectrums corresponding to background conditions and the conditions in layers between 280 and 800 meters agreed well with each other, which is an indication in favor of the wave nature of finestructure. The normalized variance of prominences, $\overset{\circ}{\sigma}_\xi^2$, is about 0.17 m^2 in the 280-405 and 550-800 meter layers; this is sufficiently close to the value obtained with the GM-75 model in the same spectral range, 0.1-1.0 cycle/meter--approximately 0.1 m^2. The distribution of $\overset{\circ}{\sigma}_\xi^2$, which is proportional to the potential energy density of internal waves, is illustrated in Figure 1 for a cyclonic eddy formation. In the center of the eddy, $\overset{\circ}{\sigma}_\xi^2 = 0.9$-$0.12$ m^2, while on its periphery it is approximately 1.0 m^2. This internal wave energy distribution is also typical of an anticyclonic eddy. Thus we can conclude that the energy of the wave field at the periphery of an eddy is about 10 times greater than the energy level in the center and in background conditions. Theoretical analysis of internal wave propagation in a nonuniform eddy velocity field can explain the observed increase in energy.

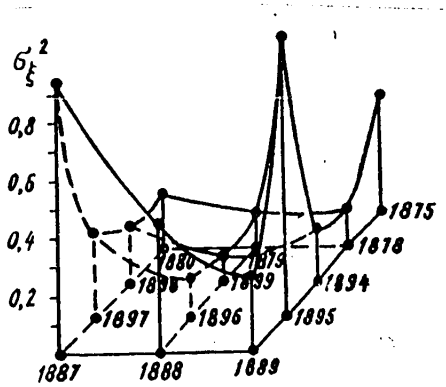

Figure 1

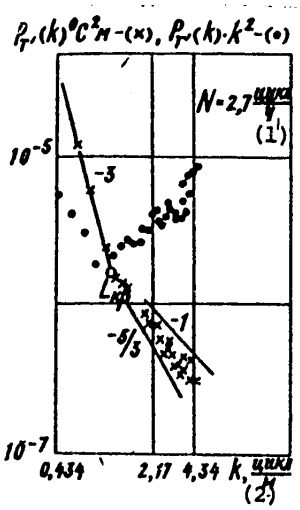

Figure 2

Key:
1. Cycles/hr
2. Cycles/meter

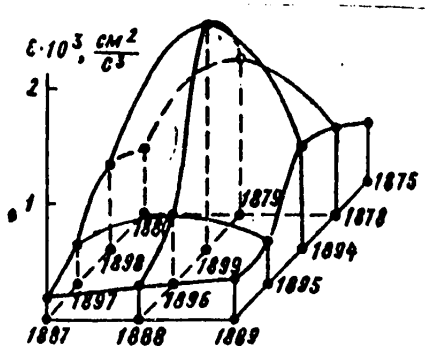

Figure 3

Analysis of the depth distribution of $\overline{\sigma^2_\xi}$ in a broad range of Vyaysyal'-Brent frequencies--1.5-15 cycles/hr--revealed significant variability: The variance of the prominences decreases abruptly in layers with large density gradients typical of a thermocline. Such a significant decrease in internal wave energy cannot be explained by the GM-75 universal-spectrum model. One of the possibility explanations may be arisal of instability in internal waves, having limitation of wave amplitude and generation of small-scale turbulence as a consequence. Thus we need to examine the joint distributions of their energy characteristics.

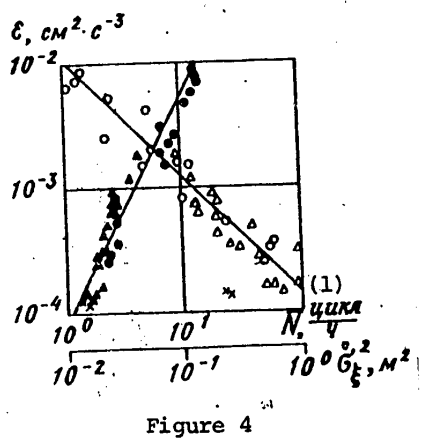

Figure 4

Key:
1. Cycles/hr

Information on finestructure and microstructure was used to reveal the dependence of the energy supply of small-scale turbulence on local hydrological conditions in the absence of significant vertical shifts in the current velocity field. Microstructure is the smallest-scale variability in the ocean, having a scale on the order of 1 mm - 1 meter. Turbulence participates in its formation; at this level, the molecular processes associated with viscosity and diffusion begin to have an effect.

The position of the boundary of the spectral range corresponding to microstructure depends on the stratification conditions (particularly on the Vyaysyal'-Brent frequency N) and on the rate of energy supply to small-scale turbulence. To determine the maximum vertical scale L_{kp}, corresponding to the boundary between finestructure and microstructure, we used "temperature dissipation" spectrums--$P_T(k)k^2$, where k is the vertical wave number (Figure 2).

Defining L_{kp} to be the external (energy-supplying) scale of turbulence, using an equation suggested in (2), $\varepsilon = CL_{kp}^2 N^3$, we determined the rate of influx of kinetic energy. The ε values were averaged on the same vertical scale used in determination of $\overline{N}$ and σ_ξ^2. Figure 3 illustrates the distribution of ε values in relation to the surface of an eddy formation within a 280-405 meter layer. Comparing the distributions of σ_ξ^2 and ε, we can note that the maximum potential energy on the periphery of the eddy corresponds to a minimum rate of influx of kinetic energy into turbulence. The reverse pattern is observed in the center of the eddy. This mutual relationship between the energy characteristics of internal waves and turbulence is typical of background conditions. In general, we can conclude on the basis of a larger quantity of data (Figure 4) that as the density gradient increases, the potential energy of the wave field decreases and the influx of kinetic energy into small-scale turbulence rises. This permits the assumption that as density gradients increase, the probability of arisal of local hydrodynamic instability in internal waves rises, owing to which the energy of internal waves is consumed in excitation of turbulence.

BIBLIOGRAPHY

1. Dykman, V. Z., Yefremov, O. I., and Panteleyev, N. A., "A Sounding Complex for Research on Vertical Finestructure of the Ocean," in "Eksperimental'nyye metody issledovaniya okeana" [Experimental Methods of Ocean Research], Sevastopol', Izd-vo MGI, 1978, pp 125-136.

2. Ozmidov, R. V., "Gorizontal'naya turbulentnost' i turbulentnyy obmen v okeane" [Horizontal Turbulence and Turbulent Exchange in the Ocean], Moscow, "Nauka", 1968, p 105.

3. Fedorov, K. N., "Tonkaya struktura vod okeana" [Finestructure of Ocean Waters], Gidrometizdat, Leningrad, 1976.

4. Gregg, M. C., and Briscoe, M. G., "Internal Waves, Finestructure, Microstructure and Mixing in the Ocean," REV. OF GEOPH. AND SPACE PHYS., Vol 17, No 7, 1979, pp 1524-1548.

Transformation of the Energy Density of Internal Waves in a Synoptic Eddy

V. Z. Dykman, A. A. Slepyshev

One of the principal objectives of the Soviet-American "Polymode" program was that of studying the local kinematics and dynamics of synoptic eddies. It would obviously be insufficient to study the large-scale structure and kinematics of an eddy if we intend to build an adequate physical model of an eddy. We would also need to analyze the energy interactions of the eddy with movements occurring at different scales, the mechanisms of energy transfer throughout the entire spectrum, and dissipation of this energy.

Research showed (2) that a moving synoptic eddy expends its principal energy on generation of the "wave background"--Rossby waves: about $2 \cdot 10^{-3}$ w/m^2. A reverse flow of energy, one of approximately the same order and promoting a quasistable energy state in the eddy, comes from average currents due to their instability. Estimates also show that dissipation of eddy energy due to mesoscale movements is approximately of the same order as energy expenditures on Rossby wave generation. But because the energy of large-scale processes balances itself out for practical purposes, the energy drain into small-scale phenomena (internal waves, turbulence) must have fundamental significance to clarifying the total local dynamic balance and to estimating the rate of dissipation of an eddy's kinetic energy.

Experimental research on the variability of the potential energy of internal waves within a zone of synoptic eddy formations, performed on the basis of estimates of the spectral density of vertical changes determined from measurements of vertical temperature finestructure with a falling probe (1), showed that wave energy on the periphery of an eddy exceeds, by 1 order of magnitude, the average "background" values (measured in an area known to be outside the eddy), and that it once again decreases toward the center of the eddy, approaching the "background" level. With depth, as the Vyaysyal'-Brent frequency N varies from 15 cycles/hr in the seasonal thermocline to 3 cycles/hr in the 800-1,000 meter layer; the energy of internal waves also changes within 1 order of magnitude, decreasing with growth of N.

On the other hand appraisal of the rate of influx of kinetic energy ε into small-scale turbulence (1) would show that ε is 5-6 times greater within an eddy than outside it. As the Vyaysyal'-Brent frequency N increases, the rate of energy influx into turbulence within the seasonal thermocline grows significantly.

The spectral density of the energy of wave trains is defined by an equation for conservation of the density of wave action (3), which in the stationary and axisymmetrical case transforms into:

$$\frac{\partial \nu}{\partial k_x}\cdot\frac{\partial}{\partial x}\left(\frac{\varepsilon}{\nu_1}\right)-\frac{\partial \nu}{\partial x}\cdot\frac{\partial}{\partial k_x}\left(\frac{\varepsilon}{\nu_1}\right)=0 \qquad (1)$$

where $\nu_1 = \nu - uk - vl = \nu - u_0 k_h \cdot \cos(\theta-\varphi)$, $k_h = \sqrt{k^2+l^2}$ --horizontal wave number, u and v--horizontal components of current velocity, $u_0 = \sqrt{u^2+v^2}$, and θ and ϕ--angular coordinates of the horizontal wave vector and the current velocity vector.

Frequency ν is the first integral of equation (1)--that is,

$$\varepsilon \sim \nu_1 \cdot \varepsilon_1(\nu) \qquad (2)$$

The spectrum of the finestructure of the ocean's temperature field is associated with the spectral energy density by the relationship (3):

$$P_T(m,z) = N^2 \int_0^{2\pi}\int_0^{k_{h\max}} \frac{\varepsilon \cdot k_h \cdot dk_h\, d\theta}{4\pi^2 \cdot \frac{m^2}{k_h \cdot N^2}} \qquad (3)$$

Using ε as stated in formula (2) and the empirically known slope of the spectrum of vertical finestructure, m^{-3}, we find that $\varepsilon_1(\nu) \sim \nu^2$.

Let us determine the potential energy density in a "floating" spectral window by integrating ε in relation to all horizontal wave numbers, and in relation to vertical wave numbers within the limits of variables γ_1, γ_2 depending on the Vyaysyal'-Brent frequency N:

$$F = \frac{1}{2}\int_{\gamma_1}^{\gamma_2}\int_0^{2\pi}\int_0^{k_{h\max}} \varepsilon\, k_h\, dk_h\, d\theta\, d\gamma = E_0 + B_0 u_0^2 \qquad (4)$$

where $\gamma = m/N$ is the vertical wave number normalized in accordance with the linear wave theory (6). The choice of values for γ_1 and γ_2--0.1 hr/meter and 1.0 hr/meter respectively--is made in accordance with the scale range of vertical finestructure under examination. E_0 is the energy density in the center of the eddy, where $u_0 \approx 0$. u_0 is the orbital velocity of the eddy, $B_0 = \frac{2\pi}{5}\left(\frac{k_{h\max}}{K_0}\right)^5 \cdot \ln\frac{\gamma_2}{\gamma_1}$, and $K_0 = 1$ cycle/meter. According to dependence (4), the energy density in the center of the eddy is close to its value outside the eddy, in the "background," where $u_0 \approx 0$.

We can attempt to associate the observed experimental variability in the rate of influx of kinetic energy from internal waves into turbulence within a synoptic eddy with the mechanism responsible for limiting wave amplitude due to local hydrodynamic instability. Presence of this instability is most probable within the layer of steep density gradients in the thermocline, where the greatest vertical shifts in velocity are usually concentrated.

Fillips (4) obtained, for a three-layer model of the ocean with a Vyaysyal'-Brent frequency $N(z)$ experiencing a sudden change in the thermocline, an equation describing limitation of the amplitude of a minimum-mode wave by the mechanism of local shear instability.

It would not be difficult to show, using a VKB approximation, that for a Vyaysyal'-Brent frequency N, changing slowly in the spatial scale of internal waves, the stability condition $R_i = N^2\left(\frac{\partial \bar{u}}{\partial z}\right)^{-2} > \frac{1}{4}$, where $d\bar{u}/dz$ is the local horizontal velocity gradient in the wave, limits the wave amplitude and, correspondingly, the potential energy density

$$N^2 a^2 = \frac{4N^4 \cdot \nu^2}{(N^2 - \nu^2)^2 k_h^2} \qquad (5)$$

If an average current with velocity shift u_{0z} exists in the ocean, the condition limiting the amplitude of internal waves would have the form:

$$N^2 a^2 = \frac{(4N^2 - u_{0z}^2)(k_h^2 + m^2)}{m^4} \qquad (6)$$

It is easy to see that as the Vyaysyal'-Brent frequency grows, the right side of equation (5) decreases.

Reaching the upper limit of energy density (5) with growth of N, the wave train should lose energy--that is, if the vertical component of group velocity is oriented in the direction of rising N, the energy density of internal waves would decrease due to the limitation mechanism indicated above. This decrease in energy may be associated with expenditure of wave energy on turbulence generation. If the vertical component of the group velocity of the wave train is oriented in the direction of decreasing N, the upper limit for energy density does not decrease, and the wave amplitude is not limited by the indicated limitation mechanism--that is, there is no drainage of energy from the waves.

Thus if we differentiate the right side of equation (6) along the trajectory of the wave train (see (5)) and take the average of the set of wave trains, we can obviously obtain the energy flux ε from the internal waves into turbulence:

$$\varepsilon = -\frac{1}{\pi \cdot K_{h\max}^2 \cdot (m_{\max} - m_{\min})} \cdot \int_{m_{\min}}^{m_{\max}} \int_0^{K_{h\max}} \int_0^{2\pi} \frac{d\omega}{dt}\left[\frac{(4N^2 - u_{0z}^2)(K_h^2 + m^2)}{m^4}\right] K_h \, dK_h \, dm \, d\theta$$

$$= \frac{8}{25} \cdot N_z \left(4N^2 - U_{0z}^2\right) K_{h\max}^3 \left(m_{\min}^{-5} - m_{\max}^{-5}\right) - \frac{4}{9} \frac{u_{0z} \cdot u_{0h} \cdot N^2}{m_{\max} - m_{\min}} K_{h\max} \left(m_{\min}^{-3} - m_{\max}^{-3}\right) \cdot$$

$$- \frac{4}{3} \frac{1}{m_{\max} \cdot m_{\min}} \cdot N \cdot N_z \cdot u_{0z}^2 \cdot K_{h\max}$$

The numerical values of $K_{h\max} \approx 10^{-2}$ cycles/meter, $m_{\max} \approx 1$ cycle/meter, and $m_{\min} \approx 10^{-3}$ cycles/meter correspond to real observed maximum and minimum horizontal and minimum vertical internal wave scales. The numerical values showed that, for

example, at $N = 6$ cycles/hr and $dN/dz = 0.1$ cycles/hr meter, and in keeping with the shifts in the current velocity, the energy flux would be $\varepsilon \sim 10^{-7}$ j/sec, which corresponds in order of magnitude to the experimental value of ε. The first term in (7) is the dominant one--that is, energy flux ε is proportional to $N^2 \cdot dN/dz$. The dependence of ε on the Vyaysyal'-Brent frequency $\sim N^2$ agrees with the experimental data (1).

Here are the basic conclusions of the research.

In an adiabatic approximation--that is, on the condition that wave action persists in a shear current, and where the energy density of wave trains was not known, we obtained the distribution of the energy density of internal waves in a synoptic eddy (4), which provides a qualitatively correct picture.

An adiabatic approximation was found to be insufficient for appraisal of the rate of flux of kinetic energy from internal waves into turbulence, and so we examined a mechanism limiting wave amplitude through local shear hydrodynamic instability.

The theoretically obtained value for energy flux from internal waves into turbulence and the dependence of energy flux on the Vyaysyal'-Brent frequency N are consistent with the experimental data.

BIBLIOGRAPHY

1. Dykman, V. Z., Yefremov, O. I., Kiseleva, O. A., and Panteleyev, N. A., "Internal Waves and Turbulence in Synoptic Eddies According to Data on Vertical Finestructure," (in this collection).

2. Korotayev, G. K., "Structure, Dynamics, and Energetics of Synoptic Variability in the Ocean," MORSKIYE GIDROFIZICHESKIYE ISSLEDOVANIYA, Ukrainian SSR Academy of Sciences Marine Hydrophysical Institute, Sevastopol', 1980.

3. Korotayev, G. K., "The Spectral Density of the Energy of Wave Trains," MORSKIYE GIDROFIZICHESKIYE ISSLEDOVANIYA, Ukrainian SSR Academy of Sciences Marine Hydrophysical Institute, Sevastopol', No 2, 1977, pp 41-47.

4. Fillips, "Dinamika verkhnego sloya okeana" [The Dynamics of the Upper Layer of the Ocean], Moscow, Izd-vo Mir, 1969, p 139.

5. Brethertone, F. P., and Carret, C. J. R., "Wavetrains in Inhomogeneous Moving Media," PROC. ROY. SOC., Ser. A., Vol 302, No 1471, 1968, pp 529-554.

6. Hayes, S. P., Joyce, T. M., and Millard, R. C., "Measurement of Vertical Finestructure in the Sargasso Sea," J. GEOPH. RES., Vol 80, No 3, 1975, pp 314-319.

Interpretation of KhVT Data in a Statistical Analysis of Density Field Variability

A. I. Yermolenko

STD data picked up by an "Istok" probe in a quasiregular measurement network were used to obtain field density figures during hydrological mapping performed in traverses under the Soviet-American "Polymode" program conducted in 1977-1978. Moreover the temperature field was measured with KhVT [not further identified] quick-action probes in a denser network along the path of the vessel. The work was done in the western Sargasso Sea in a traverse measuring 300×300 nautical miles.

The three-dimensional structure of the density and temperature fields, deduced from measurements made in nine surveys (their numbers in the program were: 2, 3, 5, 8, 9, 10, 11, 15, 16) was subjected to statistical analysis. The surveys correspondingly took 8, 14, 15, 19, 12, 10, 16 and 8 days--that is, the duration of each survey was short in comparison with the time of the complete "Polymode" program. The variability of the analyzed fields during the time of one survey is significantly lower than their annual variability; therefore in the analysis of the evolution of field structure, the measurements of one survey could be treated as applying to the midpoint of that survey's duration, while observations from all surveys can be interpreted as samples applicable to different months of the year. Figure 1 schematically shows the temporal distribution of the midpoints of the time intervals, the days in which the surveys were conducted and the survey serial numbers.

The number of measurements made in each survey vary, with KhVT sounding data making up a significant proportion of the samples. The representation of STD and KhVT measurements in the surveys is shown in Table 1.

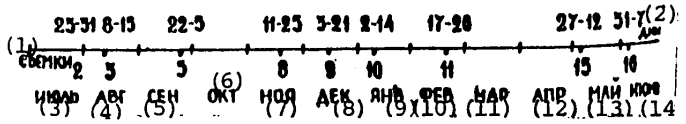

Figure 1. Distribution of Surveys Throughout the Year

Key:

1. Surveys
2. Days
3. July
4. August
5. September
6. October
7. November
8. December
9. January
10. February
11. March
12. April
13. May
14. June

Table 1

Survey No.	2	3	5	8	9	10	11	15	16
STD measurements	38	83	43	39	88	56	37	75	101
KhVT measurements	65	76	141	121	177	156	95	110	73
Total measurements	103	159	184	160	265	212	132	185	174

Availability of KhVT temperature data from a denser measurement network made it possible to subject the density and temperature fields to statistical matching, and to get more-precise data for the density field in regions in which STD measurements were not made (4).

The data to be analyzed were sampled from eight depth horizons, beginning with 0 meters, spaced 100 meters apart. Depth was limited to the 700 meter horizon because of the absence of KhVT measurements below 700-750 meters.

Statistical analysis was performed within a field of deviations from the means, computed in relation to the total measurements in the given horizon. As a consequence regularly occurring discrepancies between STD and KhVT data, varying with depth, were excluded from the analysis (5).

If there are k observations of the relative density field σ_t at points $\vec{x}_k$, and m observations of the temperature field t at points $\vec{x}_m$--that is, if $f_\sigma(\vec{x}_k)$ and $f_t(\vec{x}_m)$ are known, then the density field value f_σ at point $\vec{x}$, matched with temperature, would be sought in the form of the sum:

$$\hat{f}_\sigma(\vec{x}) = \sum_{(k)} g_1(\vec{x},\vec{x}_k) f_\sigma(\vec{x}_k) + \sum_{(m)} g_2(\vec{x},\vec{x}_m) f_t(\vec{x}_m), \qquad (1)$$

where g_1 and g_2 are weight factors determined from the conditions of minimum mean square error of interpolation by solution of a system of linear algebraic equations:

$$\begin{cases} K_\sigma(\vec{x},\vec{x}_k) = \sum_{(l)} g_1(\vec{x},\vec{x}_l) K_\sigma(\vec{x}_k,\vec{x}_l) + \sum_{(m)} g_2(\vec{x},\vec{x}_m) K_{\sigma t}(\vec{x}_k,\vec{x}_m), \\ K_{\sigma t}(\vec{x},\vec{x}_m) = \sum_{(k)} g_2(\vec{x},\vec{x}_k) K_t(\vec{x}_m,\vec{x}_k) + \sum_{(n)} g_1(\vec{x},\vec{x}_n) K_{\sigma t}(\vec{x}_n,\vec{x}_m). \end{cases} \qquad (2)$$

Here, K_σ and K_t are spatial correlation functions of fields σ_t and t respectively, $K_{\sigma t}$ is the mutual spatial correlation function of these fields, and l, m, n, and k are the number of observations falling within the correlation interval.

Then the error in determination of the density field would be defined as

$$\varepsilon(\vec{x}) = K_\sigma(0) - \sum_{(l)} g_1(\vec{x},\vec{x}_l) K_\sigma(\vec{x},\vec{x}_l) - \sum_{(m)} g_2(\vec{x},\vec{x}_m) K_{\sigma t}(\vec{x},\vec{x}_m), \qquad (3)$$

where $K_\sigma(0)$ is the variance of field σ_t.

Formulas (1)-(3) were also used to recreate the density field on the basis of measurements made only of this field. In this case the terms containing information about the other field were correspondingly absent.

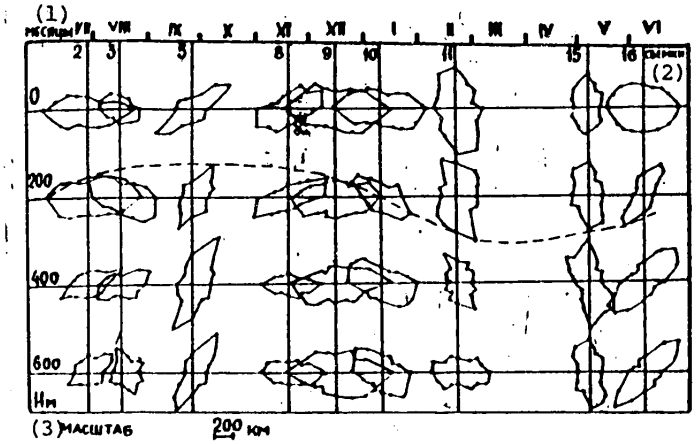

Figure 2. Change in Orientation of Correlation Ellipses at Different Horizons Throughout the Year

Key:
1. Months
2. Surveys
3. Scale

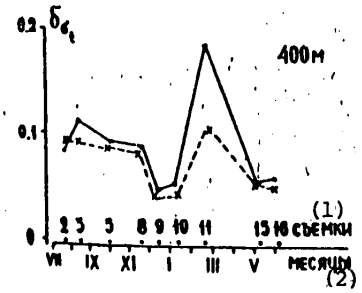

Figure 3. Behavior of the Standard Deviation in Different Surveys

Key:
1. Surveys
2. Months

Calculating the spatial correlation functions for the horizons, we analyzed their dependence on direction α. The computations were performed in accordance with the procedure explained in (3). Functions were calculated for directions of

0, 30, 45, 60, 90, 120, 135 and 150° relative to the equator for the eight horizons using data from all surveys (576 functions in all). The correlation interval was determined for each of them, and its length was plotted in each appropriate direction. The resulting figures are well-approximated by ellipses, which is an indication that the density fields are nonisotropic. Evolution of the three-dimensional statistical structure is represented in Figure 2. The ratio between the lesser and greater semiaxes of the ellipses varies between 1:1.5 and 1:2. The values of the former vary within 80-200 km, while those of the latter vary from 200 to 500 km.

It may be hypothesized that the three-dimensional statistical structure of the density field "rotates" in the course of the year, completing one revolution. The broken curve in Figure 2, which joins together the ends of the greater semiaxes of the correlation ellipses of each survey, illustrates this fact. Several eddy formations representing a single mutually associated dynamic system passed through the traverse (1). Comparing the orientation of the ellipses with the pattern of motion of the eddies (2), it would be easy to note that the mutual location and direction of the mean vector of eddy travel is fully defined by the nonisotropic nature of the density field (or the temperature field).

The mutual spatial correlation functions of fields σ_t and t exhibit negative correlation with a maximum at zero displacement. The greatest statistical correlation can be seen at distances up to 250-300 km.

When plotting the field density maps at values appearing at the intersections of a regular measurement network with a spacing of 17 nautical miles, we evaluated the degree to which these values were improved by the addition of KhVT data. With this purpose the results of two calculations--one made on the basis of STD data alone and another based on all data--were interpolated back to the observation points, and the standard deviations were computed. It was revealed as a result that all maps based on the second calculations were typified by either a smaller or a commensurate error in relation to maps based on the first calculations. As an example Figure 3 shows the typical behavior of the standard deviations of two calculations for the 400 meter horizon based on data from all surveys (filled circles correspond to the first calculations while asterisks correspond to the second). With depth, the difference in the standard deviations decreases.

Thus KhVT data from a denser measurement network provides a possibility for improving the accuracy of a density field map through its statistical matching with the temperature field; the obtained results indicate the suitability of a such a procedure.

BIBLIOGRAPHY

1. Bulgakov, N. P., "A General Description of Synoptic Eddies," in "Eksperimental'nyye issledoveniya po mezhdunarodnoy programme 'Polimode'" [Experimental Research in the International "Polymode" Program], Sevastopol', 1978, pp 44-54.

2. Grishin, G. A., and Dotsenko, S. F., "Kinematic Features of Eddy Formations in the 'Polymode' Traverse," MORSKIYE GIDROFIZICHESKIYE ISSLEDOVANIYA, Sevastopol', No 2, 1979, pp 158-166.

3. Yermolenko, A. I., Yesyunin, R. Ye., and Solodova, S. M., "Mapping Bottom Relief on the Crest of the Reykjanes Ridge by the Method of Objective Analysis," MORSKIYE GIDROFIZICHESKIYE ISSLEDOVANIYA, Sevastopol', No 5, 1971, pp 216-225.

4. Kolesnikov, A. G., Yermolenko, A. I., Novoselov, A. A., and Timchenko, I. Ye., "A Method for Plotting Chemical Element Maps for Ocean Areas Insufficiently Illuminated by Observations," MORSKIYE GIDROFIZICHESKIYE ISSLEDOVANIYA, Sevastopol', No 3, 1976, pp 5-16.

5. Flierl, G., and Robinson, A., "KhVT Measurements of Thermal Gradients in the MODE Eddy," J. PHYS. OCEANOGR., Vol 7, 1974, pp 300-302.

Numerical Models of Synoptic Variability in Delimited Regions of the Oceans and Seas

V. M. Kamenkovich, V. D. Larichev, B. V. Khar'kov

Dynamic modeling of synoptic variability in delimited regions of the seas and oceans is of interest in regard to both interpreting traverse observations and developing hydrological forecasting methods for different regions of the oceans and seas. Several numerical models have been proposed thus far. One of them will be described in sections 1 and 2, and numerical experiments with different models will be subjected to comparative analysis in section 3.

I. Dynamic Model

A frictionless quasigeostrophic model is used to describe evolution of synoptic scale movements within domain D. The grounds for the applicability of such a model to the movements under examination are provided. The model equations are:

Geostrophic relationships

$$u = -\frac{\partial \psi}{\partial y}, \quad v = \frac{\partial \psi}{\partial x}, \quad \psi = \frac{1}{\rho_0 f_0} p'$$

quasistatic relationship

$$\rho' = -\frac{\rho_0 f_0}{g} \frac{\partial \psi}{\partial z}$$

eddy equation

$$0 = \frac{\partial q}{\partial t} + (J(\psi, \Delta\psi) + \beta v)$$

entropy equation

$$\left(\frac{\partial}{\partial t} + u\frac{\partial}{\partial x} + v\frac{\partial}{\partial y}\right)\rho' - \frac{\rho_0 N^2(z)}{g} w = 0$$

The boundary conditions are:

1) $w = \frac{\partial \Gamma}{\partial t}, \quad \psi = \frac{g}{f_0}\zeta$, on the ocean surface ($z = 0$);

2) $w = u\frac{\partial h}{\partial x} + v\frac{\partial h}{\partial y}$ at mean depth H in domain D ($z = -H$);

3) the normal velocity v_n is given for the entire lateral boundary;

4) eddy $\Delta\psi$ is given for those portions of the lateral boundary where liquid flows into domain D;

5) $\frac{\partial}{\partial t}\oint_{\zeta}\frac{\partial\psi}{\partial n}d\Gamma + \oint_{\zeta}(\Delta\psi + \beta y)v_n d\Gamma = 0.$

The initial condition is:

The current function ψ is given.

Here axis x is directed eastward, axis y is directed northward, axis z is directed vertically upward, u, v, w are velocity components on axes x, y, z, ψ is the current function, ρ', p' are the density and pressure deviations from equilibrium distributions, ρ_0 is mean density, f_0 is the mean of the Coriolis parameter f, $\beta = df/dy$, N^2 is the equilibrium distribution of the square of Vyaysyal''s frequency, ζ--level, h--depth perturbations (relative to mean depth H), n--external normal to the lateral boundary, assumed to be perpendicular.

2. Difference Approximation

First a barotropic model is examined. The spatial resolution of the numerical model is determined with regard to the typical horizontal scale of perturbations. Difference approximation of advective terms in the equation for an eddy inside domain D requires the use of an (Arakava) design with second-order precision, which in turn requires establishment of the computational boundary conditions in those points of the lateral boundary where liquid flows out of domain D. A brief review of these conditions and the results of numerical calculations are presented. The problem of calculating eddy $\Delta\psi$ in relation to current function ψ in those areas or the boundary where liquid flows into domain D is discussed. The derivative with respect to time, $d\Delta\psi/dt$, within domain D is approximated by the central difference derivative; the temporal resolution of the model is chosen with regard to the typical time scales and the stability conditions of the different models. These conditions are derived for a problem involving frozen coefficients in unlimited and delimited areas; their validity in relation to the initial nonlinear problem is tested by numerical experiments. Current function ψ is calculated in relation to a known eddy $\Delta\psi$ directly (by means of a fast Fourier transform in relation to variable y and a trial run in relation to variable x). The test calculations are presented, demonstrating the advantages and shortcomings of the various difference approximations of the initial differential problem.

For the barocline problem, the difference approximation in relation to the vertical is selected in such a fashion that the laws of conservation of total energy, eddy potentials and enstrophy are satisfied for the differential difference model (entailing a difference approximation only in relation to x, y, z). Choice of the number of levels in relation to z is determined, for example, on the basis of the

accuracy of the calculations for phasal velocities of baroclinic Rossby waves in a real stratified medium (for example in the vicinity of the Polymode traverse). Inasmuch as the required number of levels is found to be high, the vertical structure of the difference problem is approximated by means of a linear combination of a barotropic mode and a small number of baroclinic modes. A numerical approximation is arrived at by colocation. The results of numerical calculations using the barocline model and illustrating the effectiveness of the method are presented.

3. Forecasting Experiments

The objective of these experiments is to determine the possibility for making a successful forecast depending on the quality of the input data (initial and boundary conditions, the forecasting interval and the parameters of the numerical design). In the first attempt, using "ideal" initial and boundary conditions applied to test examples, the parameters of the numerical design were selected in such a way that they would ensure effective integration (from the standpoint of accuracy and the computer memory and time expenditures) for a period significantly exceeding the proposed forecasting time, by 2-5 times--that is, on the order of many months. Then calculations were conducted with inaccurate or incomplete information for the boundary of the area in order to study the spread of errors from the boundaries into the area of the forecast. For example the values for the eddy or the current function at the boundary did not change throughout the entire forecasting period, which corresponds to the case where only the initial data are known. In this case the time of a satisfactory forecast did not exceed 2 weeks. Then cases were examined in which data were provided for only part of the boundary or a part of the boundary that was variable with respect to time, or in which boundary information was fed in periodically. The relative importance of information on different physical factors was evaluated in cases such as, for example, a current function that is imprecise in comparison with the eddy function. Errors resulting from inaccurate initial information were compared with errors due to imprecise boundary conditions.

Simulation of the Upper Quasi-Uniform Layer

T. R. Kil'matov, S. N. Protasov

1. A large number of mathematical models, reviewed in (1,4), describing vertical mixing in the upper layer of the ocean have recently appeared. These models are conditionally divided into two types (3) depending on the approach taken--integral or differential. The main difficulty in building integral models lies in adequate description of the production and dissipation of turbulent energy in a quasi-uniform layer. Differential models, in which mixing is described within the framework of the semi-empirical theory of turbulence, are hard to run, and they provide too much detail to the vertical structure of the quasi-uniform layer, considering that the characteristics are computed at a synoptic time scale. The model of quasi-uniform layer evolution suggested below is based on both approaches, which makes it possible to avoid both the difficulties of parametrization of energy production and dissipation and solution of the equation for turbulent energy in a semi-empirical approximation.

2. The following assumptions are made in building the model: 1) at the lower boundary of the quasi-uniform layer, $z=h$, Richardson's number attains its critical value, and the following condition must be satisfied:

$$K\left(\frac{\partial \bar{u}}{\partial z}\right)^2 + Lg\bar{Q} = 0; \qquad (1)$$

2) mixing within the quasi-uniform layer may be described by means of the turbulent exchange factor K in the following fashion:

$$K = d v_* h; \qquad (2)$$

3) below the quasi-uniform layer, drifting currents attenuate, such that $\bar{u}=0$ at $z=h$. Here, $\bar{u}$--drift velocity vector, Lg $\bar{Q}$--work done by buoyancy forces, v_*--dynamic velocity, d--constant. The first assumption defines the thickness of the quasi-uniform layer, h; the second determines vertical turbulent exchange; the third is the boundary condition for the lower boundary of the quasi-uniform layer. These assumptions are the product of the differential model (3).

Using (1) and (2) and performing simple transformations (2), the essence of which is similar to calculations associated with integral models (5), to calculate the thickness and temperature T of the quasi-uniform layer, we get

$$h\frac{dT}{dt} = Q - E\delta T\frac{dh}{dt}, \qquad (3)$$

$$E\delta T\frac{dh}{dt} = \frac{1}{d}\frac{L_1}{h}Q\left(\cos\theta + ch\,a\right)^{-1} - Q \qquad (4)$$

where $a = \sqrt{\frac{f}{d}}\frac{1}{L_1}$, L_1--Monin-Obukhov length scale, L_2--thickness of the planetary boundary layer, Q--heat flux to the ocean surface, normalized in relation to density and heat content, δT--the temperature gradient in the thermocline, E--unit function of the argument dh/dt. Equations (3)-(4) were obtained without regard to advection, salinity and penetrating radiation. The model is built and described in detail in (2).

Equation system (3)-(4) has clear physical meaning: Equation (3) describes the heat balance in the quasi-uniform layer while (4) describes deepening of the quasi-uniform layer as a result of wind-caused mixing (the first term on the right side) and owing to convection (the second term) ($Q<0$). A general description of model (3)-(4) taking account of advection, penetrating radiation and salinity is given in (2).

3. Let us examine some consequences of system (3)-(4). In the time of summer heating $Q>0$, and at the equator the thickness of the quasi-uniform layer is proportional to the Monin-Obukhov length scale, $h = (2/d)L_1$, inasmuch as $a = 0$. For moderate latitudes, expanding (4) into a series and expressing the thickness of the quasi-uniform layer explicitly we get $h = 0.5dL_1[(\ln 8fu^3/L_1gQ^3)]^{\frac{1}{2}}$, where f is the Coriolis parameter; this formula is similar, in terms of the dependence of the variables contained within it, to that derived from experimental data under the same conditions (1), which confirms the correctness of the hypothesis embodied within the model. The value of proportionality constant d, which is on the order of 0.05, agrees with the values given in (3). Thus at the equator, h is proportional to the Monin-Obukhov length scale, as we move toward higher latitudes the Coriolis parameter exerts an increasingly greater influence, and h becomes more proportional to the thickness of the planetary boundary layer.

4. Numerical experiments were conducted and natural comparisons were made in order to test the model. Calculation of the seasonal trend of the quasi-uniform layer's evolution on the basis of weather station data showed (2) that the model accurately describes the behavior of the quasi-uniform layer. The following values were obtained for the coefficient of vertical turbulent exchange in the quasi-uniform layer: $K\sim 10^2$ cm^2/sec in moderate latitudes in summer, $K\sim 10^3$ cm^2/sec in moderate latitudes in winter, and $K\sim 10^3$ cm^2/sec in lower latitudes, changing little throughout the year.

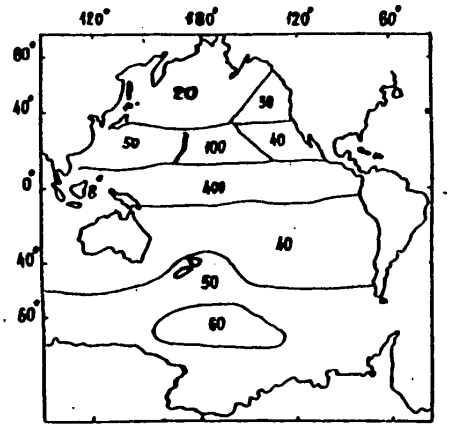

The thickness of the quasi-uniform layer was calculated with a consideration for the contribution made by salinity to the buoyancy flow in the warming period (July in the Northern Hemisphere and January in the Southern Hemisphere) in different water basins of the World Ocean. The initial data covering a 20°×20° grid were taken from atlases. The calculation results for the Pacific Ocean are shown in the figure, in which h is given in meters. The calculations show that the agreement is satisfactory, with the exception of the equatorial zone, for which the calculations produce an h value about five times greater than that observed. A possible reason for this is apparently that upwelling is observed in the equatorial region; if we consider vertical velocity W in our calculations of the thickness of the quasi-uniform layer, then we would get the following for the equator (4):

$$h = \frac{2\gamma_*^3}{\sqrt{d\Pi - \frac{g}{\rho}\frac{\partial\rho}{\partial z}W}} \qquad (5)$$

Here, Π is the buoyancy flow and $\delta\rho/\rho$ is the relative deviation of density. Using equation (5), we find that if h~100 meters at the equator, then W~$-5\cdot10^{-4}$cm/sec.

BIBLIOGRAPHY

1. Kalatskiy, V. I., "Modelirovaniye vertikal'noy termicheskoy struktury deyatel'nogo sloya okeana" [Simulation of the Vertical Thermostructure of the Ocean's Active Layer], Leningrad, Gidrometeoizdat, 1978.

2. Kil'matov, T. R., and Protasov, S. N., "A Model for Calculating the Thickness of the Ocean's Quasi-Uniform Layer," METEOROLOGIYA I GIDROLOGIYA, No 3, 1980, pp 59-64.

3. Marchuk, G. I., Kochergin, V. P., Klimok, V. I., and Sukhorukov, V. A., "Mathematical Simulation of Seasonal Variability of the Ocean's Turbulent Surface Layer," IZV. AN SSSR. FIZIKA ATMOSFERY I OKEANA, Vol 14, No 9, 1978, pp 945-955.

4. "Modelirovaniye i prognoz verkhnikh sloyev okeana" [Simulation and Forecasting of the Ocean's Upper Layers], collection of articles edited by Ye. L. Kraus, Gidrometeoizdat, 1979.

5. Kraus, E. B., and Turner, Y. S., "A One-Dimensional Model of the Seasonal Thermocline," TELLUS, Vol 19, No 1, 1967, pp 88-108.

Current and Average Three-Dimensional Spectrums of Synoptic Variability of a Current Field, According to "Polymode" Data

K. V. Konyayev, K. D. Sabinin

The two typical arrangements of current velocity vectors in the traverse have specific three-dimensional spectrums. In the period from 7 to 27 April 1978 there was an eddy in the southeastern sector of the traverse with current velocities up to 40 cm/sec. In this period the three-dimensional spectrum of the current field had the form of a half circle in the western bearing sector (Figure 1). The three-dimensional spectrum for clearly pronounced stream currents, which underwent slow deformation in the period from 28 February to 20 March 1978, appears as a narrow band along the current axis (Figure 1) (1).

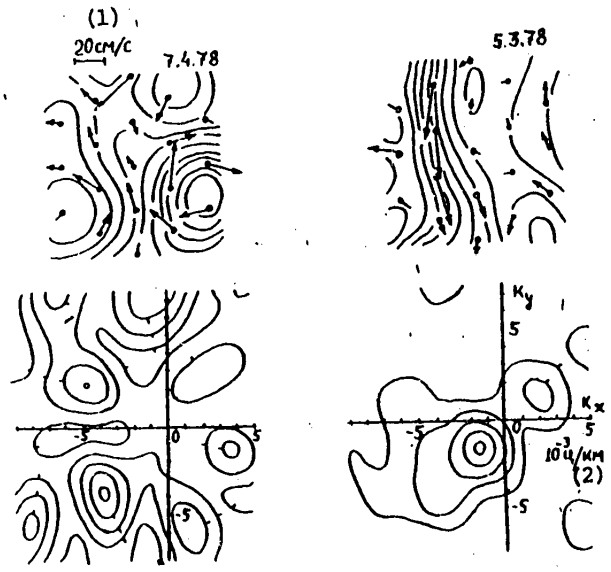

Figure 1. Arrangement of Current Velocity Vectors and the Corresponding Three-Dimensional Current Field Spectrums

Key:
1. Cm/sec
2. Cycles/km

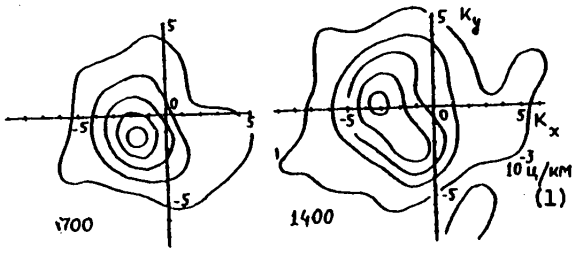

Figure 2. Cumulative Three-Dimensional Spectrums of the Current Field at the 700 and 1,400 Meter Horizons: Isolines represent 20, 40, 60, 80 and 95 percent of maximum.

When the three-dimensional spectrums are averaged for the entire period of observation, characteristics produced by selective variability disappear. For fluctuations with an observed period of 85 days, to which the main peak of the time spectrum corresponds, the three-dimensional spectrum takes the form of a narrow band, and its parameters agree with those of mode one baroclinic Rossby waves. For fluctuations within observed period of 51 days, to which the second highest peak of the time spectrum corresponds, the three-dimensional spectrum contains two peaks that promote formation of tightly packed, round eddies in space. The fluctuations are barotropic Rossby waves.

The cumulative three-dimensional spectrum (summated for all temporal frequencies) has the form of a narrow band at the 700 meter horizon (quasi-flat baroclinic waves dominate), while at the 1,400 meter horizon it is somewhat diffuse along its main axis (the role of barotropic waves traveling at an angle to one another grows).

BIBLIOGRAPHY

1. Kort, V. G., "The Polymode International Large-Scale Oceanic Experiment," OKEANOLOGICHESKIYE ISSLEDOVANIYA, Sov. radio, No 30, 1979.

A Model of the Dynamics of an Isolated Synoptic Eddy

G. K. Korotayev

Analysis of observations made during the "Polymode" experiment shows that the ocean's synoptic variability manifests itself in two forms--as intensive eddies occupying 30-40 percent of the ocean surface and as a wave background. The latter is formed mainly out of Rossby waves generated by traveling eddies. The relatively sparse distribution of eddies over the ocean surface serves as the grounds for building models of isolated eddies. Observations show that eddies are highly nonlinear, that they exist in quasi-equilibrium state and that they generate Rossby waves--that is, by analyzing real data we can formulate the principal criteria which a model of the dynamics of intensive eddies must satisfy. An eddy is henceforth defined as a certain enclosed area--a core--within which a vorticity of the same sign is initially concentrated (for the sake of concreteness, we will examine a cyclonic eddy), and an entrainment zone surrounding the core, within the limits of which particles of fluid are brought into motion on trajectories around the core. The size and shape of the entrainment zone changes as the eddy travels in view of the nonstationary nature of the process.

Motion within the entrainment zone and outside it is described in different ways (1). Within the limits of the entrainment zone, the following equation is satisfied:

$$\Delta\Psi + \beta y = -\beta\bar{y} + \Gamma_0\,\delta(x)\,\delta(y) \qquad \text{(I)}$$

Outside the entrainment zone, motion is described by a complete equation for conservation of the eddy, while at its boundary, $r = R(\theta,t)$ (r and θ are polar coordinates with their origin at the center of the eddy), we impose the conditions of "splicing" of two types of motion, used in many works devoted to research on eddy motions (2):

at $r = R(\theta,t)$ $\Psi = (V\cos\theta - U\sin\theta)R$, $\left[\frac{\partial\Psi}{\partial r}\right] = 0$,

and the condition that the current velocity turns to zero at the critical point:

at $r = R(d - \frac{\pi}{2}, t)$ $\frac{\partial\Psi}{\partial r} = \sqrt{U^2 + \bar{V}^2} = W$

where d is the angle between the direction of eddy travel and axis x.

Next we reduce the equation to its dimensionless form, selecting $\sqrt{\frac{\Gamma}{\beta}}$ as the lengthscale and $1/\sqrt{\Gamma\beta^3}$ as the time scale, and we seek their solutions in the form of series in relation to parameter $1/\bar{y}^{1/2}$, where $\bar{y} \gg 1$ is dimensionless shifting of the eddy along the meridian. When this solution method is employed, we encounter an additional difficulty associated with the nonuniformity of expansions in the vicinity of the coordinate origin when the values of variables are large. In view of this, to arrive at a uniformly suitable solution, we use the method of uniting asymptotic expansions.

The analysis shows that the structure of an eddy--its configuration and the distribution of velocities--is determined locally for the most part, without significant influence coming from distant areas. At the same time, the "external" area is significant from the standpoint of the eddy's kinematics and energetics. The equation used to find the main approximation for the external area is written in the form:

$$-U\frac{\partial \Delta\Psi_{вн}}{\partial x} - V\frac{\partial \Delta\Psi_{вн}}{\partial y} + \frac{\partial \Psi_{вн}}{\partial x} = -\left(U\frac{\partial}{\partial x} + V\frac{\partial}{\partial y}\right)\Gamma\delta(x)\delta(y) \qquad (2)$$

where Γ is the total intensity of the eddy. We can see that in the "external" area, the solution is a superimposition of quasi-stationary Rossby waves.

By uniting the solutions for the external and the internal areas, we get a uniformly suitable equation for the current function. Then, to compute the forces acting on the eddy from the surrounding fluid, we derive a formula associating pressure with the velocity field, equivalent to the Cauchy integral for potential motion of a fluid. Forces acting on an eddy have the following form:

$$\begin{aligned} X &= -\frac{\tilde{f}_0 + \tilde{y}}{\tilde{y}}V - \frac{4\pi W}{\tilde{y}^{1/2}}V + \left[\frac{6\pi W^2}{\tilde{y}} + \frac{8\pi\sqrt{W}}{\tilde{y}}K(\sin\tfrac{\alpha}{2})\sin\alpha\right]V - \\ &- \frac{4\pi\sqrt{W}}{\tilde{y}}\left[2E(\sin\tfrac{\alpha}{2}) - (1+\cos\alpha)K(\sin\tfrac{\alpha}{2})\right]U \\ V &= \frac{\tilde{f}_0 + \tilde{y}}{\tilde{y}}U + \frac{4\pi W}{\tilde{y}^{1/2}} - \left[\frac{6\pi W^2}{\tilde{y}} + \frac{8\pi\sqrt{W}}{\tilde{y}}K(\sin\tfrac{\alpha}{2})\sin\alpha\right]U - \\ &- \frac{4\pi\sqrt{W}}{\tilde{y}}\left[2E(\sin\tfrac{\alpha}{2}) - (1+\cos\alpha)K(\sin\tfrac{\alpha}{2})\right]V \end{aligned} \qquad (3)$$

The first terms on the right sides of the formulas represent that part of pressure which compensates exactly for the mean Coriolis force acting on the eddy. This is a reflection of the well known fact that when an incompressible fluid is subjected to two-dimensional motion, the Coriolis force can only cause redistribution of pressure. The meaning of the second terms on the right sides of formulas (3) becomes clear when we note that circulation of velocity along the boundary of the entrainment zone is equal to $\frac{4\pi W}{\tilde{y}^{1/2}}$. Therefore these terms represent Zhukovskiy component forces acting upon a traveling volume of rotating fluid. The third components are an addition to the Zhukovskiy force associated with presence of waveform movements in the fluid.

The energy flux elicited by Rossby waves was calculated in order to clarify the meaning behind the last terms of expressions (3). We find that $I = -XU - YV$. Consequently the last terms in formulas (3) represent the force of wave resistance experienced by the eddy as it generates Rossby waves.

Thus far we have not imposed any sort of limitations on the eddy's rate of travel--that is, for practical purposes we have solved the somewhat more-general problem of an eddy moving in a prescribed way, and we have calculated the pressures acting on the eddy. In order to get the equation for eddy movement we would need to write out the condition under which forces operating on the eddy would be balanced. We should note that in this asymptotic case, as follows from all of the previous discussion, the force of inertia is low and the motion equation is found as a quasistatic approximation, in which the Coriolis force acting upon the eddy is balanced by pressure forces.

Integrating the motion equation in relation to the area of the entrainment zone, we get

$$-\frac{\hat{f}_0+\bar{y}}{\bar{y}}V = X \qquad \frac{\hat{f}_0+\bar{y}}{\bar{y}}U - \frac{\pi}{\delta y} = Y$$

and consequently, as we had expected, the left side of the equations takes account of the average Coriolis force acting on the eddy, which is compensated exactly by pressure. Moreover an additional term appears in the left side of the second equation, associated with change in the Coriolis force in the meridional direction (Rossby, 1948).

The last formulas provide a complete description of the kinematics of the eddy formation in the asymptotic conditions examined here. That these conditions exist is established by research, which reveals that for barotropic movements, these conditions are such that the vortex moves predominantly in a westerly direction with constantly diminishing velocity, and with a small northern cyclone component. The dynamics of an intensive barotropic eddy are determined by the balance of three principal forces: forces acting in the meridional direction and brought about by variability of the Coriolis parameter, Zhukovskiy's force acting on the forward-traveling volume of rotating fluid, and the force of wave resistance. A baroclinic eddy has the form of a core--a volume of fluid within which potential vorticity of the same sign is concentrated. Within the limits of the entrainment zone, which is now a volume delimited by the ocean surface and a certain surface $z = h(x,y,t)$, the following equation is satisfied (1):

$$\Delta\psi + \frac{\partial}{\partial z}\frac{f^2}{N^2}\frac{\partial\psi}{\partial z} + \beta y = -\beta\bar{y} + \omega_0 \qquad (4)$$

where ω is the initial vorticity distribution. Given $z = h(x,y,t)$, the following condition is imposed on the boundary of the entrainment zone:

$$\psi = Vx - Uy + Q(t), \quad \left[\frac{\partial\psi}{\partial n}\right] = 0 \qquad (5)$$

Switching to dimensionless variables and appraising the order of the functions and the variables, we find that on the condition that the current function attenuates into infinity, in its lower approximation it is identically equal to zero, and within the limits of the entrainment zone it is described by the equation:

$$\Delta\psi + \frac{\partial}{\partial z}\frac{1}{N^2}\frac{\partial \psi}{\partial z} = \omega_0 - \bar{y} \qquad (6)$$

and the boundary conditions: for $z = h(x,y,t)$, $\psi = 0$, $d\psi/dn = 0$; for $z = 0$, $d\psi/dz = 0$.

A comparison of the simplest solution of this equation system and observations (3) revealed that the proposed model for the structure of an eddy is satisfactory, and consequently the structure of a baroclinic eddy is determined locally for the most part.

Computation of the kinematics and dynamics of an eddy involves calculation of the principal forces acting on it. With this purpose we calculate the next approximation of the expanded solution for the initial equation system. As in the barotropic case, the expanded solution is nonuniform, and it is found by the method of united asymptotic expansions. In this case the "internal" solution does not account for the β-effect while the "external" solution has the form of superimposed baroclinic and barotropic Rossby waves generated by a moving point eddy. Expressing pressure at the boundary of the entrainment zone by the current function of the "internal" solution, we calculate Zhukovskiy's force. Computing energy flux I, which is associated with the wave field induced by the eddy, we find that the force of wave resistance is $R = I/W$, where W is the eddy's rate of movement. Then, writing the quasistatic balance of the resultant of the Coriolis force, Zhukovskiy's force and the wave resistance force, we get the motion equation for the eddy.

BIBLIOGRAPHY

1. Korotayev, G. K., "Structure, Dynamics and Energetics of the Ocean's Synoptic Variability," Preprint No 7, Sevastopol', Izd-vo MGI AN USSR, 1980, pp 5-63.

2. Lavrent'yev, M. A., and Shabat, B. V., "Problemy gidrodinamiki i ikh matematicheskiye modeli" [Hydrodynamics Problems and Their Mathematical Models], Moscow, "Nauka", 1973, pp 187-199.

3. Fuglister, F. C., "Cyclonic Rings Formed by the Gulf Stream 1965-1966," in "Studies in Physical Oceanography," Vol 1, Gordon and Breach, 1970, pp 137-168.

Experimental Research on Synoptic Eddies in the Open Ocean

M. N. Komlyakov

Eddies in western stream-type border currents (Gulf Stream, Kuroshio, East Australian), formed by meanders cut off from these currents, were well known in the 1950's. As far as the rest of the ocean is concerned, the true structure, intensity and degree of spread of synoptic-scale movements in the ocean remained practically unclarified until the 1970's, though the first indications of the existence, in certain areas of the open ocean, of strong, deep, unstationary currents with a period on the order of several weeks or months were discovered earlier--in observations made by Dzh. Svallou and G. Stommel near the Bermuda Islands, by the Soviet "Polygon-67" expedition in the Arabian Sea, and some other observations.

The first exhaustive direct measurement of an eddy in the open ocean was made during the Soviet "Polygon-70" expedition in the Atlantic Ocean. The parameters of the eddy were reliably determined, and the numerical characteristics of its motion and evolution and its intensity were estimated. It was demonstrated that the parameters of the eddy and its motion are described well by models of baroclinic Rossby waves. Finally, indications that eddy motion is generated by baroclinic instability of a large-scale current were obtained.

The principal results of the American MODE-I experiment (1973, Sargasso Sea) were found to be close to the results of "Polygon-70." It was also shown that synoptic-scale motions encompass the sea's entire water column. Measurements of deep-water currents with neutral-buoyancy floats revealed that the field of synoptic currents is noticeably stochastic and that advective effects are well expressed in this field.

The tremendous volume of observations made during the Soviet part of the "POLYMODE" experiment (Sargasso Sea, 1977-1978) made it possible to plot a unique series of synoptic maps of the currents and subject the data to thorough statistical treatment. The high energy level of synoptic currents in the POLYMODE region was responsible for the high intensity of nonlinear effects; this relationship expressed itself, in particular, in periodic formation, within the study area, of strong quasi-isolated eddies and streams separated by areas of very weak currents. Several cases of intense interaction both between individual strong eddies and streams and between strong eddies and adjacent areas of weak currents were analyzed. Several cases were recorded in which very abrupt velocity fronts underwent formation in the main thermocline; a clear mutual relationship between temperature fronts in the upper layer of the ocean and strong eddies was also revealed. Density mapping of the research

area revealed a relatively small but very intense isolated eddy traveling across the POLYMODE area. Its upper part consisted of water carried into the research area from the southeastern part of the main circulation of the North Atlantic.

Numerous experimental studies conducted in recent years have shown that synoptic eddies are the principal form of motion of ocean waters practically throughout all of the World Ocean. In regions remote from the western border currents, the energy of eddies is approximately proportional to the energy of large-scale currents, which argues in favor of the hypothesis that baroclinic instability of large-scale currents is the principal mechanism of eddy generation. In regions adjacent to the western border currents, the principal source of energy possessed by eddies in the open ocean is, apparently, Rossby waves generated by border currents and frontal eddies created by them.

Free Rossby Waves as a Factor Responsible for Fluctuation of Synoptic-Scale Oceanological Characteristics (Using the Kuroshio and Oyashio Water Systems as an Example)

L. K. Kramareva

Investigation of changes in the state of the World Ocean having a typical time scale of 1-10 years has great significance to climate and weather forecasting. Theoretically grounded forecasts extending over such long periods are practically absent today, even though it is precisely upon their quality that the planning and organization of the work of many national economic sectors depend.

Assessment of the role played by fluctuations in hydrometeorological characteristics and of the contribution these fluctuations make to the overall variability of the ocean is a prerequisite of clarifying the physical mechanisms of these fluctuations.

An analysis of observations has permitted researchers to formulate a number of hypotheses, ones which are basically qualitative in nature and which are not always obviously valid. If we are to create theoretical models of large-scale fluctuations in oceanological fields, models having a good physical basis and exhibiting satisfactory agreement with natural processes, first of all it would be most important to analyze and test out the hypotheses published in the literature. Moreover we would need to thoroughly study nonlinear processes in the ocean. Soviet and foreign researchers have now persuasively demonstrated that a certain part of the overall variability of thermal and circulation processes in the ocean proceed under the influence of forces having a planetary scale, ones playing an important role in the formation of the ocean's hydrological climate.

Measurements made of oceanic currents and the density and temperature fields and a number of other oceanographic characteristics associated with these currents indicate significant fluctuations in the latter within a broad range of typical temporal and spatial scales. A large number of theoretical works have recently been published on physical phenomena eliciting these fluctuations. It is believed that one of the main causes is planetary waves produced by meridional change in the vertical component of the earth's angular velocity of rotation (or Rossby waves). Owing to low group velocity and, in many cases, weak dispersion, they are among the most nonlinear movements in the ocean. But a nonlinear theory of such waves has not been developed. Today, the study of the dynamics and kinematics of Rossby waves is one of the achievements of theoretical oceanology. Research on Rossby waves performed thus far has been devoted mainly to their kinematics and dynamics with a consideration for a nonstationary wind system, morphometric features of the water basin and vertical density stratification.

However, absence of models accounting for horizontal nonuniformities in the density field, the stationary current velocity field, turbulent exchange and the viscosity of the medium under analysis is a serious limitation on experimentation and application of the existing theory to calculation of the parameters of Rossby waves.

In this connection we made it our objective to study the influence of density stratification, the stationary current velocity field and turbulent exchange on the dynamics of free Rossby waves viewed as one of the factors responsible for fluctuation of oceanological characteristics on a synoptic scale. Experimental data were used as a basis for an attempt to reveal free Rossby waves in the northwestern Pacific (using the Kuroshio and Oyashio water systems as an example) and to analyze their relationship to fluctuations in the water surface temperature field. A three-dimensional hydrodynamic model of the following form was laid at the basis of the study:

$$\frac{\partial u}{\partial t} - fv = -\frac{1}{\rho_0}\frac{\partial p}{\partial x} + \mu \Delta u + \frac{\partial}{\partial z}\left(\nu \frac{\partial u}{\partial z}\right) \quad (1)$$

$$\frac{\partial v}{\partial t} + fu = -\frac{1}{\rho_0}\frac{\partial p}{\partial y} + \mu \Delta v + \frac{\partial}{\partial z}\left(\nu \frac{\partial v}{\partial z}\right) \quad (2)$$

$$\frac{\partial p}{\partial z} = g\rho \quad (3)$$

$$\frac{\partial \rho}{\partial t} + u\frac{\partial \rho}{\partial x} + v\frac{\partial \rho}{\partial y} + w\frac{\partial \rho}{\partial z} = \frac{\mu}{\rho_0}\Delta \rho + \frac{1}{\rho_0}\frac{\partial}{\partial z}\left(\nu \frac{\partial \rho}{\partial z}\right) \quad (4)$$

$$\frac{\partial u}{\partial x} + \frac{\partial v}{\partial y} + \frac{\partial w}{\partial z} = 0 \quad (5)$$

$$\nu \sqrt{\left(\frac{\partial u}{\partial z}\right)^2 + \left(\frac{\partial v}{\partial z}\right)^2} = \sqrt{cb^2} \quad (6)$$

where $u = u(x,y,z,t)$, $v = v(x,y,z,t)$, $w = w(x,y,z,t)$--current velocity components, $p = p(x,y,z,t)$--hydrodynamic pressure, $\rho = \rho(x,y,z,t)$--water density, $\mu = \text{const}$--coefficient of kinematic turbulent viscosity, ν--coefficient of vertical turbulent exchange, b--energy of turbulent pulsation, c--universal constant, x,y,z--coordinates, t--time.

We use the method of small perturbations and assume that the steady state of system (1)-(6) satisfies these conditions: 1) motion is geostrophic, 2) the continuity equation is equal to zero, 3) the isopycnicity equation and the meridional component of the velocity of the main current are equal to zero.

In this case system (1)-(6) would assume the form:

$$\frac{\partial u'}{\partial t} - fv' = -\frac{1}{\rho_0}\frac{\partial p'}{\partial x} + \mu \Delta u' + \frac{\partial}{\partial z}\left(\bar{\nu} \frac{\partial u'}{\partial z}\right) \quad (7)$$

$$\frac{\partial v'}{\partial t} + fu' = -\frac{1}{\rho_0}\frac{\partial p}{\partial y} + \mu \Delta v + \frac{\partial}{\partial z}\left(\bar{\nu} \frac{\partial v'}{\partial z}\right) \quad (8)$$

$$\frac{\partial p'}{\partial z} = g\rho' \quad (9)$$

$$\frac{\partial u'}{\partial x} + \frac{\partial v'}{\partial y} + \frac{\partial w'}{\partial z} = 0 \quad (10)$$

$$\frac{\partial \rho'}{\partial t} + \bar{u}\frac{\partial \rho'}{\partial x} + \bar{v}\frac{\partial \rho'}{\partial y} + \bar{w}\frac{\partial \rho'}{\partial z} + u'\frac{\partial \bar{\rho}}{\partial x} + v'\frac{\partial \bar{\rho}}{\partial y} + w'\frac{\partial \bar{\rho}}{\partial z} = 0 \quad (11)$$

$$\nu'^2 = \frac{cb^2}{\frac{\partial \bar{u}}{\partial z}} \quad (12)$$

Variables with a prime symbol correspond to the system's perturbed state while those without a prime symbol correspond to a steady state. The prime symbols will be dropped in the subsequent solution of equation system (7)-(12).

We solve system (6)-(12) in the presence of the following boundary and initial conditions:

$$x = 0, \ell_1 \quad u = 0 \quad \left[-A\left(\frac{1}{\rho_0}\frac{\partial p}{\partial x}\right) - \frac{1}{\rho_0}\frac{\partial p}{\partial y}\right]\Big|_{x=0,\ell_1} = 0 \qquad (I3)$$

$$y = 0, \ell_2 \quad v = 0 \quad \left[-A\left(\frac{1}{\rho_0}\frac{\partial p}{\partial y} + \frac{1}{\rho_0}\frac{\partial p}{\partial x}\right)\right]\Big|_{y=0,\ell_2} = 0 \qquad (I4)$$

where $$A = \left(\frac{\partial}{\partial t}\right)^2 - (\mu\Delta)^2 - \left(\bar{\nu}\frac{\partial^2}{\partial z^2}\right)^2$$

$$z = 0 \quad \frac{\partial u}{\partial z} = -\frac{\tau_x}{\rho\bar{\nu}} \quad \frac{\partial v}{\partial z} = -\frac{\tau_y}{\rho\bar{\nu}} \quad w = 0 \qquad (I5)$$

where τ_x, τ_y are, correspondingly, the zonal and meridional wind pressure;

$$z = H, u = v = 0, \left[-A\left(\frac{1}{\rho_0}\frac{\partial p}{\partial x}\right) - \frac{1}{\rho_0}\frac{\partial p}{\partial y}\right] = \left[-A\left(\frac{1}{\rho_0}\frac{\partial p}{\partial y} + \frac{1}{\rho_0}\frac{\partial p}{\partial x}\right)\right] = 0 \qquad (I6)$$

Solving equation system (6)-(12), we get dispersion relationships that permit us to determine formulas by which to compute Rossby wavelength L, wave frequency σ, phasal velocity c and the coefficient of attenuation (growth) γ:

$$L = 2\pi\left[2\beta^2\left(\sigma^2 + f^2\varepsilon^2 - \beta f \bar{\rho}_y \bar{\rho}_0^{-1} + \nu\beta f\right)\right]^{1/2} \qquad (I7)$$

$$\sigma = \left(\frac{2\beta^2}{\lambda^2} + \frac{\beta\bar{\rho}_0 f\varepsilon}{\bar{\rho}_y} - f^2\varepsilon^2 - \Gamma^2 - \frac{\beta\bar{\rho}_0\nu}{\bar{\rho}_x}\right)^{1/2} \qquad (I8)$$

$$c = 2\pi\sigma\left[2\beta^2\left(\sigma^2 + f^2\varepsilon^2 - \beta f\varepsilon\bar{\rho}_y\bar{\rho}_0^{-1}\right)\right]^{-1/2} \qquad (I9)$$

$$\gamma = \frac{2\beta\varepsilon\bar{\rho}_0}{\bar{\rho}_x}\left[\mu^2\left(\frac{n}{\beta} + \frac{1}{\lambda^2}\right) - 1\right] \qquad (20)$$

The calculations based on formulas (17)-(20) are analyzed for dynamically stable, unstable and attenuating wave processes.

The goal of this analysis is to study the mechanism responsible for formation of free Rossby waves, and their stability in dynamic zones of the region under analysis. Special attention is turned in the work to revealing the role of Rossby waves as a factor responsible for fluctuation of oceanological characteristics in the ocean, and particularly the water surface temperature field.

The experimental data were obtained from maps showing the distribution of water temperature over the ocean surface in the Kuroshio and Oyashio water systems (10°N. Lat.-43° N. Lat., 120°E. Long.-150°E. Long.). The entire area was divided into points, at each of which temporal series were created and subjected to spectral analysis. The research revealed that the spectrums of oscillations in the water surface temperature field differ from one another in relation to their intensity and the particular energy-contributing zones involved.

Investigation of the three-dimensional structure of fluctuations in the water surface temperature field was based on isophase maps, which permitted us to calculate experimental phasal velocities and the lengths of temperature waves, and to compare them with the theoretical phasal velocities and Rossby wavelengths. Investigation of isophase maps allow us to determine the zonal orientation of temperature waves in the central part of the region, in the northeastern branch of the Kuroshio water system, in the region of water mixing and in the area of subtropical convergence.

Consistency between theoretical and experimental results was observed in the vicinity of the main Kuroshio current and in the subtropical convergence and water mixing zones. In other regions we observed differences: The phasal velocities of Rossby waves were 20-50 cm/sec lower than those of temperature waves.

The agreement between the principal characteristics of temperature waves and the characteristics of Rossby waves in relation to magnitude and orientation indicates that fluctuations in the ocean's water surface temperature field are caused by Rossby waves.

Modeling the Water Temperature of the Baltic Sea

T. Kullas, R. Tamsalu

1. Introduction

In terms of thermal conditions, the Baltic Sea is divided into two regions. The first region includes the Gulf of Riga, the Gulf of Bothnia, the eastern part of the Gulf of Finland and the coastal zone of the open Baltic. The second region embraces the open Baltic and the western part of the Gulf of Finland.

In the first region, winter convective mixing proceeds to the bottom, while in summer the temperature drops monotonously below the uniform layer and the bottom temperature is basically the product of an upward heat flux.

In the second region, winter convective mixing proceeds only to a constant halocline. In summer, the temperature below the uniform layer first drops and then grows. The bottom temperature is basically the product of an advective heat flux through the Danish straits.

Thermal processes occurring in water basins have been studied for a long period of time by many authors. In recent years two reviews were published on this subject (2,12), and therefore there is no need to discuss these works in detail here. We will simply note that all, without exception, discuss water basins in which the temperature decreases with depth--that is, areas resembling the first region indicated above. To permit comparison of the development of temperature in the two different regions, Figure 1A shows the temporal distribution of temperature in the vicinity of the Bornholm trench, and Figure 1B shows this distribution for the Gulf of Bothnia.

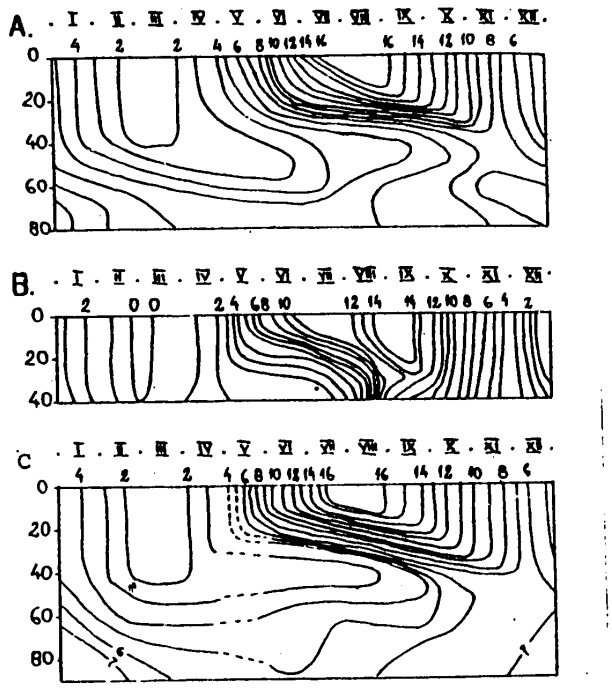

Figure 7. Temperature Distribution: A--for the Bornholm trench (10); B--for the Gulf of Bothnia (11); C--for the Bornholm trench, by computation.

2. The Equation

The large-scale temperature structure of water basins is usually described by a semi-empirical equation for turbulent diffusion of heat. The experience of numerical modeling of thermohaline processes in the Baltic (4,8) showed that it would be expedient to solve this equation in coordinate system $\eta = z/H(x,y)$; in such a case the equation would have the following form:

$$\frac{\partial T}{\partial t} + H^{-1}\left[\mathrm{div}_h\left(\vec{u} HT\right) - \mu\Delta(HT) + \frac{\partial \omega}{\partial \eta}\right] = 0. \qquad (I)$$

Here, T--temperature, H--depth, $\vec{u}$--horizontal velocity vector, μ--coefficient of horizontal turbulent diffusion, div_η--horizontal divergence, Δ--Laplace horizontal,

$$\omega = -\kappa H^{-1}\frac{\partial T}{\partial \eta} + \left(w - u\eta\frac{\partial H}{\partial y}\right)T + \eta\mu\left\{T\Delta H + 2\left(\frac{\partial H}{\partial x}\frac{\partial T}{\partial x} + \frac{\partial H}{\partial y}\frac{\partial T}{\partial y}\right) - \eta H^{-1}\left[\left(\frac{\partial H}{\partial x}\right)^2 + \left(\frac{\partial H}{\partial y}\right)^2\right]\frac{\partial T}{\partial \eta}\right\},$$

k--coefficient of vertical turbulent diffusion, w--vertical velocity. Adding to equation (1) the equations for motion, continuity, state and salt diffusion, we get a system for which a numerical solution was found in (4,8).

Analysis of numerical experiments showed that the proposed approach satisfactorily describes the thermostructure of the first region, and it is very unsatisfactory for the second region.

3. Self-Modeling

The self-modeling profile of the temperature of the ocean's active layer was first used by Kitaygorodskiy and Miropol'skiy (3). Later on, self-modeling profiles of temperature and salinity were used in many other works as well (1,2,6,9). The self-modeling temperature profile for the Baltic Sea was first discussed in (7). In contrast to the ocean, the Baltic Sea's self-modeling temperature profile embraces the entire depth of fluid stratification.

When we account for the self-modeling profile, the vertical temperature structure in the Baltic Sea is described as follows:

$$\begin{aligned} &0 \leq z \leq h && T = T_s(x,y,t) \\ &h \leq z \leq H && T = T_s(x,y,t) + \theta_i(\xi)\left[T_w(x,y,t) - T_s(x,y,t)\right] \\ &z > H && T = T_w(x,y,t) \end{aligned} \qquad (2)$$

Here h--thickness of the upper uniform layer, T_S--surface temperature, T_H--bottom temperature, $\theta_i(\xi)$--self-modeling profile.

In summer, $\theta_i(\xi)$ has the following form:

a) in the first region

$$\theta_1(\xi) = 8/3\,\xi - 2\xi^2 + 1/3\,\xi^4 \qquad (3a)$$

b) in the second region

$$\theta_2(\xi) = 9\xi - 24\xi^2 + 19\xi^3 - 6\xi^4 \qquad (3b)$$

In winter, temperature is uniform in the first region while in the second region $\theta(\xi)$ has the form:

$$\theta_3(\xi) = 1{,}5\,\xi + 1{,}5\,\xi^2 - 3{,}5\,\xi^3 + 1{,}5\,\xi^4 . \qquad (3c)$$

The distribution of $\theta(\xi)$ in different seasons and in different regions is shown in Figure 2. Dots indicate the distribution of $\theta = [T_0 - T(z)]/(T_S - T_W)$ with respect to ξ for computed temperature values borrowed from (4). This shows that the procedure suggested in (4,8) describes the vertical temperature structure in the first region well.

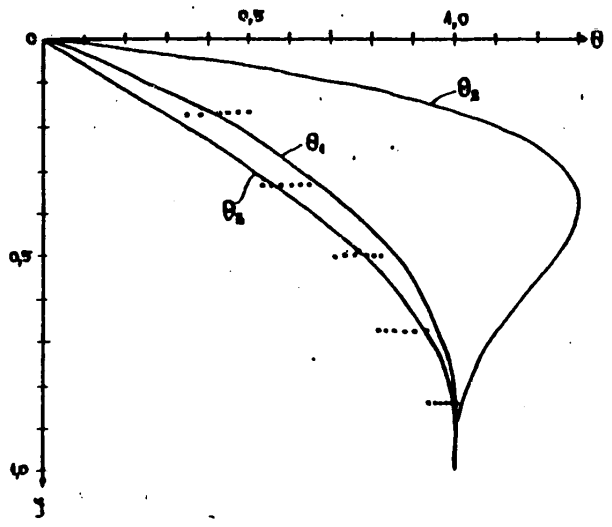

Figure 2. Self-Modeling Temperature Profiles in the Baltic Sea

4. Solution of Equation (1) Using the Self-Modeling Profile

We will solve equation (1) by the decomposition method (5). In the first step in time, we solve the equation

$$\frac{T^{t+1/2}-T^{t}}{\Delta t}+H^{-1}\left[d\omega_h(\vec{u}HT)-\mu\Delta(HT)\right]^{t+1/2}=0, \quad (4)$$

and in the second step

$$\frac{T^{t+1}-T^{t+1/2}}{\Delta t}+H^{-1}\frac{\partial\omega}{\partial\eta}=0. \quad (5)$$

Assuming that the temperature of the bottom layer is the product of advective influx--that is, that it is described by equation (4), we may write:

$$T_H^{t+1}=T\Big|_{\eta=1}^{t+1/2}$$

Next, integrating (5) with respect to η from 0 to 1 using (2) and (8), we arrive at the expression

$$T_s^{t+1}=\left(\Delta t q_s^{t+1}+\int_0^1 T^{t+1/2}d\eta-RT_H^{t+1}\right)/(1-R), \quad (6)$$

where q_B--heat flux to the surface of the sea, $R = (1-h/H)$.

Following (12), we determined the thickness of the uniform layer h using the formula:

$$\frac{\partial h^2}{\partial t} = 4N^{-2} \times \begin{cases} Av_*^3/h & q_s \geq 0 \\ Av_*^3/h + B\alpha_T g|q_s| & q_s < 0 \end{cases} \qquad (7)$$

Here, N--Vyaysyal'-Brent frequency, v_*--dynamic velocity, g--gravity, $A,B,\alpha_T = \text{const}$.

Possessing values for T_H, T_S and h at time $t+1$, we can establish the temperature profile for time $t+1$ using formula (2). The proposed algorithm was used to determine water temperature in the open Baltic. As an example Figure 1C shows the distribution of the computed temperature for the Bornholm trench.

BIBLIOGRAPHY

1. Barenblat, G. I., "Self-Modeling of Temperature and Salinity Distributions in the Upper Thermocline," IZV. AN SSSR, FAO, Vol 14, No 11, 1978.

2. Kalatskiy, V. I., "Modelirovaniye vertikal'noy termicheskoy struktury deyatel'nogo sloya okeana" [Modeling the Vertical Thermostructure of the Ocean's Active Layer], Leningrad, Gidrometeoizdat, 1978.

3. Kitaygorodskiy, S. A., and Miropol'skiy, Yu. Z., "The Theory of the Ocean's Active Layer," IZV. AN SSSR, FAO, Vol 6, No 2, 1970.

4. Kullas, T. E., and Tamsalu, R. E., "A Predictive Model for the Baltic Sea and Its Numerical Solution," VODNYYE RESURSY, No 1, 1979.

5. Marchuk, G. I., "Metody vychislitel'noy matematiki" [The Methods of Computer Mathematics], Novosibirsk, Nauka, 1973.

6. Reshetova, O. V., and Chalikov, D. V., "The Universal Structure of the Ocean's Active Layer," OKEANOLOGIYA, Vol 17, No 5, 1977.

7. Tamsalu, R. E., "Modelirovaniye dinamiki i struktury vod Baltiyskogo morya" [Modeling the Dynamics and Structure of Baltic Waters], Riga, Zvaygzne, 1969.

8. Kullas, T., and Tamsalu, R., "A Baroclinic Model of the Physical Fields of the Baltic Sea," "Ambio Special Report," Stockholm, No 5, 1977.

9. Linden, P. F., "The Deepening of a Mixed Layer in Stratified Fluid," J. FLUID MECH., Vol 71, No 2, 1975.

10. Mattaus, W., "Zur mittleren jahrezeitlichen Weranderlichkeit der Temperatur in der offenen Ostsee," BEITRAGE SUR MEERESKUNDE, No 40, 1977.

11. "Temperature and Salinity of the Fixed Finnish Stations 1965-1966," MERENTUTKIMUSLAITOKSEN JULKAISU, Helsinki, No 231, 1969.

12. Zilitinkevich, S. S., Chalikov, D. V., and Resnyansky, Yu. O., "Modeling the Oceanic Upper Layer," OCEANOLOGIA ACTA , Vol 2, No 2, 1979.

Spectral Structure of Vertical Temperature Nonuniformities in the Ocean

I. D. Lozovatskiy, N. N. Korchashkin

Vertical temperature nonuniformities in the ocean have a broad spectrum of scales--from fluctuations having dimensions on the order of several hundreds of meters to small-scale turbulent pulsations of several tenths of a centimeter and less. Basing himself on an analysis of a large quantity of temperature nonuniformity spectrums $E_t(K)$, where K is the vertical wave number, obtained by measuring temperature profiles in the main thermocline of different regions of the Pacific Ocean, Gregg (4) suggested an average statistical spectrum $E_t(K)$ within a range of scales from 10^4 to 1 cm, which was approximated by the following exponential dependencies: at $K < 6 \cdot 10^{-2}$ cycles/meter, $E_t/\overline{T_z^2} = 1.2 \cdot 10^{-1} K^{-1.9}$, while at $10^\circ > K > 6 \cdot 10^{-2}$ cycles/meter, $E_t/\overline{T_z^2} = 4.6 \cdot 10^{-3} K^{-3.1}$, where $\overline{T_z}$ is the mean vertical temperature gradient.

The results of measurements made in the ocean showed that depending on the relationships between the parameters defining the conditions of small-scale fluctuations in temperature, the finestructure subinterval in spectrum $E_t(K)$, where $E_t = A\overline{T_z^2}K^3$ ($A = 4.5 \cdot 10^{-3}$), may transform directly into a buoyancy interval, where $E_T = \alpha_1 \varepsilon_T^{3/5} \beta^{-1/5} K^{-1/5}$, or into an inertial-convective interval $E_T = \alpha_2 \varepsilon_T \varepsilon_u^{-1/3} K^{-5/3}$ or into a viscous-convective interval ($E_T = \alpha_3 \varepsilon_T t_\eta K^{-1}$). Here, α_1, α_2, α_3--universal constants, E_u--turbulent energy dissipation rate, E_t--temperature nonuniformity equalization rate, β--buoyancy parameter, $t_\eta = (\nu/E)^{1/2}$--Kolmogorov's time scale, ν--coefficient of molecular viscosity. Taking account of the asymptotic nature and differences in dimensions of spectrum $E_t(K)$ at large and small K, Lozovatskiy (1) obtained expressions describing spectrum $E(K)$ in the transitions from the finestructure subinterval to one of the turbulence subintervals. These expressions contain typical scales L_t^* L_t and L_t^η separating the finestructure interval from the buoyancy, inertial-convective and viscous-convective intervals respectively:

$$L_T^* = c_1 \varepsilon_T^{1/5} \beta^{-1/5} \overline{T}_z^{-2/5}, \quad L_T = c_2 \varepsilon_T^{3/4} \varepsilon_u^{-1/4} \overline{T}_z^{-3/2}, \quad L_T^\eta = c_3 \varepsilon_T^{1/4} t_\eta^{1/2} \overline{T}_z^{-1},$$

and c_1, c_2, c_3 are dimensionless constants defined as follows:

$$c_1 = (A/\alpha_1)^{-3/5}, \quad c_2 = (A/\alpha_2)^{-}, \quad c_3 = (A/\alpha_3)^{-1/2}.$$

Measurements of the vertical structure of the temperature field and simultaneous observations of the internal wave field showed that in the finestructure interval, spectrum $E_t(K) = A\overline{T_z^2}K^{-3}$ for sufficiently well developed short-period internal waves, while for waves of small amplitude, $E_t(K) \sim K^{-(4-5)}$, and the spectrum is characterized by a lower level. It may be possible that confluence of the internal wave field is precisely what causes smoothing of mesoscale nonuniformities in profile $T(z)$. However, we still do not have a firm idea about the dominant mechanisms responsible for the form of spectrum $E_t(K)$ in the range of scales from 10^4 to (10^2-10^1) cm. Therefore, staying within the framework of dimensional theory, we will attempt to reveal the dominant parameters that may indicate the mechanisms responsible for redistribution of the deviations of temperature fluctuations in relation to the scale spectrum and making it possible to obtain an expression by which to describe the average spectrum at $K<(10^{-1}-10^{-2})$ cm^{-1} (4). If we assume that in a certain layer of the thermocline, the main processes influencing formation of the fine vertical structure of profiles $T(z)$ are turbulence and (or) nonlinear interactions in the internal wave field, than change in temperature in the vicinity of a fixed point would be the product of, in particular, turbulent flows of momentum and heat. We know that in the presence of intense, stable stratification, which is observed in an ocean thermocline, heat exchange is significantly encumbered in comparison with momentum exchange (for an experimental confirmation of this, see for example (3)). That is, the main contribution to the heat flux spectrum is made by fluctuations with scales l_q that are much smaller than for momentum flux spectrum, l_τ. Therefore the values for the heat flux $q = \overline{T'w'}$ and momentum flux $\tau = -\overline{u'w'}$ per unit mass would be the external parameters defining nonuniformities with scales $l<l_q$ and $l<l_\tau$ respectively. At $l>l_q$ and $l>l_\tau$ the external parameters would be no longer the turbulent fluxes q and τ themselves, but some averaged characteristics of their change on the vertical axis, for example the mean gradients $\tilde{q}_z = \langle \frac{\Delta \overline{T'w'}}{\Delta z} \rangle$ and $\tilde{\tau}_z = \langle -\frac{\Delta \overline{u'w'}}{\Delta z} \rangle$. Thus within the scale range $l_q<l<l_t$ the defining parameters are $\tilde{q}_z$ and τ, while at $l>l_q$, the defining parameters are $\tilde{q}_z$ and $\tilde{\tau}_z$. Next, considering dimensionality, we get the following expressions for spectrum $E_t(K)$:

$$E_T(K) = \gamma_1 \tilde{q}_z^2 \tilde{\tau}_z^{-1} K^{-2} \qquad (K<K_\tau) \qquad (1)$$

and

$$E_T(K) = \gamma_2 \tilde{q}_z^2 \tilde{\tau}^{-1} K^{-3} \qquad (K_\tau<K<K_q) \qquad (2)$$

where γ_1 and γ_2 are some dimensionless constants. Formulas (1) and (2) are consistent with experimental spectrums in relation to the form of their dependence on K at $K<K_0$ and $K>K_0$ respectively. The interpolation formula for $E_t(K)$ for the entire range of scales under examination may be represented as follows:

$$E_T(K) = \gamma_2 \tilde{q}_z^2 \tilde{\tau}^{-1} K^{-3} \left[\frac{L_\tau K}{1+L_\tau K}\right] \qquad (3)$$

where scale L_τ is defined as $L = (\gamma_1/\gamma_2)\tau/\tau_z$. At $L_\tau K \gg 1$, $E_t(K)$ is described by formula (2), while when $L_\tau K \ll 1$, it is described by formula (1). According to the available data, [symbol left out; possibly L_τ] varies basically within 10 and 20 meters. To directly confirm the possibility of using expression (3), we would need to calculate parameters $\tilde{q}_z$, τ and $\tilde{\tau}_z$ using experimental data, and determine dimensionless constants γ_1 and γ_2. The first information on nonuniform distribution of the heat flux of a thermocline, obtained by means of instrumental measurements, is presented in (2). Heat flux estimates were obtained in (3) with the help of indirect calculations for individual layers; these estimates also vary noticeably in relation to z; at present, however, direct instrumental measurements of vertical profiles $\overline{u'w'}(z)$, suitable for appraisal of τ and τ_z, are unavailable.

Expression (3), which describes spectrum $E_t(K)$ in the finestructure interval, and formulas obtained in (1) for the transitional area between the finestructure interval and one of the subintervals of small-scale turbulence, permit us to derive general interpolation formulas for spectrum $E_t(K)$ within the entire range of wave numbers--from 10^{-4} to 10^{0} cm^{-1}. Naturally in this case the combination $A\tilde{T}_z^2$ in the expressions for scales L_t^*, L_t and L_t^{ν} must be substituted by $\gamma_2 \tilde{q}_z^2 \tilde{\tau}^{-1}$. Then, depending on whether the finestructure interval is followed by the buoyancy, inertial-convective or viscous-convective interval, the spectrum of temperature nonuniformities $E_t(K)$ would be described by one of the following equations:

$$E_T(K) = \alpha_1 \varepsilon_T^{4/5} \beta^{-2/5} K^{-2/5} \left[1 + \frac{L_t K/(1+L_\tau K)}{(L_\tau K)^{4/5}}\right] \quad (4)$$

$$E_T(K) = \alpha_2 \varepsilon_T \varepsilon_u^{-1/3} K^{-5/3} \left[1 + \frac{L_\tau K/(1+L_\tau K)}{(L_\tau K)^{4/3}}\right] \quad (5)$$

$$E_T(K) = \alpha_3 \varepsilon_T \chi_t K^{-1} \left[1 + \frac{L_\tau K/(1+L_\tau K)}{(L_\tau K)^{2}}\right] \quad (6)$$

Considering that $L_\tau > L_t$, L_t^*, L_t^{ν}, at $L_\tau K \ll 1$ these formulas reduce to expression (1), at $L_\tau K \gg 1$ and at $L_\tau^* K$ or $L_t K$, $L_t^{\nu} K \ll 1$ we get the "power of negative three interval," as represented by formula (2), and at $L_t^* K$, $L_t K$ or $L_t^{\nu} K \gg 1$ we get one small-scale turbulence interval or the other. In those cases where scale L_* is found to be greater than the typical scales of deformation of mean temperature and velocity fields--L_τ, the buoyancy interval would be absent from the temperature nonuniformity spectrum, and the general interpolation formula for $E_t(K)$, describing a succession of intervals with powers -2, -3, -5/3 and -1 with growth in K, would be written in the form:

$$E_T(K) = \alpha_2 \varepsilon_T \varepsilon_u^{-1/3} K^{-5/3} \left[1 + \frac{L_\tau K/(1+L_\tau K)}{(L_\tau K)^{4/3}} + (L_\varepsilon K)^{2/3}\right], \quad (7)$$

where $L_\varepsilon = (\alpha_3/\alpha_1^{3/2}) l_\nu$ and $l_\nu = (\nu^3/\varepsilon)^{1/4}$--Kolmogorov's scale. Depending on the relationship between the sizes of scales L_τ, L_t and L_ε in spectrum $E_t(K)$, both the finestructure subinterval, where $E_t \sim K^{-3}$, and the inertial-convective interval may be absent. The results of comparing these formulas with the experimental data showed the possibility of their use to describe $E_t(K)$ spectrums in an ocean thermocline.

We should note in conclusion that if we take the approach indicated above in our analysis of the spectrums of vertical finestructure nonuniformities in the velocity field, then at $K^{-1}>L_T$ spectrum $E_u(K)$ may have the form:

$$E_u(K) = c\tilde{\varepsilon}_2 K^{-2}, \qquad (8)$$

where c is a certain constant. The available information on $E_u(K)$ spectrums calculated on the basis of measurements of the finestructure of the ocean's velocity field, indicates that at $K^{-1}>8$-10 meters, in a number of cases we observe a scale interval for which $E_u(K)\sim K^{-2}$. Inasmuch as L_T is close to 10 meters, use of expression (8) to describe $E_u(K)$ may probably be justified in these experiments.

BIBLIOGRAPHY

1. Lozovatskiy, I. D., "The Spectrum of Vertical Nonuniformities in the Temperature Field of the Ocean Thermocline," IZV. AN SSSR, FAO, Vol 15, No 11, 1979.

2. Lozovatskiy, I. D., and Ozmidov, R. V., "Statistical Characteristics of the Local Structure of Developed Turbulence in the Kuroshio Current," OKEANOLOGIYA, Vol 19, No 5, 1979.

3. Lozovatskiy, I. D., and Ozmidov, R. V., "The Relationship Between the Characteristics of Small-Scale Turbulence and the Parameters of Water Stratification in the Ocean," OKEANOLOGIYA, Vol 19, No 6, 1979.

4. Gregg, M. C., "Variations in the Intensity of Smallscale Mixing in the Main Thermocline," J. OF PHYS. OCEANOGR., Vol 7, No 3, 1977.

A Particular Model of Turbulence Interstratification

M. M. Lyubimtsev

Signals representing variables (pulsations in velocity, temperature and so on) measured in experimental research on ocean turbulence are recorded by low-inertia sensors in the form of a succession of pulses (of varying shape and width) separated by noise intervals of irregular duration. Such pulse modulation of signals is the consequence of turbulence interstratification. An elementary model is suggested for description of such signals. It is used as a framework for examining the influence of interstratification parameters on some statistical characteristics of small-scale turbulence.

Let us examine random process $\xi(t)$, which is the product of stationary random process $u(t)$ with a mean $\langle u(t)\rangle = 0$) and pulse process $I(t)$, in which the time of arisal t_i and duration θ_i of the i-th pulse ($i = 1,2,\ldots$) of unit amplitude are random. Process $I(t)$ may be represented in the form $I(t)=\sum_i I_i(t)$, where $I_i(t)$ is the i-th pulse located randomly on the time axis. Then process $\xi(t)$ may be written in the form

$$\xi(t) = \sum_i u_i(t)\,1\left(\frac{t-t_i}{\theta_i}\right) = \sum_i F_i(t) \qquad (1)$$

Here $1(x) = \chi(x) - \chi(x-1)$, $\chi(x)$ is Heaviside's unit function. Argument $x = (t-t_i)/\theta_i$ was selected in such a fashion that as t varies from t_i to $t_i + \theta_u$--that is, within the limits of the i-th pulse, x varies from 0 to 1; in this case $I(x) = 1$. Outside the limits of pulses, $I(x) = 0$. We will treat process $\xi(t)$ as a model of a unidimensional section of the turbulence field.

To calculate the statistical characteristics of process $\xi(t)$, we would need to introduce a number of hypotheses on its probability structure: 1. The probability that exactly n pulses would arise in time interval T depends on T but not on the position of this interval on the time axis--that is, uniformity of the pulse process is presupposed. 2. The number of pulses arising in nonintersecting time intervals is independent of random variables--that is, there is no "after-effect". 3. The probability that more than one pulse would arise in a small time interval dt is one order of magnitude less than dt--that is, as $dt \to 0$, this probability becomes equal to $0(dt)$. From a physical standpoint this means that arisal of two pulses simultaneously is impossible. 4. All $u_i(t)$, t_i and θ_i are statistically

independent from one another, and their probability distributions do not depend on the pulse number. It may be shown that under these conditions the probability $P_T(n)$ that n pulses will appear in time T would be described by a Poisson distribution with intensity $\lambda = \langle n \rangle / T$.

Let us find the characteristic function $\phi_\xi(s)$ for variable $\xi(t)$ (at a fixed t, this is a random variable, given within interval $[-T/2, T/2]$. The probability of event A--satisfaction of the inequality $x < \xi(t) \leqslant x+dx$--may be written as: $P\{A\} = W_\xi(x)\,dx$, where $W_\xi(x)$ is the probability distribution density for $\xi(t)$. Event A occurs together with one of events B_η ($n = 0,1,\ldots$) forming a complete set of mutually exclusive events, where B_η represents arisal of exactly n pulses in interval $[-T/2, T/2]$. Obviously, $P\{B_\eta\} = P_T(n)$. The conditional probability of event A' is $P\{A|B_\eta\} = W_\xi(x|n)\,dx$ where $W_\xi(x|n)$ is the conditional density. Using the formula for total probability, we can write

$$P\{A\} = \sum_{n=0}^{\infty} P\{B_n\}\, P\{A|B_n\} = W_\xi(x)\,dx = \sum_{n=0}^{\infty} P_T(n)\, W_\xi(x|n)\,dx \qquad (2)$$

Averaging variable $\exp(iS\xi)$ in relation to probability (2), we get the characteristic function

$$\varphi_\xi(s) = \sum_{n=0}^{\infty} P_T(n)\, \varphi_\xi(s|n) \qquad (3)$$

where $\phi_\xi(s|n)$ is the characteristic function of variable $\xi_n(t) = \sum_{i=1}^{n} F_i(t)$. In view of the fourth hypothesis all F_i are statistically independent, and their probability distributions do not depend on number i. Therefore we can write

$$\varphi_\xi(s|n) = [\varphi_F(s)]^n, \qquad (4)$$

where the characteristic function of variable $F(t)$ has the form

$$\varphi_F(s) = \int_{-\infty}^{\infty} W_u(u)\,du \int_0^{\infty} W_\theta(\theta)\,d\theta \int_{-T/2}^{T/2} \exp\left\{is u(t) I\left(\frac{t-\tau}{\theta}\right)\right\} W_t(\tau)\,d\tau \qquad (5)$$

Here, $W_u(u)$ and $W_\theta(\theta)$ are the probability distribution densities for variable $u(t)$ and θ. After some simple transformations we arrive at the formula

$$\varphi_\xi(s) = \exp\left\{\lambda \int_{-\infty}^{\infty} W_u(u)\,du \int_0^{\infty} \theta W_\theta(\theta) \int_{-\infty}^{\infty} \left[e^{isuI(\tau)} - 1\right] d\tau\right\} \qquad (6)$$

Using formula (6), we can find the semi-invariants of the distribution of $\varkappa_k(\xi)$ to the power of k:

$$\varkappa_k(\xi) = \lambda \int_{-\infty}^{\infty} u^k w_u(u)\,du \int_0^{\infty} \theta w_\theta(\theta)\,d\theta \int_{-\infty}^{\infty} I^k(\tau)\,d\tau = \mu \langle u^k \rangle \quad (7)$$

Here parameter $\mu = \lambda \langle \theta \rangle = \langle n \rangle \langle \theta \rangle / T$ is the average interstratification coefficient. In the absence of interstratification, $\mu = 1 (\langle \theta \rangle = T, \langle n \rangle = 1)$ and $\varkappa_k(\xi) = \langle u^k \rangle = \varkappa_k(u)$ for $k = 1, 2, 3$. However, for $k > 3$ these semi-invariants are not coincident, probably due to the rigid conditions imposed on the model.

Let us find correlation function $B_\xi(t, \tau) = \langle \xi(t) \xi(t+\tau) \rangle = \langle \xi \xi_\tau \rangle$. Similarly as when we obtained formula (2), we can obtain an expression for the probability of an event consisting of simultaneous satisfaction of the inequalities

$$x < \xi \leq x + dx \quad \text{and} \quad y < \xi_\tau \leq y + dy$$

Averaging the product $\xi \xi_\tau$ in relation to this probability, we get the expression

$$B_\xi(t, \tau) = B_u(\tau)\, B_I(\tau) = B_\xi(\tau), \quad B_I(\tau) = \lambda \int_\tau^{\infty} (\theta - \tau) w_\theta(\theta)\,d\theta \quad (8)$$

where $B_u(\tau)$ is the correlation function of process $u(t)$, and $B_I(\tau)$ is a dimensionless correlation function satisfying the conditions

$$B_I(0) = \mu, \quad \left.\frac{dB_I(\tau)}{d\tau}\right|_{\tau=0} = -\lambda, \quad B_I(\tau)\Big|_{\tau \to \infty} \to 0 \quad (9)$$

We can see from (7) and (8) that $\xi(t)$ is a steady-state process, at least in the broad sense, and therefore its energy spectrum is a Fourier transform of function $B_\xi(\tau)$.

In order to find function $B_I(\tau)$ in explicit form, we would have to give density $W_\theta(\theta)$ in analytical form. Let us assume, as the evolutionary scheme of turbulent "spots," their independent fragmentation. Then the distribution of the probabilities of the dimensions of such "spots" must be described by a log-normal function

$$w_\theta(\theta) = \frac{1}{\sqrt{2\pi}\,\sigma_{\ln\theta}} \exp\left\{ -\frac{(\ln\theta - m_{\ln\theta})^2}{2\sigma^2_{\ln\theta}} \right\}, \quad (10)$$

where $m_{\ln\theta} = \langle \ln\theta \rangle$, $\sigma^2_{\ln\theta} = \langle (\ln\theta - m_{\ln\theta})^2 \rangle$. Substituting (10) in (8), we get the equation

$$B_I(\tau) = \mu\left[N(x_\tau - \sigma_{\ln\theta}) - \frac{\tau}{\langle\theta\rangle} N(x_\tau)\right], \qquad (11)$$

where $$N(z) = 1 - \frac{1}{\sqrt{2\pi}} \int_{-\infty}^{z} e^{-v^2/2}\, dv, \quad x_\tau = (\ln\tau - m_{\ln\theta})/\sigma_{\ln\theta}$$

Function (11) decreases monotonously with growth of τ, and it satisfies conditions (9). At $\mu = 1$ ($\langle\theta\rangle = T$), function $B_I(\tau) = (1-\tau/T)$. As the length of the realization under consideration increases (as $T\to\infty$), function $B_I(\tau)\to 1$.

Thus the correlation function $B_\xi(\tau)$ of process $\xi(t)$ decreases with growth of τ faster than the correlation function $B_u(\tau)$ of process $u(t)$. In this case spectrum $E_\xi(f)$ of process $\xi(t)$ will decrease with growth in frequency f more slowly than spectrum $E_u(f)$ of process $u(t)$, since in the limiting case a uniform "white noise" spectrum corresponds to a delta-correlated process. Here lies the influence of interstratification on the correlation and spectral functions. Unfortunately we cannot obtain spectrum $E_\xi(f)$ (which is a convolution of spectrums $E_u(f)$ and $E_I(f)$)) in explicit form and evaluate the influence of interstratification parameters on the spectral components of process $u(t)$ in different intervals of frequencies (scales), since we do not know function $B_u(\tau)$ (or function $E_u(f)$), while the Fourier transform of function (11) cannot be expressed by either elementary or special functions, and it requires numerical computer calculation.

Use of Dynamic Stochastic Models for Integrated Treatment of Oceanological Measurements

V. A. Moiseyenko

High cost is a typical feature of oceanographic expeditionary research. Therefore to raise the effectiveness of expeditions, we usually make integrated measurements of a large number of oceanographic and meteorological parameters using a relatively rare network of observations. A broad complex of measurements are made today in traverses: measurements by autonomous buoy stations, density maps plotted with the help of hydrological stations and depth, temperature and salinity probes, and so on. Clearly by raising the informativeness of measurements made at each station, we can increase the accuracy of a particular hydrophysical field under analysis (2). Therefore when we plot hydrophysical field maps we must consider the question of integrated use of all available information, both on the field itself and on other fields and statistical relationships existing between different fields.

When we study synoptic variability, which reveals itself in analysis of different fields of the ocean, we must consider the asynchrony of the measurements and the irregularity of their spatial representation; otherwise maps plotted directly from such data by traditional methods may reveal a smoothed-out picture (5). Dynamic-stochastic models permit optimum treatment of practically any quantity of measurements of different kinds, reported at arbitrary moments of time from different points in space. The essence of the dynamic-stochastic approach lies in "numerical" forecasting based on a thermohydrodynamic model providing for simultaneous correction of calculated values by observed data (1,2).

This paper discusses a dynamic-stochastic model permitting joint treatment of measurements of density fields and the horizontal component of current velocities. If we limit ourselves to a quasigeostrophic approximation and an approximate determination of surface level (4), we could calculate the correlation and mutual correlation functions for discrepancies in the horizontal components of current velocity using the formula

$$P_{\delta v_i \delta v_j}(\vec{x},\vec{x}',t_m)=(-1)^{i+j}\left(\frac{g}{f\rho_0}\right)^2\frac{\partial^2}{\partial x_i \partial x_j'}\int_0^H\int_0^H P_{\delta\rho}(\vec{x},\vec{x}',t_m)\,d\zeta\,d\zeta',$$

where $i,j=1,2$, $x_1=y$, $x_2=x$, $P_{\delta\rho}(\vec{x},\vec{x}',t_m)=E\{\delta\rho(\vec{x},t_m)\cdot\delta\rho(\vec{x}',t_m)\}$ --correlation function of the density field prediction errors, f--Coriolis parameter, g--gravity, ρ_0--density of sea water.

Correlation function $B_{\delta\rho}(\vec{x},\vec{x}',t)$ has a large scale. Therefore in order to be able to calculate it with a computer of average capacity, as a rule we resort to some sort of approximation. In this model $B_{\delta\rho}(\vec{x},\vec{x}',t)$ was represented by the following approximate formula:

$$P_{\delta\rho}(x,y,z,x',y',z',t)=D(x,y,t)\cdot D(x',y',t)\cdot P_0(x-x',y-y')\cdot f_0(z,z').$$

where $D(x,y,t)$ is an unknown function (standard deviation) and P_0 and f_0 are known functions (6).

Let us examine the use of the proposed model (6) to process measurements of density fields and the horizontal component of current velocity vectors. The calculations were performed for the central part of the traverse ($\phi=27°01'$ and $30°59'$ N. Lat., $\lambda=68°$ and $72°$ W. Long.). The selected region was covered with an observation network having a spacing $\Delta x=\Delta y=17$ nautical miles in the horizontal plane and $\Delta z=200$ meters in the vertical plane to a depth of 1,600 meters. The time interval was 1 day. The density of sea water at the boundaries was corrected after each batch of observations were received; this made it possible, in the final analysis, to account for evolution of real boundary conditions.

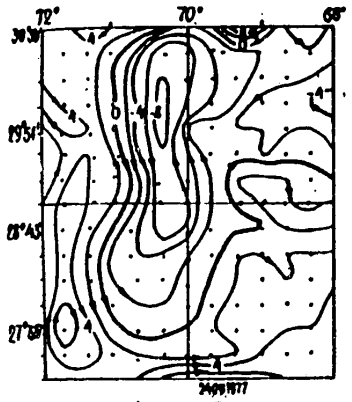

Figure 1

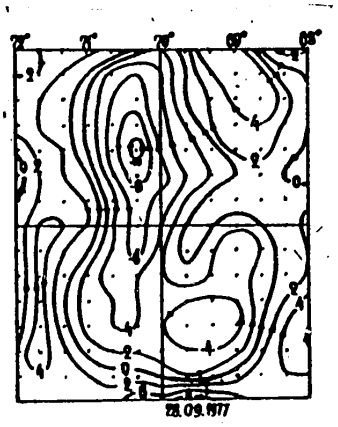
Figure 2

Using the suggested procedure for joint treament of diverse measurements, we plotted density field maps, the surface level and current velocities with a time interval of 1 day.

Figures 1-3 are maps showing the surface levels for the traverse (arrows indicate the direction of surface gradient current, and numbers on isolines indicate the surface level in centimeters).

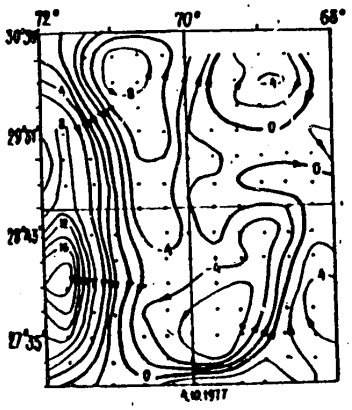

Figure 3

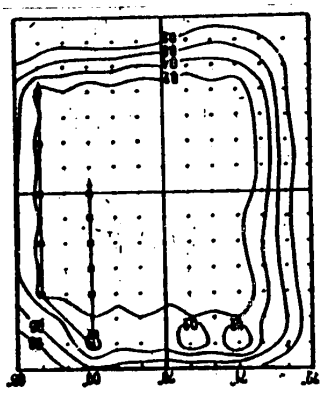

Figure 4

Analysis of surface level maps plotted successively each day allows us to trace the evolution of surface level in the traverse and appraise the direction and velocity of travel of eddy formations, as well as trace invasion of the traverse by new eddy formations.

Concurrently with optimal assessment of the fields under analysis, this dynamic-stochastic model permits computation of maps indicating their reliability, which was determined on the basis of the dispersion of assessment errors. A sequence of such maps allows us to plan the measurement scheme to be implemented in real time (Figure 4).

A comparison of results from processing measurements obtained by our procedure with others (3) permits the assertion that the maps we obtained exhibited greater detail in relation to both time and space.

BIBLIOGRAPHY

1. Gandin, L. S., and Kagan, R. L., "Statisticheskiye metody interpretatsii meteorologicheskikh dannykh" [Statistical Methods for Interpreting Meteorological Data], Leningrad, Gidrometeoizdat, 1976, pp 312-339.

2. Nelepo, B. A., and Timchenko, I. Ye., "Sistemnyye printsipy analiza nablyudeniy v okeane" [Systemic Principles of Analysis of Observations in the Ocean], Kiev, "Naukova Dumka", 1978, 250 pp.

3. Nelepo, B. A., Knysh, V. V., and Timchenko, I. Ye., "Evolution of Synoptic Eddies According to Materials From Density Surveys Made by the Ukrainian SSR Academy of Sciences Marine Hydrophysical Institute in the Polymode Traverse," Preprint #3, Sevastopol', Izd-vo MGI AN USSR, 1978.

4. Sarkisyan, A. S., "Chislennyy analiz i prognoz morskikh techeniy" [Numerical Analysis and Prediction of Marine Currents], Leningrad, Gidrometeoizdat, 1977, pp 28-33.

5. Knysh, V. V., Moiseyenko, V. A., and Timchenko, I. Ye., "Assimilation of Hydrophysical Measurements in a Numerical Model of Ocean Density and Current Fields," MORSKIYE GIDROFIZICHESKIYE ISSLEDOVANIYA, Sevastopol', No 4 (83), 1978, pp 65-77.

6. Timchenko, I. Ye., Knysh, V. V., and Moiseyenko, V. A., "Integrated Use of Hydrophysical Information in an Algorithm for Four-Dimensional Analysis," MORSKIYE GIDROFIZICHESKIYE ISSLEDOVANIYA, Sevastopol', No 1 (88), 1980, pp 65-76.

The Concept of Finestructure and Its Discrimination in the Ocean

V. V. Navrotskiy

When we refer to the vertical finestructure of hydrophysical characteristics in the ocean, we imply presence of layers having properties exhibiting vertical gradients that change abruptly; in this case the thickness of such layers is much less than the associated integral vertical scales (total depth, thickness of the baroclinic layer and so on). In similar fashion we can interpret fast fluctuation of properties in horizontal coordinates as a manifestation of horizontal finestructure, but for the moment it is of lesser interest to us.

The importance of studying finestructure stems from its interaction with all dynamic processes in the ocean--currents, internal waves and turbulence. A universally accepted definition of finestruction does not exist, and different authors discriminate finestructure in different ways: as a deviation from some temporal mean (3,6), as a deviation from a hypothetical linear profile (7) and so on. In all cases discrimination of finestructure from fluctuations in characteristics elicited by dynamic properties, especially internal waves (4,5), is a major problem. And yet such discrimination is necessary, inasmuch as the methods of mathematical description of hydrophysical processes require us to give the characteristics of the medium as parameters of a process, or vice versa.

The physical grounds for referring to changing parameters either as an attribute of the medium's structure or as a process are the widely different scales of variability--that is, the great differences in the rates at which these parameters change. In this case those parameters of the medium which change little in the time (or space) it takes for certain classes of processes to occur are applied to the structure of the medium. The division made between medium structure and process is arbitrary, and definitions of structure in most cases imply a process, the scale of which is significantly smaller than the scale of the medium's structure.

In our case in addition to indicating the class of processes in relation to which finestructure is a "structure," we need to explain the meaning of the word "fine"--that is, we need to indicate those processes which take no notice of such a structure. This is rather easy to do: Large-scale currents, mesoscale eddies and tidal waves do not for practical purposes react to finestructure--that is, averaging in relation to the scales of these processes would reveal the distinction between unfine, coarse structure in the low frequency range and finestructure in the high frequency range. But in this case finestructure and processes with scales less than the discrimination scale would be mixed together.

Internal waves are the most significant and universal dynamic process reacting responsivelyto finestructure. But the rangesof scales of internal waves and finestructure intersect practically completely, and therefore it is impossible to discriminate between them absolutely. Moreover, as was shown earlier (2), internal waves cause arisal of irreversible changes in the vertical gradients of properties (when averaged over a time period on the order of tens of wave cycles), and therefore they may be a significant factor in finestructure formation. At the same time, internal waves and finestructure distort one another kinematically.

Defining the finestructure concept with an indication of one of two filtration scales, both of which are associated with internal waves, is suggested. The first, smaller scale distinguishes structure (at large scale) from process (at small scale). The second, larger-scale filtration distinguishes coarse (meso-) structure from finestructure. For temperature in particular, this definition would have the following form:

$$T(z,t) = \hat{T}(z,t) + T'(z,t) = \bar{\hat{T}}(z,t) + \hat{T}_f(z,t) + T'(z,t) \quad (1)$$

Here, $\hat{T}$--the complete structure--that is, the low frequency part of function $T(z,t)$ when filtration time is equivalent to the period of internal waves propagating in the layer under examination; T'--process occurring in the structure; $\bar{\hat{T}}$--meso- (coarse) structure--that is, the low frequency part of function $\hat{T}(z,t)$ in relation to the second filtration scale; $\hat{T}_f$--vertical finestructure of parameter T. Distortions in finestructure caused by internal waves may be deleted by changing the averaging process: Rather than function $T(z,t)$, we would need to time-average the reciprocal function $z(T,t)$ for the range of values of T of interest to us. This procedure produces mutually unique correspondence between T and z in segments of monotonous change in $T(z)$. Given this assumption, for structure $\bar{T}$ obtained by inverse averaging and regression to the temperature profile, expression (1) would have the form:

$$T(z,t) = \check{T}(z,t) + T'(z,t) = \bar{\check{T}}(z,t) + \check{T}_f(z,t) + T'(z,t) \quad (2)$$

Inasmuch as the internal wave spectrum is very broad, this definition implies that the kinematic effects of low frequency and large-scale internal waves would be described as a structure for high frequency and small-scale internal waves, while finestructure elements with a life span less than the filtration scale would fall into the process category, and they may drop out from the averaging process. Physically and methodologically, such a situation is entirely reasonable, since we are always interested in specific ranges of scales and periods, into which internal waves and finestructure must (and can) be divided.

Large-scale filtration with respect to time, performed with the purpose of discriminating between coarse and finestructure, would best be substituted by filtration in relation to the vertical coordinate, inasmuch as the vertical scales of large-scale processes are well known.

An analysis of the results of several soundings of temperature and current velocity fields from the standpoint of the proposed definitions and discrimination methods demonstrated their suitability. Distortions in finestructure arising due to vertical movements and appearance of compression-rarefaction zones in isolines during the

passage of internal waves decrease significantly. Maximum gradients increased while minimum gradients decreased by approximately two times in observations of a not-too-abrupt finestructure in the upper 40-meter layer. Differences in abruptly stepped structures grow in this case. In terms of reducing distortions, description of finestructure by means of probability distributions is equivalent (1).

The proposed definition, which uses internal waves as the reference-point process for discriminating finestructure, does not exclude the role of numerous other factors (laminar advection, double diffusion, turbulence in response to disruption and so on) in formation of finestructure, but it may change their position in relation to finestructure. Thus irrespective of vertical scales, long-period laminar advection may fall within mesostructure, while the effects of turbulence having periods less than the Vyaysyal' frequency do not necessarily fall within the finestructure category (the highest-frequency internal waves are found to represent the lower boundary of microstructure). Therefore the advantages and shortcomings of this interpretation of the finestructure concept require discussion.

BIBLIOGRAPHY

1. Navrotskiy, V. V., "Distribution of the Probability Characteristics of Finestructure in the Shelf Zone of the Sea," IZV. AN SSSR. FIZIKA ATMOSFERY I OKEANA, in press.

2. Navrotskiy, V. V., "Finestructure and Internal Waves in the Ocean," DOKLADY AN SSSR, Vol 231, No 5, 1976, pp 1080-1083.

3. Fedorov, K. N., "The Finestructure of Hydrophysical Fields in the Ocean," in "Seriya 'Okeanologiya', fizika okeana" ["Oceanology" Series, Physics of the Ocean], Vol 1: [Hydrophysics of the Ocean], Chapter III, Nauka, Moscow, 1978, pp 113-147.

4. Joyce, T. M., "Finestructure Contamination of Moored Temperature Sensors: A Numerical Experiment," J. PHYS. OC., Vol 4, No 2, 1974, pp 183-190.

5. Joyce, T. M., and Desaubies, Y. J. F., "Discrimination Between Internal Waves and Temperature Finestructure," J. PHYS. OC., Vol 7, No 1, 1977, pp 22-32.

6. Hayes, S. P., "Temperature Finestructure Observations in the Tropical North Pacific Ocean," J. GEOPHYS. RES., Vol 83, No C10, 1978, pp 5099-5104.

7. Siedler, G., "The Finestructure Contamination of Vertical Velocity Spectra in the Deep Ocean," DEEP-SEA RES., Vol 21, No 1, 1974, pp 37-46.

Intrusions and Differential-Diffusional Convection in Cromwell's Current

V. T. Paka

The scientific research vessel "Dmitriy Mendeleyev" sailed its 24th trip in February-March 1980 with the purpose of studying circulation and the structure of hydrophysical fields in the equatorial system of Pacific Ocean currents (2). A traverse was selected between 163°W. Long. and 167°W. Long., 2°N. Lat. and 2° S. Lat.. The main effort was concentrated on meridional sections at the eastern and western edges of the traverse, with 11 stations and 5 buoys on each section. The hydrological measurements were made according to the usual procedure, and they were supplemented by detailed measurements of drifting current curves, inasmuch as the number of current recorders on buoys was not enough to study the profile of current shifts in the vicinity of Cromwell's current, which was the principal object of the study. Microstructural measurements were made with a falling "Baklan" probe (3) containing sensors for velocity pulsation u', electrical conductivity σ', and the means of electrical conductivity $\overline{\sigma}$ and temperature $\overline{t}$.

The World's Ocean equatorial currents are known as a region of intense, constant shearing action coupled with a corresponding rise in the intensity of turbulent mixing (5,7). This feature manifested itself in our measurements as well, as can be seen for example in Figure 1, showing oscillograms for vertical soundings of u' on the background of a cross section of the zonal component of the current velocity, plotted by V. A. Bubnov and V. D. Yegorikhin. In normal regions with a moderate wave state, the thickness of turbulent layers does not exceed 10-30 meters, while in a region with shearing action we often observe turbulent layers with a thickness of 50 meters and more, sometimes reaching 120 meters. The weakly stratified layer above the center of Cromwell's current exhibits dominant turbulence. The center itself is not turbulent, and as we found in our case, this permitted development of other forms of mixing. A unique frontal zone is known to exist in the salinity field along the equator in the Pacific (1). At the depth of Cromwell's current its maximum is to the south and its minimum is to the north of the equator. Owing to the convergent nature of circulation in the central part of the equatorial zone, currents of different salinity invade into the center of Cromwell's current from peripheral regions, resulting in formation of temperature inversions. This phenomenon is illustrated by Figure 2, which shows the sounding profiles for σ'. The leftward peaks on these profiles correspond to temperature inversion gradients. Inversions were observed on all cross sections and in all profiles intersecting the axial region of Cromwell's current, while in the periphery they were found to be atypical. It is interesting that inversions were not observed in Gregg's measurements made further east, at 155° W. Long. (5). Such differences are apparently associated with the unique features of the convergent regime of the equatorial current system.

A detailed analysis of the inversions showed that they vary in scale and nature of accompanying phenomena. Large inversions in thick layers (10 meters and more) are often accompanied by higher activity of microstructural pulsations of σ', and sometimes of u' as well, indicating active intrusion and turbulent injection of water into the intruding layer out of over- and underlying layers. Thin inversions (less than 1 meter) are observed as a rule between quasi-uniform layers without signs of active or relict turbulence. It would be logical to hypothesize the action of differential-diffusional convection, for the arisal of which all of the prerequisites exist: Temperature inversions are accompanied by an increase in salinity coupled with maintenance of sustained density stratification, as is evidenced by the results of selective measurements of the finestructure of temperature, salinity, and density with an AIST probe. The density ratio $R_\rho = \beta \Delta S / \alpha \Delta T$ for such inversion interlayers is close to 2, which is typical of the action of double diffusion (4).

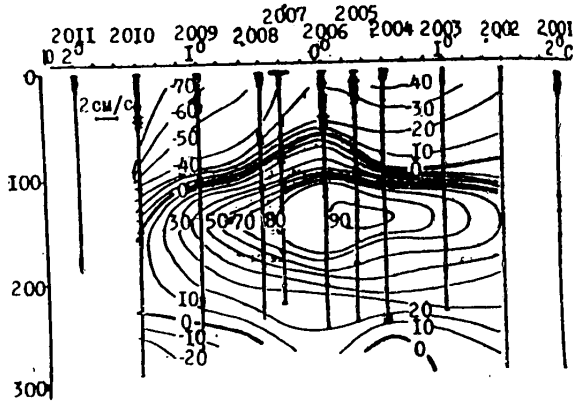

Figure 1. Velocity Pulsation Profiles for the Center of Cromwell's Current

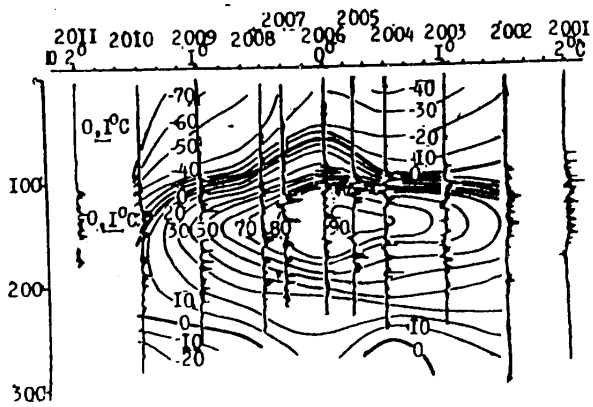

Figure 2. Profiles of Finestructure Electrical Conductivity Gradients and Pulsations in the Center of Cromwell's Current

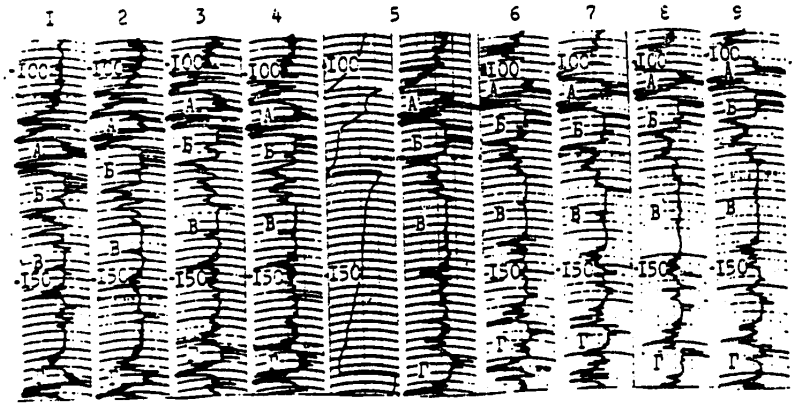

Figure 3. A Series of Successive Soundings of σ' in the Center of Cromwell's Current, Station 2004: The polarity of the signal is the inverse of that in Figure 2.

Figure 3 shows a series of nine successive profiles (the profile for $\bar{t}$ is also given for the fifth sounding). This series demonstrates different types of inversions and their evolution. In Figure 3, the inversions are directed to the right. The letter A represents a major inversion with a gradually attenuating microstructure; Б--a quasi-uniform layer with typical thin inversion interlayers; В--apparently the end result of double diffusion; Г--a layer in which inversion interlayers are gradually forming.

Thus is can be asserted that the finestructure of the center of Cromwell's current in the region of the traverse forms as a result of convergent phenomena stimulating development of intrusions from the periphery into the axial zone, and that differential-diffusional convection was the principal factor defining the evolution of these intrusions. Stratification typical of the action of double diffusion was observed for 2 months, and it was so well developed that it could serve as a tracer for Cromwell's current.

BIBLIOGRAPHY

1. Burkov, V. A., "Obshchaya tsirkulyatsiya Mirovogo okeana" [The General Circulation of the World Ocean], Leningrad, Gidrometeoizdat, 1980.

2. Paka, V. T., Pozdynin, V. D., and Bubnov, V. A., "The 24th Trip of the Scientific Research Vessel 'Dmitriy Mendeleyev'," OKEANOLOGIYA, in press, 1980.

3. Paka, V. T., "Apparatus for Studying the Finestructure of Hydrophysical Fields," in the present collection, 1980.

4. Terner, Dzh., "Effekty plavuchesti i khidkostyakh" [Effects of Buoyancy in Liquids], Moscow, "Mir", 1977.

5. Gregg, M. C., "Temperature and Salinity Microstructure in the Pacific Equatorial Undercurrent," J. GEOPHYS. RES., Vol 81, No 6, 1976, pp 1180-1196.

6. Gregg, M. C., "Microstructure and Intrusions in the California Current," J. PHYS. OCEANOGR., Vol 5, 1975, pp 253-278.

7. Osborn, T. R., and Crowford, W. R., "Microstructure Measurements in the Atlantic Equatorial Undercurrent During GATE," DEEP SEA RES., in press, 1979.

Apparatus for Studying the Finestructure of Hydrophysical Fields

V. T. Paka

When studying small-scale nonuniformities in hydrophysical fields, it is fundamentally important to reduce, to a necessary minimum, interference caused by vibration and yawing of the sensor carrier owing to poor streamlining of the housing or effects exerted by the cable used to submerge or tow the instrument. One of the simplest ways to achieve this goal is to use freely falling probes. Different variants of such probes are known, differing in the particular way smooth motion is achieved and information is transmitted: The completely self-contained probe (3); a probe which, as it falls, unwinds a thin conductor from a reel, typically used in disposable temperature probes (4); a probe permanently connected to the vessel by an unweighted neutral-buoyancy cable that is dropped into the water (2). The "Baklan" probe described here is similar to the last of the falling probe variants mentioned here. Information is transmitted by a thin, flexible type KG 3-3-70 (KTSh-03) cable. Presence of a strong cable makes recovery of the probe to the surface and its reuse possible. The "Baklan" probe is equipped with sensors for electrical conductivity σ, velocity pulsations u', temperature t and depth h. The electrical conductivity sensor, developed by the Special Design Office of Oceanological Technology, has as its sensitive element a platinum microelectrode with a diameter of 0.5 mm, which permits high spatial resolution. Electric filters divide the signal into constant and pulsating components, which are then recorded separately. In this case the right channel records the profile of fine stratification while the second records the superimposed profiles of microstructural pulsations and finestructural gradients. The latter are recorded owing to the action of an electric filter that operates as a differentiating unit at frequencies measured in units of Hertz. In the first approximation, the electrical conductivity profiles reflect temperature profiles, and they are graduated in degrees. A signal from the temperature sensor, which due to the inertia of the thermistor does not bear information on fine stratification itself, is used to account for nonlinearity and zero drift.

The sensitive element of the velocity pulsation sensor is a pair of point electrodes located within the field of a strong magnet in such a way that when sea water streamlines the sensor along its axis, pulsations of the oncoming flow's longitudinal components are recorded (1). The channel's sensitivity is about 0.5 mm/sec.

Depth is measured by a standard vibration-frequency pressure gage with an error of about 1.5 meters; however, because of the high smoothness of its movement, the thickness and mutual arrangement of individual layers can be determined with an accuracy in the units of centimeters.

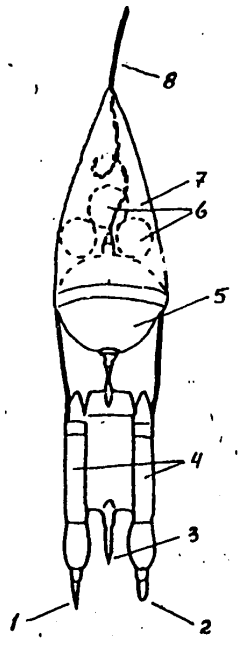

Figure 1. Structure of the "Baklan" Falling Microstructural Probe: *1*--σ sensor, *2*--u' sensor, *3*--t sensor, *4*--cylindrical sealed containers, *5*--spherical sealed container, *6*--(kukhtyli), *7*--cone, *8*--cable

The structure of the probe is shown in Figure 1. Motion is retarded by the use of a spherical sealed container with positive buoyancy; the latter, however, was found to be insufficient. Additional weight compensation is achieved by polyethylene (kukhtyli) from fishing trawls with a buoyancy of 3 kg each, secured to the inside of the cone. The cone is made from close-woven fabric stretched over a framework. The batteries are located in the spherical container, while the electronic blocks of the measuring circuit are in the cylindrical containers. The signal is transmitted by cable in analog form (besides the FM depth signal, which is demodulated aboard the vessel), and it is recorded on magnetic tape and by high-speed stylus recorders. The magnetic recording may be made both in analog form (using type NO-62 or R-400 tape recorders) and in digital form with a quantization frequency of 200 Hz. This system is supported by a specially developed complex based on an "Elektronika 100 I" computer and a connected 17-track LMR tape recorder designed by the Special Design Office of the USSR Academy of Sciences Institute of Physics of the Earth. This provides a possibility for immediate raw data processing, as a result of which all of the primary signals are plotted in a scale convenient to analysis as functions of depth, and the profiles for the mean square values of pulsations, dissipation velocities ε and χ, and Cox' number can be calculated and plotted in the same scale. Parameters χ and c are calculated for the profiles of electrical conductivity, which

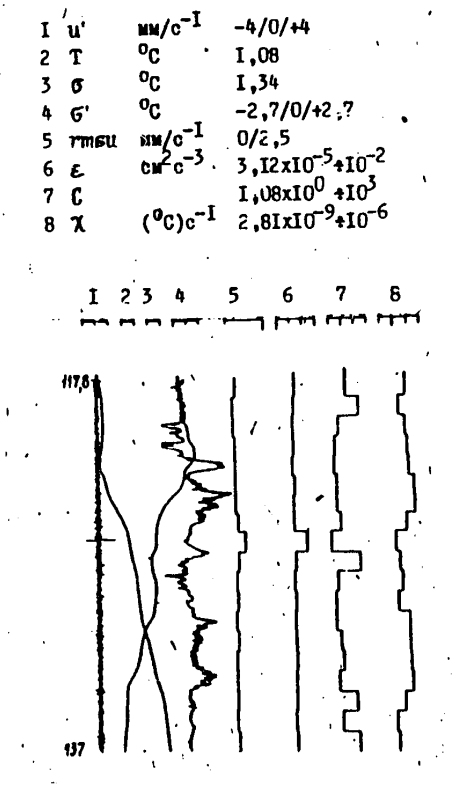

Figure 2. Examples of Sounding Results Following Computer Processing. The scale is in keeping with a "Konsul" printout; each scaling segment corresonds to a line in the table above, indicating the units and values of the scaling marks.

is used as an analog of temperature, though with a consideration for the nonlinearity of the sensor's characteristic. Statistical calculations are made for series of 200 terms, which at a probe submergence rate of about 1 meter/sec corresponds to a layer thickness of 1 meter. Figure 2 shows an example of data plotted successively profile after profile with a two-coordinate H 306 recorder. Scaling segments are printed out simultaneously, and all numerical characteristics of the scales, to include the initial and final depth marks, are printed out and then graphed.

The probe is used with a cable up to 500 meters long. The actual sounding depth depends on the length of the cable, while the rate of submergence (1 meter/sec) and the probe's rate of drift relative to the vessel depend on the resultant action of wind drift and deep-water currents. The greatest drift was observed in research on Lomonosov's and Cromwell's undercurrents; when the cable was completely played out in these areas, the sounding depth was 300 meters.

The "Baklan" probe has enjoyed broad application in hydrophysical studies by various vessels, aboard which it was used as a rule together with freight winch drums. Practice has shown that the resultant recording error, in relation to layers for which pulsations in μ' and σ' could be assumed to be absent on the basis of general physical considerations, does not exceed 1 mm/sec for the u' channel and 10^{-3}°C for the σ' channel, in a frequency range from 5 to 100 Hz in all sea states. Its simplicity and reliability are sufficient to many purposes. Its sensitivity and all-weather capacity make the probe's future look promising.

BIBLIOGRAPHY

1. Golubev, Yu. Ye., Vasilevskiy, V. V., and Turenko, V. V., "A Sensor Determining the Flow Rate of Electrically Conductive Water. USSR Author's Certificate No 685954," BYULL., No 34, 1979.

2. Galagher, B., "Vertical Profiles of Temperature and Fine-Scale Velocity Structure in the Thermocline," J. GEOPHYS. RES., Vol 81, No 6, 1976, pp 1201-1206.

3. Gregg, M. C., and Cox, C. S., "Measurements of the Oceanic Microstructure of Temperature and Electrical Conductivity," DEEP SEA RES., No 18, 1971, pp 925-934.

4. Osborn, T. R., and Crowford, W. R., "Microstructure Measurements in the Atlantic Equatorial Undercurrent During GATE," DEEP SEA RES., in press, 1979.

Activation of Small-Scale Turbulence by Internal Waves in the Presence of Fine Microstructure

Ye. N. Pelinovskiy, I. A. Soustova

Internal waves are known to interact with turbulence in different ways: On one hand internal waves may be damped by external turbulence produced, for example, by wind waves, while on the other hand as a result of shear instability internal waves may generate "secondary" turbulence located in small interstratifications.

This report examines a number of questions associated with generation of "secondary" hydrodynamic turbulence.

1. The relationship between internal waves and turbulent perturbations B', generated by internal waves, is found.

2. The life span of turbulent perturbations is determined within the framework of the unstationary problem of generation of "secondary" turbulence by the shear instability of internal waves.

3. Change in equilibrium density distribution is determined on the basis of the calculated level of turbulent pulsations B'.

Let us dwell in greater detail on each of these problems.

1. In the absence of wave-caused perturbations, together with the boundary conditions the system of semi-empirical turbulence equations [symbol omitted from original] determines some stationary equilibrium distribution defined by the functions $P_0(z)$--equilibrium pressure, $\rho_0(z)$--the density, and the energy of turbulent fluctuations--$B_0(z)$ (z is oriented along the nonuniformity gradient). The appearance of this equilibrium distribution depends significantly on the type of boundary conditions. Thus for example, one of the possible types of stationary distributions is $B_0(z) = \text{const}$; in this case the buoyancy flux $\Pi \sim K_{\rho z}(d\rho_0/dz)$ (where $K_{\rho z}$ is the diffusion coefficient for density) and the turbulent energy flux $M \sim K_{Bz}(dB_0/dz)$ (where K_{Bz} is the diffusion coefficient for turbulent energy) are correlated. This situation is not typical of VPS [not further identified] (turbulence occupies an area of limited depth). However by calculating the level of turbulent fluctuations B' on background B_0, we can appraise the relative value of these perturbations, and from the shift in phases we can appraise their three-dimensional structure. Analyzing propagation of turbulent perturbations,

$b' \sim \exp i(\omega t - i\kappa_x x - i\kappa_z z)$ generated by internal waves $u' \sim \exp i(i\omega t - i\kappa_x x - i\kappa_z z)$ on the background $B_0 = \text{const}$, we get

$$b' = \frac{i u' \Pi \kappa_x}{\omega' R}\left(1 + \kappa_z^2 K_{pz} \Pi / 2 b_0 \omega' R\right) \qquad (1)$$

Here, K_x, K_z--horizontal and vertical wave numbers, ω--internal wave frequency, u'--amplitude of horizontal velocity,

$$R = (1 - i\omega^{-1} T_{dif}^{-1})(1 - i\omega^{-1} T_{dif}^{-1} - i\omega^{-1} T_{dis}^{-1} - i\omega^{-1}\Pi/2b_0) ,$$

T_{dis}--typical dissipation time for turbulence energy into heat, $T_{dif} \sim (K_{px}\kappa_x^2 + K_{pz}\kappa_z^2)$--diffusion time for tubulence energy. It would not be difficult to show that if the wave period is small ($T \ll T_{dif}, T_{dis}$), the amplitude of turbulent perturbations B' would be associated with the amplitude of horizontal velocity by the relationship

$$\begin{aligned} b'/b_0 &= u'/v_\phi (R_i T)^{1/2} N/\omega \qquad l_{Tz} \ll 2\pi\kappa_z^{-1} \\ b'/b_0 &= u'/v_\phi (R_i T)^{1/2} N/\omega \left(1 + N^2/\omega^2\right) \quad l_{Tz} \simeq 2\pi\kappa_z^{-1} \end{aligned} \qquad (2)$$

where $R_i T = l_{Tz}^2 N^2/b_0$, $v_\phi = \omega/\kappa$

In this case the "turbulent" structure is shifted $\pi/2$ relative to the wave structure. If, however, the wave period becomes commensurate with one of the characteristic times T_{dis} or T_{dif}, then the phase shift ϕ depends on frequency, and it is defined by the relationship $\varphi = \arctg(\omega^{-1} T_{dif}^{-1})$

Thus the level of "secondary" turbulence changes significantly depending on $R_i T$, l_{Tz}. Thus if $l_{Tz} \ll 2\pi\kappa_z^{-1}$, then at $R_i \simeq 0.1$ and $B'/B_0 \simeq u'/V_\phi$, $\omega = 0.3N$; but if $l_{Tz} \simeq 2\pi K_z^{-1}$, then $\omega \simeq 0.7N$.

2. Using the nonstationary equation for the balance of the kinetic energy of turbulent fluctuation, we analyze activation of "secondary" turbulence by the shear instability of an internal wave. Assuming that a) the instability condition $(du'/dz)^2 > 4N^2$ is satisfied (where du'/dz is the vertical shift of horizontal velocity and $N^2 = g\rho_0^{-1}(d\rho_0/dz)$ is the square of the Vyaysyal' frequency); and b)

$(du'/dz)^2 N^{-2} > u'/v_\phi$ (where V_ϕ is the phasal velocity of internal waves), then for the conditions of the real ocean this equation has the typical form

$$\frac{\partial b}{\partial t} - u'\frac{\partial b}{\partial x} - v'\frac{\partial b}{\partial z} - \frac{\partial}{\partial x}\left(K_{bx}\frac{\partial b}{\partial x}\right) - \frac{\partial}{\partial z}\left(K_{bz}\frac{\partial b}{\partial z}\right) = K_{pz}\left(\frac{du'}{dz}\right)^2 N^2 - \varepsilon \qquad (3)$$

Here, u', v'--horizontal and vertical velocity of average wave motion, $K_{\rho\vec{r}} \sim \varkappa_\rho K_{\vec{r}}$, $K_{b\vec{r}} \sim \varkappa_b K_{\vec{r}}$--diffusion coefficients for density ρ_0 and energy B, $K_{\vec{r}} = l_{\vec{r}} \sqrt{B}$--coefficient of turbulent viscosity, l_{tr}--turbulence scales, $\varepsilon \sim \alpha$, $(K_x/l_{tx}^2 + K_z/l_{tz}^2)$--dissipation of the energy of turbulence into heat. We will assume scales l_{tr} to be given in regard to activation of secondary turbulence.

If $u(u',v')$ is a flat traveling wave propagating in a medium with $N = \text{const}$, then it would not be difficult to show that the main contribution to activation of "secondary" turbulence in time $T \ll T_{dif}$ is made by a constant shift component $(du/dz)^2$. Inasmuch as in this case $(du/dz)^2$ does not depend on the coordinates, (3) becomes significantly simpler. Thus

$$b = \frac{\varkappa_\rho}{\alpha} l_{tz} \frac{(2K_z^2 u^2 - N^2)}{(K_x + K_z)} \left\{ th\left(t \varkappa_\rho l_{tz} (2K_z^2 u^2 - N^2) \alpha^{-1} (K_x + K_z)^{-1}\right) \right\}^2 \quad (4)$$

At small t, the level of B grows in proportion to t, while the rate of growth is $dB/dt \sim u^4$. At large t, B attains a value on the order of

$$b_{cr.} = \varkappa_\rho l_{tz} (2K_z^2 u^2 - N^2)/\alpha (K_x + K_z)$$

The typical growth time is $t_н \simeq l_{tz} u^{-1} (\varkappa_\rho \alpha)^{-1/2}$.

When the internal wave is "switched off" (when $du/dz = 0$) the stationary distribution dissipates in time $t \approx (\varkappa_\rho \alpha N^2)^{-1/2} \ll T_{dif} \approx (K_z K_{bz})^{-1}$. Inasmuch as the growth time depends on the size of shift du'/dz), at large shift values $t_{нар.}$ may be significantly lower than the dissipation time (or the diffusion time) of secondary turbulence. This means that the generated perturbations are long-lived (T_{dif} is on the order of several hours, t ≈1-10 min).

3. The "secondary" turbulence diffusion problem must be solved as a nonlinear problem with a consideration for natural turbulence. To describe this process, we need to use the equation for the balance of turbulent energy with boundary conditions

$$K_{bz} \frac{db}{dz} = -M \qquad K_{\rho z} \frac{d\rho}{dz} = \Pi \quad \begin{matrix} (z=0) \\ (z=-H) \end{matrix} \qquad b = b_0 \qquad (5)$$

Moreover we need to introduce the source of "secondary" turbulence into the right side of the balance equation; we represent this source as $b_0 \Delta l \, \delta(z-z_0) \delta(t)$

where Δl--characteristic dimension of the region within the interstratification in which turbulence is generated, $\delta(z-z_0)\delta(t)$ --Delta function, z_0--depth of

interstratification. Inasmuch as adjustment of the equilibrium profile $B_0(z), \rho_0(z)$, determined by boundary conditions (5), proceeds slowly (T_{dif} is on the order of several hours), we can solve the stationary problem $\delta B/\delta t = 0$ at a low level of secondary turbulence. Relative change in the equilibrium density profile may be described in this case by the expression

$$\Delta\rho_0/\rho_0 = 10^3 \Pi^{-1} M^{4/3} K_{bz} \Delta\ell\, b_0 (\ell_{Tz}^4 g)^{-1} \qquad (6)$$

Considering the unperturbed distribution of density $\rho_0(z)$, we can find the shift in level connected with change in density, $\xi = -\Delta\rho_0/\rho_0 g N^2$. Given typical parameters for the upper layer of the ocean, the level drops by 50 cm due to "secondary" turbulence.

Space-Time Spectrum Analysis of the Temperature Field of "Polymode" Traverse

V. G. Polnikov

1. Space-time spectrum analysis of data attained in the course of the "Polymode" program was first conducted in (1,2,4). Buoy velocity measurements from all 19 buoys, covering a period of about a year, were used in (4), while (1,2) made use of temperature data from hydrological surveys of the entire traverse, covering a period of about 7 months. Only the first baroclinic mode of Rossby waves was identified at horizons down to 1,000 meters, and a barotropic mode was identified at the 1,400 meter horizon.

The traditional procedure for calculating the space-time spectrum $S(\vec{k},\omega)$ was used in these works. Most of the space-time scales of the studied fields produced a certain large-scale picture--that is, the best resolution in appraisal of $S(\vec{k},\omega)$ was achieved in relation to waves with length comparable to or greater than the dimensions of the traverse under consideration. The results of adaptive spectrum analysis of the temperature field presented below indicate a more-complex wave structure for the field at a synoptic scale.

2. Estimation of $S(\vec{k},\omega)$ by the method of maximum likelihood (3) requires synchronous values for the field at several fixed points in the traverse. Out of the data at our disposal for analysis, we selected the synoptic component of the buoy temperature measurements (with a quantization interval $\Delta = 1$ day): Five measurements at the 100 meter horizon (buoys 2, 3, 4, 5, 6) based on 48 readings each, and three measurements at the 700 meter horizon (buoys 5, 13, 15) based on 80 readings (5). These data apply to the season extending from December 1977 to March 1978 (the fifth and sixth buoy drops), and they correspond to the central and southern part of the buoy traverse (Figure 1). We were unable to select more-representative synchronous samples, or samples similar to those above for other seasons and horizons.

Time spectrums $S(\omega)$ were plotted for the noted time series by the adaptive method proposed in (6). Spectral curves $S(\omega)$ for different buoys and horizons differ significantly in quantiative respects. The qualitative behavior of the $S(\omega)$ curves was identical. The most typical $S(\omega)$ spectrums for both horizons are shown in Figure 2. One significant feature of the time spectrums is presence of two clearly isolated peaks. This indicates existence of two isolated groups of waves in the field under examination with characteristic periods of $T_1 \approx 40$-45 days and $T_0 \approx 10$-15 days. Oscillations with shorter periods are significantly less intense, and they are not analyzed here. Peaks with periods T_1 and T_0 can be identified only following an analysis of the space-time spectrums.

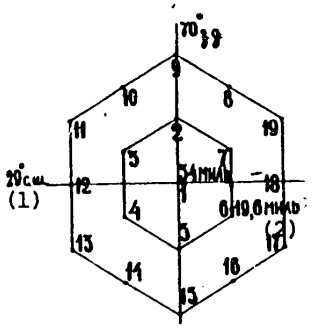

Figure 1

Key:
1. N. Lat.
2. Nautical miles

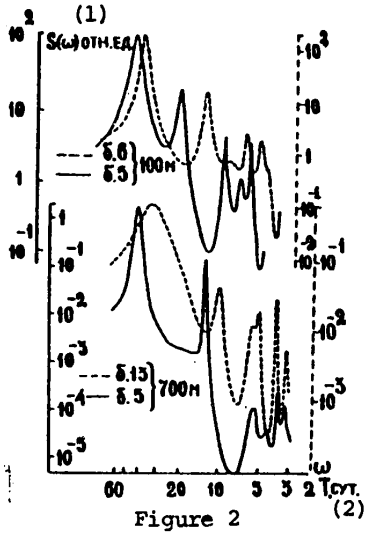

Figure 2

(The scale for the broken curves is on the right.)

Key: 1. Relative units 2. Days

$\vec{S}(\vec{k},\omega)$ spectrums for the 100 meter horizon were plotted using different combinations of sets of buoys. A set consisting of three buoys {4,5,6} was found to be the most suitable; for it, the $\vec{S}(\vec{k},\omega)$ spectrum did not have (Eliayzing) secondary peaks. The same was true for buoy set {5,13,15} for the 700 meter horizon. The results of calculating $\vec{S}(\vec{k},\omega)$ are shown in Table 1, which gives period T, corresponding to angular frequency ω, the coordinates of the principal maximum in space $\vec{k}$--k_x, k_y, and the value for $S_{max}(\vec{k},\omega) = S_m(\omega)$.

Table 1. Results of Calculating Space-Time Spectrums

100 м					700 м				
1) T, сутки	$\omega \cdot 10^6$, 2) сек$^{-1}$	$k_x 10^6$, м$^{-1}$	$k_y 10^6$, м$^{-1}$	$S_m 10^2$, отн.ед.	T, сутки	$\omega \cdot 10^6$, сек$^{-1}$	$k_x 10^6$, м$^{-1}$	$k_y 10^6$, м$^{-1}$	$S_m 10^2$, отн.ед.
240	0,3	-24	6,5	3) 7,3	360	0,2	I,6	2,2	I,9
I92	0,38	-I9,4	6,5	7,7	240	0,3	0	5,4	3,2
I60	0,45	-I9,4	6,5	7,3	I80	0,4	-3,2	I2	4
I20	0,6I	-I9,4	6,5	6,9	I60	0,45	-3,2	I2	4,7
80	0,9I	-I9,4	8,6	I0,3	I20	0,6I	-6,5	I7,5	I,9
60	I,2I	-I9,4	I9,4	I8,8	80	0,9I	-6,5	I2	0,2
48	I,5I	-I9,4	30	32,8	60	I,2I	-5,4	34,5	I,4
40	I,82	-I9,4	43,2	45,4	45	I,6I	-I2	40	3,5
34	2,I2	-I9,4	36,7	57,8	32	2,26	-I7,5	30	I3,3
30	2,42	-I9,4	43,2	54	30	2,42	-I9,4	35,7	37,8
24	3,03	-I6,2	49,6	I5,2	27,4	2,56	-I9,4	45,4	6,6
22	3,33	-I9,4	58,5	3	20	3,63	-35,6	75,5	0,3
20	3,63	-24	64,8	I,I	I2	6,04	-37,8	65	4,I
I6	4,54	-36,6	9I	20,5	II,4	6,34	-4I	6I,5	4,I
I2	6,04	-47,5	I06	8,I	I0	7,2	-56	76,5	0,5

Key:
1. Days
2. Sec^{-1}
3. Relative units

In the examined frequency range, functions $S_m(\omega)$ have two clearly isolated maximums for each of the two horizons: For the 100 meter horizon the maximums correspond to periods of $T_1 \approx 34$ days and $T_0 \approx 16$ days, while for the 700 meter horizon the maximums correspond to periods of $T_1 \approx 30$ days and $T_0 \approx 12$ days. This behavior of $S_m(\omega)$ agrees well with the dependence $S(\omega)$ (Figure 2). The sharp drop in intensity between the peaks and the noticeable displacement of the position of $S_m(\omega)$ from peak to peak provide the grounds for separately identifying each peak of $S(\vec{k},\omega)$ within its own range of frequencies.

The principle of identification entails minimization of the mean square deviations of the calculated (at given ω) coordinates k_x, k_y from the variance curve for linear Rossby waves:

$$\omega = -\frac{\beta k_x}{k_x^2 + k_y^2 + R_m^{-2}} + k_x u + k_y v \qquad (I)$$

by varying the mode parameter R_m^{-2}. In (1), β is the rate of change of the Coriolis parameter with latitude, R_m is the deformation radius of the m-th mode, and u and v are the components of the mean transfer velocity, determined in the identification procedure by the least square method, on analogy with (2).

As a result the $S_m(\omega)$ peak for the 700 meter horizon corresponding to period T_0 was identified as the zero mode of Rossby waves, while the peak corresponding to period T_1 was identified as the first mode. The velocity components for the different peaks differed from one another, and on the average they were $u = -0.09$ m/sec, $v = 0.03$ m/sec, with an accuracy on the order of 20 percent. Identification of peaks for the 100 meter horizon produced similar results, with the components being $u = -0.06$ m/sec, $v = 0.03$ m/sec. The results permit us to evaluate, with an accuracy of about 30 percent, the typical period T and wavelength λ of the noted Rossby wave modes.

Table 2. Parameters of Identified Rossby Waves

	700 Meters		100 Meters	
Mode	0	1	0	1
T, days	240	380	200	310
λ, km	90	160	70	150

3. The obtained results supplement the results given in (1,2,4). In our opinion absence of the signs of a zero mode at horizons less than 1,000 meters, seen in these works, is connected with the absence of mutual correlation of this mode at 300-400 km scales and wavelength $\lambda \approx 90$-100 km.

In this connection it would be interesting to note the fundamental possibility for identifying the second baroclinic mode of Rossby waves. As an example using results shown in Table 1, we can independently examine the diffuse maximum of $S_m(\omega)$ for the 700 meter horizon, corresponding to a period of $T_2 \approx 160$ days. Given the u and v values indicated above, it may be identified as the second baroclinic Rossby wave

mode, with parameters $T \approx 1{,}500$ days and $\lambda \approx 510$ km. However, for final resolution of this question, we would need to perform calculations with larger samples and scales providing reliable information for periods on the order of T_2.

BIBLIOGRAPHY

1. Yefimov, V. V., "Space-Time Spectrums of Horizontal Temperature Nonuniformities in the Northwest Atlantic," OKEANOLOGIYA, 1980 (in press).

2. Yefimov, V. V., Korotayev, G. K., and Shevchenko, E. A., "Spectral Characteristics of Synoptic-Scale Wave Motions," MORSKIYE GIDROFIZICHESKIYE ISSLEDOVANIYA, Sevastopol', No 1, 1980 (in press).

3. Keypon, Dzh., "Space-Time Spectrum Analysis With High Resolution," TIIER, Vol 57, No 8, 1969, pp 69-79.

4. Sabinin, K. D., and Konyayev, K. V., "Space-Time Spectrum of the Kinetic Energy of Synoptic Eddies in the 700 Meter Horizon," OKEANOLOGIYA, Vol 20, 1980, pp 356-357.

5. "Otchet o rabotakh v 26 reyse NIS 'Akademik Kurchatov'" [Report on Projects Conducted During the 26th Trip of the Scientific Research Vessel "Akademik Kurchatov"], Moscow, IO AN SSSR, Vol 3, Part 4, 1978, p 128.

6. Polnikov, V. G., and Timchenko, I. Ye., "A Method of Adaptive Spectrum Analysis of Random Hydrophysical Processes," MORSKIYE GIDROFIZICHESKIYE ISSLEDOVANIYA, Sevastopol', 1980 (in press).

Laws Governing the Distribution and Variability of the Characteristics of the Thermohaline Finestructure of the Northwest Pacific

I. D. Rostov

Functional cause-and-effect relationships between the distribution of finestructure parameters and processes responsible for formation and transformation of finestructure are complex, and in most cases they do not yield to strict description. One of the reasons making analysis and interpretation of the results and their generalization within the framework of the appropriate models difficult is the inadequacy of integrated traverse observations. An analysis of the amplitude-frequency properties of perturbations in profiles recorded by means of sounding instruments would lead to the conclusion that the structure forming processes are significantly unstable, and that their characteristics exhibit significant variability in space and time. It would be interesting in this connection to examine the laws governing the distribution and variability of finestructure parameters obtained as a result of analyzing and classifying large amounts of information on the basis of the methods of probability theory and mathematical statistics.

The Pacific Ocean Oceanological Institute has formed a bank of data on the finestructure of temperature and salinity fields, using YeS EVM magnetic discs, and it has developed a specialized complex of programs for processing sounding data. The bank contains data from more than 200 soundings made through cross sections and at 24-hour stations, basically in the Northwest Pacific. The new experimental material was used as a basis to study the unique features of fine-scale stratification in different structural zones of the ocean, to generalize appraisals of the amplitude-frequency composition and probability characteristics of different regions, to establish the limits for the variability of the parameters of theoretical laws approximating empirical distributions of finestructural elements, and to study the stability of the obtained appraisals.

It was established that differences in structures are well noticeable on the basis of statistical characteristics. This permits us to hypothesize that processes generating finestructure in some regions of the ocean are quasistationary.

Using the methods of factor and regression analysis, we studied the dependence of the values of a number of variables: the means of layer thicknesses, the standard deviations of layer thicknesses and gradients, the amplitudes of profile perturbations, the slope of spectral curves and the parameters of distribution laws, all in dependence upon the sum total of the factors characterizing the background hydrological conditions.

Anisotropic Spectrums of Waveform Turbulence in the β-Plane

A. G. Sazontov

This report analyzes the anisotropic spectrums of weak turbulence of nondivergent barotropic Rossby waves generated by quasi-zonal external effects, and it discusses the local nature of the obtained distributions.

As we know, nondivergent barotropic Rossby waves are described by the equation

$$\frac{\partial}{\partial t}\Delta\psi + \beta\frac{\partial\psi}{\partial x} + \mathfrak{J}(\psi, \Delta\psi) = 0 \qquad (1)$$

Here, ψ--current function, $\beta = \frac{d\Omega}{dy} = \text{const}$, Ω--Coriolis parameter, $\mathfrak{J}$ --Jacobian functional determinant, $\vec{r} = (x, y)$--Cartesian coordinates.

In a Fourier representation, equation (1) would have the form

$$\frac{\partial a_{\vec{k}}}{\partial t} + i\omega_{\vec{k}} a_{\vec{k}} = \int V_{\vec{k}\vec{k}_1\vec{k}_2} a_{\vec{k}_1} a_{\vec{k}_2} \delta(\vec{k}_1 + \vec{k}_2 - \vec{k})\, d\vec{k}_1\, d\vec{k}_2 \qquad (2)$$

where $a_{\vec{k}} = \frac{1}{(2\pi)^2}\int \psi(\vec{r}, t) e^{-i\vec{k}\vec{r}}\, d^2\vec{r}$ --Fourier component of the current function, $(a_{\vec{k}} = a^*_{-\vec{k}})$, $\omega_{\vec{k}} = -\beta\frac{k_x}{k^2}$ --the variance law for Rossby waves $(K \equiv \sqrt{K_x^2 + K_y^2})$, and $V_{\vec{k}\vec{k}_1\vec{k}_2} = \frac{1}{2k^2}(k_1^2 - k_2^2)(\vec{z}\cdot[\vec{k}_1 \times \vec{k}_2])$ --matrix element of interaction ($\vec{z}$--unit vector directed vertically upward).

As was shown by Longuet-Higgins and Gill (4), nonlinear interaction of Rossby waves is possible at as low as the first order of the theory of perturbations, assuming satisfaction of synchrony conditions:

$$\begin{aligned} \omega_{\vec{k}} + \omega_{\vec{k}_1} + \omega_{\vec{k}_2} &= 0 \\ \vec{k} + \vec{k}_1 + \vec{k}_2 &= 0 \end{aligned} \qquad (3)$$

Therefore within the framework of the theory of weak turbulence, interaction occurs at the second-order level in relation to wave energy. Kenyon (3) obtained the appropriate kinetic equation for spectral energy density $F_{\vec{k}}$, defined by the relationship $\frac{1}{2}k^2\langle a_k a_{k_1}^*\rangle = F_{\vec{k}}\,\delta(\vec{k}-\vec{k}_1)$:

$$\frac{\partial F_{\vec{k}}}{\partial t} = 2\pi \int \frac{U_{\vec{k}\vec{k}_1\vec{k}_2}}{k^2 k_1^2 k_2^2}\left\{U_{\vec{k}\vec{k}_1\vec{k}_2} F_{\vec{k}_1}\cdot F_{\vec{k}_2} + U_{\vec{k}_1\vec{k}_2\vec{k}}\cdot F_{\vec{k}_2}\cdot F_{\vec{k}} + U_{\vec{k}_2\vec{k}\vec{k}_1} F_{\vec{k}}\cdot F_{\vec{k}_1}\right\}\delta(\vec{k}+\vec{k}_1+\vec{k}_2)\,\delta(\omega_{\vec{k}}+\omega_{\vec{k}_1}+\omega_{\vec{k}_2})\,d\vec{k}_1\,d\vec{k}_2 \tag{4}$$

where $U_{\vec{k}\vec{k}_1\vec{k}_2} = k^2\cdot V_{\vec{k}\vec{k}_1\vec{k}_2}$

Interaction coefficients $U_{\vec{k}\vec{k}_1\vec{k}_2}$ for resonance surface (3) satisfy the Jacobian identities:

$$U_{\vec{k}\vec{k}_1\vec{k}_2} + U_{\vec{k}_1\vec{k}_2\vec{k}} + U_{\vec{k}_2\vec{k}\vec{k}_1} = 0 \tag{5}$$

$$k^2 U_{\vec{k}\vec{k}_1\vec{k}_2} + k_1^2 U_{\vec{k}_1\vec{k}_2\vec{k}} + k_2^2 U_{\vec{k}_2\vec{k}\vec{k}_1} = 0 \tag{6}$$

$$\frac{k_y}{\omega_{\vec{k}}} U_{\vec{k}\vec{k}_1\vec{k}_2} + \frac{k_{y_1}}{\omega_{\vec{k}_1}} U_{\vec{k}_1\vec{k}_2\vec{k}} + \frac{k_{y_2}}{\omega_{\vec{k}_2}} U_{\vec{k}_2\vec{k}\vec{k}_1} = 0 \tag{7}$$

In this case (5) and (6) are the consequences of, respectively, the laws of conservation of energy $\int F_{\vec{k}}\,d\vec{k}$ and enstrophy $\int k^2 F_{\vec{k}}\,d\vec{k}$; (6) is also equivalent to the law of conservation of the projection of momentum in the zonal direction $\int k_x/\omega_{\vec{k}}\,F_{\vec{k}}\,d\vec{k}$; (7) reflects the law of conservation of the projection of momentum in the meridional direction.

First of all let us find the equilibrium stable solutions to equation (4). For this purpose we rewrite the integrand in (4) as

$$U_{\vec{k}\vec{k}_1\vec{k}_2} F_{\vec{k}}\cdot F_{\vec{k}_1}\cdot F_{\vec{k}_2}\left(U_{\vec{k}\vec{k}_1\vec{k}_2}\cdot F_{\vec{k}}^{-1} + U_{\vec{k}_1\vec{k}_2\vec{k}} F_{\vec{k}_1}^{-1} + U_{\vec{k}_2\vec{k}\vec{k}_1}\cdot F_{\vec{k}_2}^{-1}\right)\delta(\vec{k}+\vec{k}_1+\vec{k}_2)\times$$
$$\times\,\delta(\omega_{\vec{k}}+\omega_{\vec{k}_1}+\omega_{\vec{k}_2})$$

from which it is evident that in view of (6), equation (4) permits the solution

$$F_{\vec{k}} = \text{const} \tag{8}$$

Another solution is a distribution of the form

$$F_{\vec{K}} = \frac{1}{C_1 + C_2 K^2} \quad (C_1 \text{ и } C_2 - \text{const}) \qquad (9)$$

which transforms the collision integral to zero in view of the law of conservation of enstrophy (6).

The most general solution is the drift equilibrium solution,

$$F_{\vec{K}} = \frac{1}{C_1 + C_2 K^2 + \vec{K}\vec{U}/\omega_{\vec{K}}} \qquad (10)$$

which transforms the collision integral to zero in view of conservation of momentum. Vector $\vec{U}$ is an additional distribution parameter proportional to the system's total momentum.

Note that spectrums (8)-(10) may hold in exceptional situations when the sources and flows of turbulence may be ignored.

Equation (4) also has other solutions describing nonequilibrium flow distributions. For the moment we are aware of only one way to analytically find the corresponding solutions, based on a factoring procedure (1). In this case transformation of the kinetic equation into factored form would be convenient not only to explicit derivation of power spectrums but also to determination of the directions of the corresponding flows and the level of turbulence (2). For Rossby waves, the factoring method is not directly applicable because, in view of the anisotropy of the problem, the variance law and the coefficients of interaction are not uniform functions of their arguments. However, in the case where Rossby waves are generated by quasizonal external effects ($K_x^2 \ll K_y^2$, where K_x and K_y are projections of the wave vector correspondingly in the zonal and meridional directions), the appropriate anisotropic spectrums may be found exactly. And in fact, the condition $K_x^2 \ll K_y^2$ ($K^2 \approx K_y^2$) is satisfied in this situation for generated waves; in this case the law of variance and the coefficients of interaction exhibit scaler invariance:

$$\omega_{\lambda K_x, \xi K_y} = \lambda^{\alpha} \xi^{\beta} \omega_{K_x, K_y} \quad (\alpha = 1, \beta = -2); \quad U_{\substack{\lambda K_x \lambda K_{x_1} \lambda K_{x_2} \\ \xi K_y \xi K_{y_1} \xi K_{y_2}}} = \lambda^{t} \xi^{r} U_{\substack{K_x K_{x_1} K_{x_2} \\ K_y K_{y_1} K_{y_2}}}$$

$$(t = 1, r = 3).$$

Let us find the solution to equation (4) in the form $F_k = A K_x^{-s} \cdot K_y^{-p}$ where A is a constant and α and β are unknowns.

Performing a conformal transformation in relation to K_x and K_y in the standard fashion (1), we can rewrite the integral expression in (4) as

$$\int \frac{U_{\vec{K}\vec{K}_1\vec{K}_2}}{K^2 K_1^2 K_2^2}\left\{\left(K_x K_{x_1} K_{x_2}\right)^{-S}\cdot\left(K_y K_{y_1} K_{y_2}\right)^{-P}\left[U_{\vec{K}\vec{K}_1\vec{K}_2}+\left(\frac{K_x}{K_{x_1}}\right)^{X}\cdot\left(\frac{K_y}{K_{y_1}}\right)^{Y}\cdot U_{\vec{K}_1\vec{K}_2\vec{K}}+\right.\right.$$
$$\left.\left.+\left(\frac{K_x}{K_{x_2}}\right)^{X}\left(\frac{K_y}{K_{y_2}}\right)^{Y}\cdot U_{\vec{K}_2\vec{K}\vec{K}_1}\right]\delta\left(\vec{K}+\vec{K}_1+\vec{K}_2\right)\delta\left(\omega_{\vec{K}}+\omega_{\vec{K}_1}+\omega_{\vec{K}_2}\right)d\vec{K}_1 d\vec{K}_2$$

where $X=2t+2-\alpha-2S;\ Y=2r-4-\beta-2p$

Obviously the integrand transforms to zero at the following values of S and P:

$$1)\ S=3/2,\ P=2\ (X=Y=0);\ 2)\ S=3/2,\ P=3\ (X=0,\ Y=-2)$$
$$3)\ S=1,\ P=7/2\ (X=1,\ Y=-3)$$

Anisotropic spectrums reflecting constancy of energy flux $F_K \sim K_x^{-3/2} K_y^{-2}$ and enstrophy $F_K \sim K_x^{-5/2} K_y^{-3}$, correspond to the first two solutions. In this case the second solution is also equivalent to a spectral distribution satisfying constancy of the flow of momentum in the zonal direction. The last solution corresponds to constancy of the flow momentum in the meridional direction.

We emphasize that the found spectrums were obtained as approximations with weak nonlinearity, and they are based on the hypothesis of local interaction.

The applicability condition for weak turbulence is satisfied when $\omega_K \cdot \tau_{int} \gg 1$, where τ_{int} is the characteristic time of nonlinear interaction of Rossby waves with scale K^{-1}. Using (4), we can arrive at this estimate for it: $\tau_{int}^{-1} \sim \omega_K^{-1} K^4 F_K$.

Obviously the applicability condition for weak turbulence is violated in the ranges of small wave numbers, where nonlinear effects become significant, and spectrum $F_K \sim K_x^{-5/2} K_y^{-2}$ must transform into the spectrum obtained by Rhines (5).

Next, in order that the found distributions would have physical meaning, the local nature of turbulence must be demonstrated. What this means physically is that interaction of waves with a scale of the same order is much stronger than interaction of waves of different scales. Formally, the property of being local requires that the integrals in (4) would converge upon the obtained distributions.

Elementary analysis shows that within the range $\vec{K}_1, \vec{K}_2 \gg \vec{K}$, the integrals in (4) converge to the found distribution. Let us examine convergence in the range $\vec{K}_1 \ll \vec{K}$ ($\vec{K}_2 \sim \vec{K}$) in greaterdetail. In this case the most "dangerous" terms (with which the greatest divergence is associated) would be ones proportional to $F_{\vec{K}_1}$. Integrating in relation to $\vec{K}_2$ in accordance with the law of conservation of the momentum, we get the following for the "dangerous" terms:

$$\int d\vec{K}_1 \delta(\omega_{\vec{K}} + \omega_{\vec{K}_1} + \omega_{(\vec{K}+\vec{K}_1)}) \frac{U_{\vec{K}\vec{K}_1-(\vec{K}+\vec{K}_1)}}{K_1^2} \left\{ U_{\vec{K}\vec{K}_1-(\vec{K}+\vec{K}_1)} F_{-(\vec{K}+\vec{K}_1)} + U_{-(\vec{K}+\vec{K}_1)\vec{K}_1\vec{K}} F_{\vec{K}} \right\} F_{\vec{K}_1}$$

At small $\vec{K}_1 << \vec{K}$, decomposing the argument of the δ-function and $U_{\vec{K}\vec{K}_1\vec{K}_2}$ we get an integral of the form:

$$\int d\vec{K}_1 \frac{(\vec{K}\vec{K}_1)}{K_1^2} \left[K_{x_1} K_y - K_x K_{y_1} \right]^2 \delta\left(\frac{K_{x_1}}{K_1^2} + \frac{2K_{x_1}(\vec{K}\vec{K}_1)}{K^4} \right) F_{\vec{K}_1}$$

We can see from the expression for the argument of the δ-function that when we integrate in relation to angular dimensions, because $K_1 << K$ the integral transforms to zero. Thus the found spectrums are local.

BIBLIOGRAPHY

1. Kadomtsev, B. B., and Kontorovich, V. M., "Turbulence Theory in Hydrodynamics and Plasma," IZV. VUZOV. RADIOFIZIKA, Vol 17, No 4, 1974, pp 511-540.

2. Kats, A. V., "Spectral Direction of Energy Pumping and [one word illegible] Numbers in Stationary Exponential Solutions of Kinetic Wave Equations," ZHETF, Vol 71, No 6, 1976, p 2105.

3. Kenyon, K., "Discussions," PROC. ROY. SOC., Vol A299, 1967.

4. Longuet-Higgins, M. S., and Gill, A. E., "Resonant Interactions Between Planetary Waves," PROC. ROY. SOC., Vol A299, 1967.

5. Rhines, P. B., "Waves and Turbulence on a Beta-Plane," J. FLUID. MECH., Vol 69, No 3, Pt 3, 1975, pp 417-444.

Eddy-Resolving Numerical Models of Ocean Currents

D. G. Seidov, K. K. Rusetskiy

The significant role played by synoptic-scale eddies in the general circulation of the ocean is not doubted today. But at the same time even qualitative research on in the interaction between eddies and average currents is extremely difficult owing to the nonlinear nature of this interaction. The sole sensible alternative for analytical research is numerical modeling of general circulation, which presumes resolution of synoptic processes with a network analyzer--that is, creation of so-called eddy-resolving models of ocean currents (henceforth abbreviated as EM's). The first EM was Holland and Lin's two-layer model (5). This EM presupposes constant density in two layers of liquid, and the sole driving force is wind-caused friction on the ocean surface. Under the action of wind-driven circulation in the upper layer, the interface deviates from its equilibrium horizontal state, resulting in activation of the mechanism of baroclinic instability. In this case the available potential energy is released with intensification of horizontal currents, and it causes intensification of the barotropic instability of average currents. The release of energy occurs in the form of synoptic eddies, the kinetic energy of which is comparable to the kinetic energy of large-scale circulation. In view of the fact that it assumes presence of two layers, this EM contains a number of significant shortcomings. We can cite, for example, the fact that differential heating, which has been found to be extremely important (2,6,7), is absent from this EM, and deviations of the interface from its equilibrium state are small, which contradicts the known fact that the amplitudes of isopycnic surfaces in the ocean are significant. As a result this EM obviously overstates the effect of baroclinic instability.

Another EM developed by Robinson et al. (6,7) is based on complete equations for the balance of momentum, heat and mass in a continuously stratified ocean. This is the most complete EM, which is in a certain sense its weakness, because retention of all wave motions up to internal waves (surface waves are excluded by the condition that there is a "hard lid" on the ocean surface) imposes stringent requirements on temporal spacing. The numerical network of this EM is a high-level network, retaining certain motion integrals, having a second-order approximation with respect to time, and being free of nonlinear instability. But for practical purposes these merits of the network are also the weak points of the EM, inasmuch as they preclude the possibility for numerical simulation of its most attractive side--the possibility for broad variation of parameters in large experimental series. Even using very high-capacity computers, the authors of this EM were able to perform only two experiments. In the model, motion is generated and supported by the zonal pressure exerted by

wind friction and by heat flux proportional to the difference between the temperature of the surface layer of water and the given zonal air temperature. The basic conclusion here was that the role of barotropic instability of the average circulation is significant. However, it was rather difficult in the two experiments to indicate the role of particular factors in the mechanism of eddy formation and in interaction of eddies and central currents.

Mention should be made of Holland's recent work (8), which in physical nature is close to the Holland-Lin model, but it has been simplified, and it is a two-layer quasi-geostropic EM. This approximation significantly increases the effectiveness of the EM, but it hardly distorts its physics, inasmuch as only internal waves are filtered out. In our opinion however, as in (5), the assumption that there are two layers present is unjustifiably inflexible, and it excludes extremely important thermal effects.

One of the authors suggested the EM 3-63, which is practically as complete as the EM suggested in (6,7) in physical respects, having the sole simplification of calculating vertical velocity with a quasi-geostrophic (stationary or complete) equation of eddy balance, instead of the initial continuity equation (this is the way internal waves are filtered out). The numerical algorithm of our EM differs fundamentally from the diagrams for the models of the American scientists. It is based on a division method using (Laks-Vendroff) diagrams ((Leys-Rikhtmayr) or Euler-Lagrange diagrams; see (3)) applied to advection stages. The order of approximation with respect to time decreases; as was shown, however, artificial viscosity is not only not detrimental to the calculations, but it may even be useful, inasmuch as it filters out high-frequency harmonics generated in the network while practically not distorting long waves (including synoptic eddies), which are of principal interest in the analysis of large-scale circulation.

First we will formulate the general premises arrived at in (5,6-8), and then we will summarize our experiments, which supplement the research cited above and shed light on some important aspects of synoptic processes in the ocean and on their relationship to thermohydrodynamic large-scale circulation.

The main physical result of the EM experiments was the revelation of the significant role played by synoptic eddies in large-scale circulation. It was demonstrated that even when external conditions (wind and air temperature, if the latter was taken into account) are stable, quasi-stationary conditions do exist, accompanied by significant transfer of momentum and heat due to the action of the eddies specifically. Thus eddies in the EM describe horizontal advection processes brought about by other than the average currents. Synoptic eddies are generated as a result of the baroclinic and barotropic instability of currents experiencing vertical and horizontal velocity shifts. Transferringenergy from certain parts of a water basin into others, eddies redistribute the system's energy, and they can either dissipate this energy in boundary layers through small-scale turbulence (parametrized within the framework of the semi-empirical theory of turbulence (1)) or intensify average currents as a result of nonlinear interactions (the so-called negative viscosity effect (1,4)). We should note, however, that the negative viscosity effect was not dominant in the experiments under discussion here, since such dominance would require a significant influx of heat into the system (see below, and (2,4)).

We emphasize that dynamic equilibrium of general circulation and synoptic eddies is an important element of the EM experiments.

The authors performed the following experiments within the framework of the EM discussed above (see (2,3)). Under the action of the stable zonal pressure of wind friction and a heat flux over the surface of the ocean, proportional to the difference between the temperature of the water surface and the zonal air temperature, which decreases linearly from south to north, currents arise, develop and persist in a rectangular, enclosed basin of constant depth approximating a beta-plane.

The role of different physical and computational parameters in the problem was studied in a series of experiments. Variations were made in: the circulation configuration (two circulation gyres with a free flow in the middle of the basin, or one gyre with a northern boundary current); the intensity of small-scale turbulent exchange of momentum and heat (different coefficients of turbulent exchange); the intensity of the flow of momentum across the ocean surface (different amplitudes of wind pressure); the intensity of differential heating (different values for the air temperature differences in the meridional direction); the horizontal dimensions of the area; the resolution of the computation network and, finally, the structure of the model (we ignored eddy advection--that is, we excluded nonlinear interactions; in this case eddy formation did not occur--that is, nonlinear effects were the most important element of the EM).

The results of this series permitted the following conclusions:

1. Circulation configuration has important significance. The principal physical result is that presence of a free, meandering flow results in a dynamic cycle fundamentally different from that of single-gyre circulation, with not only baroclinic and barotropic instability but also negative viscosity playing a significant role.

2. The heat flux turns out to be an extremely important factor. When differential heating grows more intense, eddy formation intensifies, and the effect of negative viscosity grows larger.

3. Baroclinic instability occurs in slow return currents, while negative viscosity is concentrated in areas where the flow breaks away from the shore. Barotropic instability manifests itself in the eastern regions of the meandering flow.

4. There exists a special zone near the place where the flow breaks away from the shore; in it, intensification of this flow due to eddies may attain 50 percent of its "climatic" expenditures (that is, expenditures arrived at with the use of models of nonresolving eddies).

5. Finally, revelation of north-south asymmetry is extremely important. In the case of two-gyre circulation, eddy activity in the vicinity of the anticyclone (the southern gyre) is significantly higher than in the cyclonic, northern gyre. We know from observation that south of the Gulf Stream, for example, synoptic processes are much more intense than north of this current. The asymmetry is intensified when the meridional gradient of atmospheric temperature increases.

Today the most important problem is to arrive at sufficiently reliable parametrization of synoptic effects in models of large-scale circulation, inasmuch as the objective need for accounting for these effects in simulation of general ocean circulation, as well as in climate models and in long-range weather forecasts, is obvious.

BIBLIOGRAPHY

1. Monin, A. S., and Yaglom, A. N., "Statisticheskaya gidromekhanika" [Statistical Hydromechanics], Part 1, Moscow, "Nauka", 1965.

2. Seidov, D. G., "A Numerical Diagram For Analyzing Synoptic Eddies in the Ocean," IZV. AN SSSR. FIZIKA ATMOSFERY I OKEANA, Vol 14, No 7, 1978.

3. Seidov, D. G., "Synoptic Eddies in the Ocean. A Numerical Experiment," IZV. AN SSSR. FIZIKA ATMOSFERY I OKEANA, Vol 16, No 1, 1980.

4. Starr, V., "Fizika yavleniy s otritsatel'noy vyazkost'yu" [The Physics of Negative Viscosity Phenomena], Moscow, "Mir", 1971.

5. Holland, W. R., and Lin, L. B., "On the Generation of Mesoscale Eddies and Their Contribution to the Oceanic General Circulation," J. PHYS. OCEANOGR., Vol 5, No 4, 1975.

6. Robinson, A. R., Harrison, D. E., Mintz, Y., and Semtner, A. J., "Eddies and the General Circulation of an Idealized Ocean Gyre," J. PHYS. OCEANOGR., Vol 7, No 2, 1977.

7. Semtner, A. J., and Mintz, Y., "Numerical Simulation of the Gulf Stream and Mid-Ocean Eddies," J. PHYS. OCEANOGR., Vol 7, No 2, 1977.

8. Holland, W. R., "The Role of Mesoscale Eddies in the General Circulation of the Ocean. Numerical Experiments Using a Wind-Driven Quasi-Geostrophic Model," J. PHYS. OCEANOGR., Vol 8, No 3, 1978.

Formation of the Synoptic Variability of Seas Experiencing Free and Limited Exchange With the Ocean, and the Problems of Its Computation and Prediction

Yu. V. Sustavov

The influence of the nature of water exchange between the seas and the ocean was studied in application to formation of synoptic-scale processes on the basis of a comparison between the unique features of the variability of cyclic characteristics of two marginal seas--Barents and Baltic.

The Barents Sea is a typical through water basin experiencing free exchange. The waters of the Atlantic (the Norwegian Sea) spread through the entire depths of the sea via the western boundary section throughout the entire year (Figure 1A). These waters circulate within it and then drain out, determining the basic traits of the water dynamics and creating the unique thermal cycle of the Barents Sea. Under these conditions the interaction of the sea with the atmosphere above it is supplemented by two processes associated with water exchange: variations in the advective component resulting from variability in the velocity of the principal branches of the North Cape Current and variability in the thermal state of water masses entering the western boundary section from the ocean (1,2). The variability of all of these processes has a complex polycyclic structure, with each component exhibiting significant instability.

The Baltic Sea is one of the seas with one-way water exchange, which occurs through the system of Danish straits. Salt water from the ocean (the North Sea) penetrates into the Baltic Sea in the bottom horizons during summer when the thermocline forms (Figure 1B). Filling the deep layers, this denser water has a fixed upper boundary taking the form of a zone exhibiting stable stratification (the halocline), which prevents interaction between the deep layers of the sea and the atmosphere As a consequence the variability of processes in the Baltic Sea depends mainly on development of short-period wave motions in the basin connected with the static reaction of the water column to varying atmospheric pressure and to internal-wave, inertial and eddy movement (3,4,6).

Of interest is the fact that while the cause is the same (water exchange with the ocean), the situation is such that in the presence of different water exchange conditions, its effect produces diametrically opposed fundamental consequences.

Penetrating into the Barents Sea, warm Atlantic waters bring with them the unique variations in hydrophysical fields typical of the ocean, which superimpose themselves

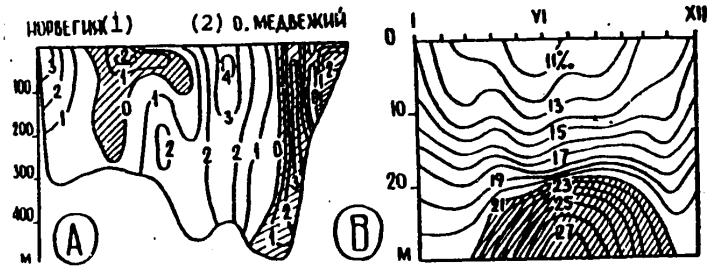

Figure 1. A) Distribution of the Normalized Velocity of the North Cape Current (Not Cross-Hatched) in July; B) Mean Annual Trend of the Depth of Isohalines in the Fehmarn-Baelt Strait

Key:
1. Norway
2. Bear Island

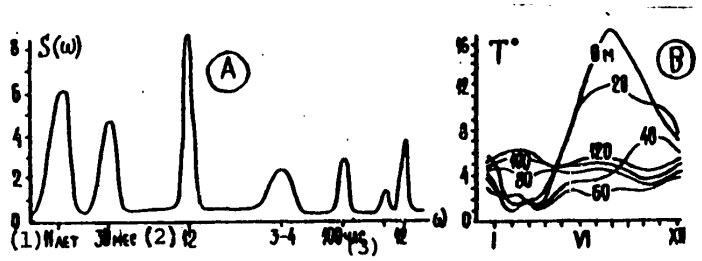

Figure 2. A) Hypothetical Spectrum of Water Temperature Variability in the 0-200 Meter Layer of the Southern Barents Sea; B) Mean Annual Trend of Water Temperature in Horizons of the Central Baltic Sea

Key:
1. Years
2. Months
3. Hours

over the general background produced by the natural variability of processes in the Barents Sea, thus complicating their already complex pattern (Figure 2A). In this case the roles of "oceanic" and local variability are comparable in their contribution, and in certain periods of time they may predetermine the orientation in which processes within the sea develop; it follows from this that a significant part of the problems experienced in the Baltic Sea have their causes outside it, and they necessitate consideration of the variability of the thermal and dynamic state of water masses intruding into the sea from the Atlantic.

On the other hand salt water from the North Sea "arrests" a significant part of the waters of the Baltic below the halocline, in which even an annual temperature trend is absent (Figure 2B), thus creating an additional problem for vertical exchange between layers and for aeration of abyssal layers where, as we know, stagnation

processes develop with detrimental consequences to the entire sea. In this case the state of the sea depends on the activity of processes penetrating into the sea.

These considerations predetermined the overall strategy behind the design of the mathematical models: The key problem in relation to the Barents Sea was to consider the probability structures of the processes and their instability, while in relation to the Baltic Sea it was to consider wave and internal wave processes connected with the unique features of the water basin's vertical stratification and with processes developing in the thermocline and halocline zones.

The physical statistical model described here for variability of thermal conditions in the principal standard cross section through the Barents Sea is based on an equation for the balance of water temperature variability in the 0-200 meter layer, given in spectral form (2). The left side of the equation contains the sum of the variability spectrums of the processes, while the right side contains the similar sum of variability spectrums for the predictors:

$$S(\omega)_{T_w} + S(\omega)_{T_a} + S(\omega)_{\Delta T_{нсх}} = S(\omega)_{T_b} + S(\omega)_{H-\bar{H}} + S(\omega)_{\Delta T_a}$$

Here $S(\omega)_{T_w}$ is the spectrum of water temperature fluctuations produced by heat exchange with the atmosphere, dominated by a cyclicity of 12 months; $S(\omega)_{T_a}$ is the spectrum of fluctuations associated with variability in the advective component exhibiting 30, 12 and 3-4 month cycles; $S(\omega)_{\Delta T_{нсх}}$ is the spectrum of fluctuations of anomalies in the initial state of the water masses entering the western border section, in which cycles of 8-11 years and 30 and 3-4 months are clearly pronounced. The last two components also exhibit cycles of 100, 24 and 12.4 hours. Due to their pronounced periodicity, these short-period processes, connected with the passage of pressure systems above the Barents Sea and with tidal phenomena, do not have a significant influence on formation of the basin's thermal conditions, and they are not accounted for in the model. But at the same time failure to account for trend components (8-11 years and 30 months) that serve as the background for development of synoptic-scale processes in the computational and forecasting models makes the overall problem meaningless, inasmuch as these trends may have a dominant effect.

The predictor spectrums in the right side of the equation include: $S(\omega)_{T_b}$--the variability spectrum for air temperature; $S(\omega)_{H-\bar{H}}$--the spectrum for sea level fluctuations; $S(\omega)_{\Delta T_a}$--the spectrum for fluctuations in air temperature anomalies. In terms of their structure, these spectrums correspond fully with the spectrums of the resulting processes (2).

The physical basis for the forecasting method is presence of a spectral phase of mutual fluctuation at all frequencies that reflects the inertia of the processes, a different one for each frequency band.

The instability of the inertia interval in the first component is accounted for with the use of a nomogram (Figure 3A); it is accounted for in the second component by change in time of the spectral phase (Figure 3B); it is accounted for in the third component by extrapolation of trend components by means of an expansion of the form

$$\Delta T = \sum_{i}^{n} A_i \sin(\omega_i t + \gamma_i).$$

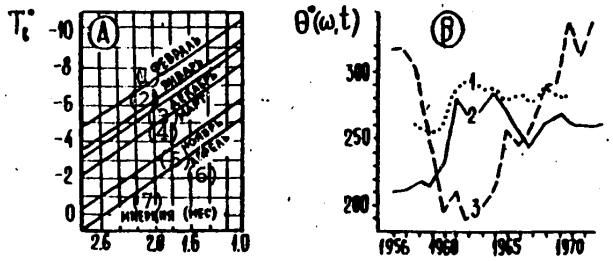

Figure 3. A) Dependence of the Inertia Interval on Mean Monthly Air Temperature (T_b°); B) Change in Spectral Phase ($\Theta°\omega,t$) at Different Sections: 2.52 (*1*), 6.28 (*2*), and 15.7 (*3*) radians per year, in mutual fluctuations of sea level and the advective component

Key:

1. February
2. January
3. December
4. March
5. November
6. April
7. Inertia (months)

The model has been used successfully to calculate and predict the thermal conditions of the Barents Sea.

The nonstationary model of thermodynamic processes in the Baltic Sea is based on solution of equations for the dynamics of a two-layer liquid in which a quasi-uniform layer of constant density and variable depth is located above a layer with density varying vertically. The problem is nonstationary and nonlinear, and it requires consideration of vertical and horizontal turbulent exchange. A Bussinesk approximation and a hydrostatic approximation are used. The upper quasi-uniform layer, the depth of which varies with time, is represented by a sum of three variables: the depth of the interface in the given season (month), shifts in the depth of the interface caused by internal wave processes, and fluctuations of the free surface. The dynamics of the interface between water layers of different densities are accounted for by an approximation of the vertical pressure profile for the upper and lower layers (5).

Some approximations of this model have been used successfully to calculate the fields of internal wave currents and sea level.

BIBLIOGRAPHY

1. Sustavov, Yu. V., "A Method for Calculating Water Temperature in the Southern Barents Sea on the Basis of Separate Consideration of Thermal Interaction and and Heat Advection By Currents," TR. AANII, Vol 321, 1975, pp 133-142.

2. Sustavov, Yu. V., "A Physical Statistical Model of Variability in the Water Temperature of the Barents Sea, and the Method for Calculating and Predicting Its Components," TR. GOIN, No 147, 1978, pp 34-44.

3. Sustavov, Yu. V., and Chernysheva, Ye. S., "Numerical Simulation of Internal Waves of the Baltic Sea Based on Solution of Two-Dimensional Equations for the Dynamics of a Two-Layer Liquid," TR. GOIN, No 147, 1978, pp 103-110.

4. Sustavov, Yu. V., Chernysheva, Ye. S., and Mikhaylov, A. Ye., "Concealed Eddies of the Baltic Sea," TR. GOIN, No 152, 1980.

5. Sustavov, Yu. V., and Chernysheva, Ye. S., "A Two-Layer Mathematical Model for the Dynamics of the Waters of the Baltic Sea," TR. GOIN, No 152, 1980.

6. Sustavov, J. V., Chernyshova, E. S., and Mikhaylov, A. E., "On the Synoptic Eddy Genesis in the Baltic Sea," in " XI Conf. of Baltic Oceanogr.," Vol 2, 1978, pp 795-805.

Linear Reaction of a Stratified Ocean to a Moving Tropical Cyclone

G. G. Sityrin

Interest in studying the variability of the ocean's physical fields connected with the influence of tropical cyclones has risen significantly in recent years. Analysis of unique observations made during expeditions sponsored by the State Committee for Hydrometeorology and Environmental Control and the USSR Academy of Sciences has shown that following the passage of a tropical cyclone, significant changes in the temperature field and salinity persist in both the upper layer of the ocean and in the main oceanic thermocline (1,2,5). The principal traits of the response of the ocean's upper layer to a moving tropical cyclone have been studied theoretically within the framework of two-layer models (4,7,8).

To analyze the response of an unlimited rotating ocean to a tropical cyclone moving at constant velocity, we introduce a Cartesian coordinate system (x,y,z) moving together with the tropical cyclone, and we examine steady-state motion, produced by stably distributed wind pressure $\underset{\sim}{\tau}^{\alpha}$ and atmospheric pressure anomalies p^{α} in the ocean, proceeding along axis x with velocity v.

We divide the ocean into an upper layer with thickness H_0, consisting of a mixed layer with density ρ_0 and a seasonal thermocline with density gradient $\varepsilon\rho_0$, a main thermocline with thickness H_T, for which the Vyaysyal'-Brent frequency is $N(Z)>0$, and an abyssal layer with thickness H_A, for which $N=0$. We will treat motion in the ocean as being isopycnic, with the density being $\rho=\rho(S)$, where S is the Lagrange coordinate, determined in relation to an unperturbed state for which $S=Z$.

In a quasi-Lagrange coordinate system (x,y,S), quasi-static motion is described in a Bussinesk approximation by the following equation system and boundary conditions (11):

$$(\underset{\sim}{v}\cdot\nabla)\underset{\sim}{v} + f\underset{\sim}{k}\times\underset{\sim}{v} + \nabla\hat{\pi} = \frac{1}{\rho_0(1+\sigma)}\frac{\partial\underset{\sim}{\tau}}{\partial S}, \qquad (1)$$

$$\nabla(1+\sigma)\underset{\sim}{v} = 0, \qquad (2)$$

$$\frac{\partial\hat{\pi}}{\partial S} + N^2(S)\zeta = 0, \qquad (3)$$

$$\underset{\sim}{\tau} = \underset{\sim}{\tau}^{\alpha}, \quad \hat{\pi} = \frac{p^{\alpha}}{\rho_0} - g\zeta \quad \text{at } S=0, \qquad (4)$$

$$\underset{\sim}{\tau} = 0, \quad \zeta = 0 \quad \text{at } S=H, \qquad (5)$$

$$v_x = U, \quad v_y = 0, \quad \zeta = 0, \quad \hat{\pi} = 0 \quad \text{at } x\to-\infty. \qquad (6)$$

Here $\underset{\sim}{v} = (v_x, v_y)$ is the horizontal current velocity, $\nabla = (d/dx, d/dy)$ at $S = \text{const}$, f is the Coriolis parameter, $\underset{\sim}{k}$ is a unit vector directed vertically downward, $\hat{\pi} = (p - \rho g \zeta)/\rho_0$, p is pressure perturbation, g is gravity, $\zeta = Z(x,y,S) - S$ is the vertical displacement of the isopycnic surface, $\sigma = dS/dS$, $\underset{\sim}{\tau}$ is momentum flux, and $H = H_0 + H_T + H_A$.

Below the seasonal thermocline, we will assume $\underset{\sim}{\tau} = 0$. At $f = \text{const}$, we have the following linear relationship from equations (1) and (2):

$$f\sigma = \underset{\sim}{K}(\nabla \times \underset{\sim}{V}). \qquad (7)$$

Integrating equations (1) and (2) in relation to S from $S = 0$ to $S = H_0$, we calculate, as a linear approximation, the total change in potential vorticity in the upper layer of the ocean in response to a tropical cyclone:

$$\frac{f + \underset{\sim}{K}(\nabla \times \underset{\sim}{V}^0)}{1 + \eta/H_0} - f = \frac{1}{\rho_0 U H_0}\int_{-R}^{R} \underset{\sim}{K}(\nabla \times \underset{\sim}{\tau}^a)\,dx \equiv f\frac{A}{H_0}\omega(y), \qquad (8)$$

where η is the shift in the boundary of the seasonal thermocline (we ignore the contribution made by sea level to change in the thickness of the upper layer), $\underset{\sim}{v}^0$ is the mean current velocity in the upper layer and R is the radius of the tropical cyclones. For an axisymmetrical tropical cyclone, $\omega(y)$ is a symmetrical function and $\omega(0) = 1$:

$$A = \frac{2}{\rho_0 U f}\int_0^R \tau_\varphi^a(r)\frac{dr}{r} = \frac{\tau_A}{\rho_0 U f}.$$

For the distribution $\tau_\varphi^a = \tau_m r^2/L^2 \exp(1 - r/L)$ (8,9), $\tau_A = 3{,}7\tau_m$; for $\tau_\varphi^a = \tau_m r/L$ at $r<L$ and $\tau_\varphi^a = \tau_m L/r$ at $r \geqslant L$ (3), $\tau_A = 4\tau_m$.

In a two-layer model of the ocean, if $U > C$ (where $C = \sqrt{\varepsilon g H_0}$ is the rate of propagation of long internal waves), gravitational-inertial fluctuations occur in the interface in a wedge-shaped area behind the center of the tropical cyclone, attenuating at $x \to \infty$ (8). When continuous stratification is present in the main thermocline, isopycnic variations exist no matter what the rate of movement of the tropical cyclone. However, at a sufficient distance from the coordinate origin in the wake of the tropical cyclone ($x \to \infty$), the solution of the problem does not depend on x. Atmospheric pressure p^a and the radial component of wind pressure τ_r^a do not influence the structure of the wake of a tropical cyclone, given a linear problem.

Flow in the wake of a tropical cyclone becomes geostrophic, $\underset{\sim}{k}(\nabla \times \underset{\sim}{v}) = d^2\hat{\pi}/dy^2/f$, and at $N = \text{const}$ we can write the solution to system (3), (7) with boundary conditions

$$\hat{\pi} = \hat{\pi}^0 - \varepsilon g \eta, \quad \tau = \eta \cdot \quad S = H_0, \quad \tau + H_A \partial^2 R/\partial y^2/f = 0$$

at $S = H_0 + H_T$, with a consideration for a somewhat simplified version of relationship (8), $H_0 \partial^2 \hat{\pi} / \partial y^2 / f^2 - \eta = A\omega / (1 + A\omega / H_0)$, in the form

$$\zeta(y, S) = -\frac{f_1}{N^2} \frac{\partial \hat{\pi}}{\partial S} = -A \int_0^\infty q(\ell) G(\ell, S) \cos \frac{\ell y}{L} d\ell. \quad (9)$$

where $$q(\ell) = \frac{2}{\pi} \int_0^\infty \frac{\omega(y)}{1 + A\omega(y)/H_0} \cos \frac{\ell y}{L} dy,$$

$$G(\ell, S) = \frac{ch[M\ell(\lambda H_T + H_0 - S)/H_T]}{ch M\ell\lambda(1 + M_\eta \ell^2 + M_0 \ell \operatorname{cth} M\ell\lambda)}, \lambda = 1 + \frac{\operatorname{arcth} M_A \ell}{M\ell}. \quad (10)$$

The structure of kernel (10) depends on four dimensionless parameters:

$$M = L_T / L, M_\eta = L_\eta^2 / L^2, M_0 = L_0 / L, M_A = L_A / L,$$
$$L_T = NH_T / f, L_\eta = c / f, L_0 = NH_0 / f, L_A = H_A N / f.$$

Here L is the radius of maximum winds in the tropical cyclone, varying within 20-150 km. At stratification parameters typical of the ocean's tropical zone, $N = 4 \cdot 10^{-3}$ sec^{-1}, $H_T = 1.2$ km, $\xi = 2 \cdot 10^{-3}$, $H_0 = 200$ meters, $H_A = 3.5$ km and $f = 7 \cdot 10^{-5}$sec^{-1}, we have $L_T = 70$ km, $L_\eta = 30$ km, $L_0 = 10$ km, $L_A = 200$ km.

Analysis of expression (10) would show that as M increases, displacement of isopycnics in the main thermocline decreases faster with depth. As $M_A \to \infty$, which corresponds to a baroclinic approximation, $\lambda = 1$. Maximum displacement of isopycnics occurs in the seasonal thermocline, in which case the influence stratification in the main thermocline has on the magnitude of η is small, inasmuch as it may be assumed that $M_0 << 1$. In this case for $\omega = 1$ at $y < L$ and $\omega = 0$ at $y \geq L$ calculation of $\eta_m = \eta(0)$ gives

$$\eta_m = -\frac{A}{1 + A/H_0} (1 - e^{-L/L_\eta}). \quad (11)$$

Thus presence of a density gradient in the seasonal thermocline noticeably reduces displacement of isopycnics in the wake of a tropical cyclone at $L \sim L_\eta$.

It should be noted that in distinction from Geisler's linear theory (8), in this case linearization was performed only for the purpose of calculating changes in potential vorticity (8); therefore the solution remains limited for any value $A: |\zeta| < H_0$.

Evolution of the wake of a tropical cyclone in the β-plane was studied in (9), the results of which we can use to estimate the typical time of existence of a baroclinic wake--several months. The hypothesis that the comb-shaped wake of a tropical cyclone may transform into a system of eddies comparable with synoptic eddies encountered in the open ocean was suggested in (6) on the basis of an analysis of observations made of the wake of typhoon Tess (1975). Analysis of expression (8) would show that flow within the wake of a tropical cyclone satisfies the necessary instability conditions obtained in (10); in particular, $d\omega/dy$ changes sign in the upper layer of the ocean. However, additional research would have to be performed in order to reveal the possibility for development of instability, and to estimate the typical time of its development.

Cyclonic eddies may form in the ocean directly in response to a tropical cyclone in areas typified by local minimums for the rate of travel of the thermocyclone. Formation of a sufficiently intense eddy, comparable with synoptic eddies, requires that the effect of the tropical cyclone persists for an average of a day (3). Formation of a synoptic-scale cyclonic eddy in response to typhoon Virginia (1978), which remained in practically the same place for about 3 days, was documented by measurements made in the ocean (2).

At $U = 0$, the dome-shaped wake of a tropical cyclone is described by similar equations analyzed in (3). In this case maximum displacement of isopycnics may be appraised using formula (11), where $A = 2T\tau_m/\rho_0 fL$ and T is the time of influence of the tropical cyclone. This formula gives the following figures for tropical cyclones Ella (1978), Tess (1975) and Virginia (1978): $A = 35$ meters, $\eta_m = -25$ meters; $A = 70$ meters, $\eta_m = -50$ meters; $A = 300$ meters, $\eta_m = -120$ meters. This agrees completely with the results of observations given in (1,2,5). Isopycnic displacement decreases with depth fastest in the first case ($M \sim 3$), more slowly in the second ($M \sim 1.5$), and it changes little in the main thermocline in the third ($M \sim 1$).

BIBLIOGRAPHY

1. Pudov, V. D., Varfolomeyev, A. A., and Fedorov, K. N., "Vertical Structure of the Wake of a Typhoon in the Upper Layer of the Ocean," OKEANOLOGIYA, Vol 18, No 2, 1978, pp 218-225.

2. Pudov, V. D., "The Mesostructure of Temperature and Current Velocity Fields in the Baroclinic Layer of the Ocean in the Wake of Typhoon Virginia," OKEANOLOGIYA, Vol 20, No 1, 1980, pp 19-27.

3. Sutyrin, G. G., "The Energetics of a Stratified Ocean in the Presence of a Stationary Tropical Cyclone," IZV. AN SSSR, FIZIKA ATMOSFERY I OKEANA, Vol 15, No 10, 1979, pp 1076-1083.

4. Sutyrin, G. G., "Reactions of the Upper layer of the Ocean to a Moving Typhoon," METEOROLOGIYA I GIDROLOGIYA, No 9, 1980.

5. Fedorov, K. N., Varfolomeyev, A. A., Ginzburg, A. I., Zatsepin, A., G., Krasnopevtsev, A. Yu., Ostrovskiy, A. G., and Sklyarov, V. Ye., "Thermal Reaction of the Ocean to Passage of Hurricane Ella," OKEANOLOGIYA, Vol 19, No 6, 1979, pp 992-1001.

6. Fedorov, K. N., Krasnopevtsev, A. Yu., and Varfolomeyev, A. A., "The Possibility of Arisal of Synoptic Eddies in the Ocean Under the Direct Influence of Hurricanes and Typhoons," in "Issledovaniye izmenchivosti fizicheskikh protsessov v okeane" [Investigation of the Variability of Physical Processes in the Ocean], IO AN SSSR, 1978, pp 35-40.

7. Chang, S. W., and Anthes, R. A., "Numerical Simulations of the Ocean's Nonlinear, Baroclinic Response of Translating Hurricanes," J. PHYS. OCEANOGR., Vol 8, No 3, 1978, pp 468-480.

8. Geisler, J. E., "Linear Theory of the Response of a Two Layer Ocean to a Moving Hurricane," GEOPHYS. FLUID DYN., Vol 1, No 4, 1970, pp 249-272.

9. Loguet-Higgins, M. S., "The Response of a Stratified Ocean to Stationary or Moving Wind Systems," DEEP-SEA RES., Vol 12, No 6, 1965, pp 923-973.

10. Pedlosky, J., "The Stability of Currents in the Atmosphere and the Ocean. Part 1," J. ATMOS. SCI., Vol 21, No 2, 1964, pp 201-219.

11. Robinson, A. R., "Three-Dimensional Model of Inertial Currents in a Variable Density Ocean," J. FLUID MECH., Vol 21, Part 2, 1965, pp 211-233.

A New Viewpoint on Fronts in the Ocean

K. N. Fedorov

Oceanic fronts can obviously be interpreted as a horizontal equivalent to the fine vertical thermohaline structure of ocean waters. In this interpretation the close relationship between the initial processes leading to frontogenesis and to fine separation of the stratified ocean water columns becomes especially obvious. In this case fronts represent the first stage in transformation of large-scale horizontal nonuniformities in the distribution of heat, salt, and motion into vertical nonuniformities; in particular, they represent the principal generators of the fine vertical structure of ocean waters (3). We can now assume it to be an established fact that frontal zones in the ocean contain an abundance of different forms of fine thermohaline structure, among which intrusive forms occupy the most important place, as a rule initiating differential-diffusive convective processes ("salt fingers" for example) (4). Inasmuch as fine thermohaline structure is always a sign of active mixing of ocean waters, it may be concluded that frontal zones and oceanic fronts are areas of the most intensive mixing of waters, and of the most significant vertical transfer of heat, salt and momentum through a hydrostatically stable pycnocline deep in the ocean. Formation of a fine intrusive thermohaline structure at fronts is connected with ageostrophic motions, which can include centrifugal components arising as fronts meander, and inertial fluctuations. Intrusive sags in isotherms and isohalines may also arise during frontogenesis itself in layers near the surface (10).

The importance of the contribution made by fronts to the transfer of the heat, salt, and momentum into the ocean water column through a hydrostatically stable pycnocline becomes even more obvious after we appraise the frequency with which fronts recur in different areas of the World Ocean (1). Use of satellites to observe the thermal state of the ocean surface in combination with traditional shipboard measurement resources has made such appraisal possible. It has been found that in coastal regions, and especially wherever intensive rising of deep waters (upwelling) occurs, in inland seas and straits, and within the vast frontal zones of large boundary currents, the average distance between thermal fronts $\overline{l}$ is equal to 30-50 km, while actual changes in l are within 5-100 km. In all frontal zones of climatic origin in the open areas of the ocean (for example in subtropical convergences), the typical value of $\overline{l}$ approaches 100 km. In the open ocean, in areas away from the main frontal zones and coasts, $\overline{l}$ values rise to 500-1,000 km (1). In special conditions, in connection with large internal waves ((solitony) for example), frontal phenomena may arise near the ocean surface, succeeding one another in space with an interval from 1 to 15 km. Inasmuch as arisal of such internal waves is associated with tides, the passage of series of such fronts may recur in certain tidal phases. Such phenomena have been observed in the Andaman Sea and at the Serpent's Mouth south of Trinidad. The

technical possibilities for measuring the actual horizontal temperature, salinity and density gradients in oceanic fronts have improved significantly in recent years. Use of new measurement methods has made it possible to establish that the actual horizontal temperature gradients are greater by one or two orders of magnitude than those which had been discussed earlier in the literature in connection with fronts on the basis of traditional hydrological data. In fronts of the Oregon upwelling for example, horizontal temperature gradients attain 4-5°C/km. The same can be said about upwelling fronts in the Gulf of Tehuantepec on the Mexican coast (8). Even in the open ocean, fronts have been discovered for which a temperature contrast on the order of 3°C was concentrated within a narrow band only 10-30 meters wide (7). Salinity contrasts in fronts occurring in the open ocean rarely exceed 1‰; however, given a front width of 100 meters to 1-5 kilometers on the surface, this means significant horizontal gradients. The strongest salinity contrasts and gradients are associated with river plume fronts, delimited by fresh water draining from large rivers in coastal regions of the ocean. Here, salinity contrasts may attain 10 and more ‰ in distances of just 100-200 meters, while in the most dramatic cases they may attain 4-5 ‰ in 20-25 meters (5). The corresponding density contrasts at such fronts are also very great, inasmuch as temperature contrasts between river plumes and surrounding waters are small as a rule.

Most thermal fronts in the ocean are accompanied by horizontal salinity contrasts. However, we can encounter both purely thermal and purely saline fronts. The latter, however, are encountered about 10 times less frequently than thermal fronts. A density gradient across a front, elicited either by thermal or by salinity contrasts or by both together, usually exists in quasi-geostrophic equilibrium with the velocity gradient transverse to the front. The latter always promotes cyclonic eddy motion within the frontal zone. The only exception is found with small-scale fronts (river plume fronts for example), for which the frontal Rossby number

$$Ro_\phi = \frac{u_\phi}{L_\phi \cdot f},$$

where u_ϕ--typical current velocity, L_ϕ--typical transverse scale of the front, and f--Coriolis parameter, is too great (about 30). Such fronts are not affected by earth rotation. For most fronts in the open ocean, however, $Ro_\phi = 1$. Hence it follows that in terms of their dynamics, fronts may be divided into two basic groups: a) large-scale, in relation to which earth rotation is significant, determining the inclination of the frontal surface through the ratio of density and velocity gradients; b) small-scale, the dynamics of which are governed mainly by viscous friction and turbulent intrusion through the frontal surface. However, unique thermohaline fronts that do not fit in either of these categories are encountered as well. In them, the density contributions made by horizontal temperature and salinity gradients compensate fully for one another, such that a resultant density contrast is absent. If these fronts are able to exist for a period of any length without breaking down due to intrusive stratification and differential-diffusional convection, their dynamics would have to include dominant factors entirely different from those existing in the two other cases--compression occurring with displacement for example.

Many conceptions developed in research on frontogenesis in the atmosphere, particularly the "deformation fields" conception, are useful to analysis of frontogenesis in the ocean. Practically all conditions favoring frontogenesis in the ocean may be interpreted as one type of deformation field or another. The typical values for

the intensity of deformation fields in the ocean are within 10^{-6}-10^{-5}sec^{-1}. Deformation fields of the highest intensity are associated with a typical frontal density contrast formation time from 3-4 to 10 days, which is confirmed well by the agreement of the results of modeling experiments (2,6,9) and natural observations.

A significant share of frontogenesis in the ocean is associated with synoptic-scale eddies. If we interpret eddies and fronts as manifestations of mesoscale two-dimensional quasi-geostrophic turbulence, then fronts would play the role of the required mechanism transferring enstrophy downward along a scalar cascade. Developing on fronts and interacting with them, internal waves may apparently cause parallel transfer of kinetic energy (11). In turn, owing to the baroclinic instability of fronts, eddies of smaller scale than those which had created the initial deformation field and which were the primal cause of frontogenesis may arise. This process may repeat itself several times in the direction of decreasing scale. The possibility is not excluded that this is precisely the way that three-dimensional variability of hydrophysical fields in the upper layer of the ocean is carried over from global scales to the scales of dissipation phenomena.

BIBLIOGRAPHY

1. Karabasheva, E. I., Paka, V. T., and Fedorov, K. N., "Are Thermal Fronts Encountered Often in the Ocean?," OKEANOLOGIYA, Vol 18, No 6, 1978, pp 1004-1012.

2. Kuz'mina, N. P., and Kutsenko, B. Ya., "Some Models of Oceanic Frontogenesis," in "Issledovaniye izmenchivosti fizicheskikh protsessov v okeane" [Investigation of the Variability of Physical Processes in the Ocean], edited by K. N. Fedorov, Institute of Oceanology, USSR Academy of Sciences, Moscow, 1978, pp 83-89.

3. Fedorov, K. N., "Tonkaya termokhalinnaya struktura vod okeana" [Fine Thermohaline Structure of Ocean Waters], Gidrometeoizdat, Leningrad, 1976.

4. Feodorov, K. N., "Intrusive Finestructure in Frontal Zone and Indication of Double Diffusion," in "Marine Turbulence," Jacques C. J., Nihous (Editor). Elsevier Oceanographic Series, Vol 28, 1980, pp 57-63.

5. Garvine, R. W., and Monk, J. D., "Frontal Structure of a River Plume," J. GEOPHYS. RES., Vol 79, No 15, 1974, pp 2251-2259.

6. Kao, T., Pao, H. P., and Park, C., "Surface Intrusions, Fronts and Internal Waves: A Numerical Study," J. GEOPHYS. RES., Vol 83, No C9, 1978, pp 4641-4650.

7. Knauss, J. A., "An Observation of an Oceanic Front," TELLUS, Vol 9, No 2, 1957, pp 234-237.

8. Legeckis, R.," A Survey of Worldwide Sea Surface Temperature Fronts Detected by Environmental Satellites," J. GEOPHYS. RES., Vol 83, No C9, 1978, pp 4501-4522.

9. Macvean, M. K., and Woods, J. D., "Redistribution of Scalars During Upper Ocean Frontogenesis: A Numerical Model," Q. JOUR. ROY. MET. SOC., Vol 106, No 448, 1980, pp 293-311.

10. Woods, J. D., "The Generation of Thermohaline Finestructure at Fronts in the Ocean," OCEAN MODELING, July 1980.

11. Woods, J. D., "The Physics of Energy and Enstrophy Cascades in the Ocean," (Preprint), 1980.

Simulation of Hydrodynamic Processes in the Sea With a Model of Rotationally Anisotropic Turbulent Flows

Ya. Kheynloo

Growth in interest toward eddy formation is one of the most typical trends in the present stage of development of the teaching on turbulence. The eddy concept is now being encountered more and more frequently in the scientific literature on turbulence, including in the literature on oceanology. The concept of eddies as specific carriers of turbulent current is evolving slowly, but more and more definitely. All of this is now having an effect on both the way turbulent current fields are studied and on the way concrete models of turbulent currents are set up. One of the main stumbling blocks to significant progress in this direction is the difficulty associated with imparting more or less strict meaning to the concept of a turbulent eddy. An original means of accounting for the eddy structure of a turbulent current field, one which permits us to avoid this uncertainty at least partially, was suggested in (1). The idea suggested in (1) essentially entails accounting for the eddy structure of a current field through the correlation between the kinematic and some geometric characteristics of the current field. This tactic affords a possibility for considering a number of characteristics of eddy structure important to average description of turbulent currents, ones such as the orientation and rotation rate of eddies in the environment, some aspects of the cascade nature of eddy fragmentation, and so on, without having to provide an exact definition of the concept of a turbulent eddy. As the main characteristic of eddy structure, we introduce the variable

$$\vec{\Omega} = \overline{\vec{v}' \times \frac{\partial}{\partial s}\left(\frac{\vec{v}'}{v'}\right)} \qquad (1)$$

where $\vec{v}'$--pulsation component of the velocity field; s--length of the arc of the current line of the velocity field's pulsation component; the bar above the expression represents averaging. The condition $\vec{\Omega} \neq 0$ determines a class of turbulent mediums referred to in (1) as rotationally anisotropic.

The motion equations derived in (1) for turbulent mediums having a rotationally anisotropic eddy structure have the form:

$$\rho \frac{D}{Dt}\vec{v} = -\nabla p + (\mu+\beta)\Delta\vec{v} + 2\beta\nabla\times\vec{\Omega} + \rho\vec{f}$$
$$\rho J\frac{D}{Dt}\vec{\Omega} = \theta J(\Delta\vec{\Omega} + \tfrac{1}{3}\nabla\nabla\cdot\vec{\Omega}) - 4(\beta+\varkappa)\vec{\Omega} +$$
$$+ 2\beta\nabla\times\vec{v} + \rho J(\nabla\vec{v})\cdot\vec{\Omega} + \rho\vec{m} \qquad (2)$$

in which, in application to the case of marine currents under discussion here,

$$\vec{f} = \frac{\rho^*}{\rho}\vec{g} + 2\vec{\omega}^0\times\vec{v},$$
$$\vec{m} = \vec{g}\times\left(\kappa^{(1)}\nabla\frac{\rho^*}{\rho} + \kappa^{(2)}\left(\nabla\frac{\rho^*}{\rho}\right)\times\vec{\Omega}\right) + J\vec{\Omega}\times\vec{\omega}^0 \qquad (3)$$

(ρ--some medium density typical of the current area of interest to us; ρ^*--true medium density; p--thermodynamic pressure; $\vec{g}$--gravity; $\vec{\omega}^0$--angular velocity of the earth's rotation; μ, γ, $\varkappa$, θ--viscosity coefficients for the medium; J--effective moment of inertia of eddies).

Equations (2) should be integrated jointly with the equation for mass balance:

$$\frac{D}{Dt}\rho^* = \kappa\Delta\rho^* + \nabla\cdot\left[\left(\kappa^{(1)}\nabla\rho^* + \kappa^{(2)}\nabla\rho^*\times\vec{\Omega}\right)\times\vec{\Omega}\right] \qquad (4)$$
$$(\kappa,\ \kappa^{(1)},\ \kappa^{(2)} = \text{const})$$

Let us examine some particular situations described by equations (2), (4).

1. $\vec{v}=0,\ \vec{\Omega}=\vec{\Omega}(t),\ \nabla\rho^* = \left(0, 0, \frac{\partial\rho^*}{\partial z} = \text{const}\right)$. In correspondence with (2), (4), in this case we have

$$\frac{\partial\vec{\Omega}}{\partial t} = -\frac{1}{\rho J}\left[\left(4(\beta+\varkappa)+\kappa^{(2)}\vec{g}\cdot\nabla\rho^*\right)I - \kappa^{(2)}\nabla\rho^*\vec{g}\right]J\vec{\Omega} + \vec{\Omega}\times\vec{\omega}^0 \qquad (5)$$

(I--unit tensor).

It would not be difficult to distinguish, on the basis of the appearance of equation (5), the two effects described by this equation: procession of vector $\vec{\Omega}$ about vector $\vec{\omega}^0$ caused by the moment of pulsation of the Coriolis force, and differences in the rates of attenuation of different components of vector $\vec{\Omega}$ caused by stratification of the medium. In the particular case where the moment of pulsation of the Coriolis force may be ignored, differences in the attenuation rates of different components of vector $\vec{\Omega}$ would cause rotation of vector $\vec{\Omega}$ to vector $\nabla\rho^*$. Achievement of this situation would preclude the further influence of the medium's stratification on attenuation of $\vec{\Omega}$. The situation is different when the pulsation moment of the Coriolis force is present. In this case $\vec{\Omega}$, which is oriented at a certain moment

in time along $\nabla\rho^*$, will be turned in a subsequent moment of time in relation to $\nabla\rho^*$ by the pulsation moment of the Coriolis force--that is, it would acquire a component perpendicular to $\nabla\rho^*$, and it would once again be under the power of the suppressing action of the medium's stratification. Hence we conclude that the Coriolis force, when combined with medium stratification, plays an important role in suppression of eddy motion in the environment.

2. $\vec{v}=0, \vec{\Omega}=\vec{\Omega}(z)$, $\rho^*=\text{const}$. Equations (2), (3) lead us to the following equation for $\vec{\Omega}$:

$$\theta J\left(\Delta\vec{\Omega}+\frac{1}{3}\nabla\nabla\cdot\vec{\Omega}\right)-4(\gamma+\varkappa)\vec{\Omega}+\rho J\,\vec{\Omega}\times\vec{\omega}^0=0$$

which describes diffusion of $\vec{\Omega}$ at the time of simultaneous attenuation of $\vec{\Omega}$ owing to friction and fragmentation of eddies and rotation of vector $\vec{\Omega}$ about vector $\vec{\omega}^0$ (during motion along axis z).

3. $\vec{v}=0$, $\vec{q}=(0,0,q)$, $\vec{\Omega}=\vec{\Omega}(z,t)$, $\Omega_z=0$; $\rho^*=\rho^*(z,t)$. The pulsation moment of the Coriolis force may be ignored. Given our assumptions, instead of (2), (4) we have

$$\begin{aligned}\frac{\partial}{\partial t}\vec{\Omega}&=\frac{\theta}{\rho}\frac{\partial^2\vec{\Omega}}{\partial z}-\frac{1}{\rho J}\left[4(\gamma+\varkappa)+\kappa^{(1)}q\frac{\partial\rho^*}{\partial z}\right]\vec{\Omega}\\ \frac{\partial\rho^*}{\partial t}&=\frac{\partial}{\partial z}\left[(\kappa+\kappa^{(1)}\Omega^2)\frac{\partial}{\partial z}\rho^*\right]\end{aligned}\qquad(6)$$

Let $\vec{\Omega}$ be generated by upsetting of surface waves or by drift current instability. Because Ω decreases in relation to depth z in such a case, the typical diffusion time for ρ^* also decreases with depth. Owing to this the near-surface layer would be mixed in a shorter period of time than would the layer beneath the surface layer, and for a certain period of time these two layers would be separated by a "discontiniuty" layer--an area of relatively fast change in ρ^*. Note that stable stratification--that is, a time of descent of isosteric surfaces--is a prerequisite of formation of this discontinuity. In the case of unstable stratification, isosteric surfaces rise; in this case the rate of their ascent increases with growth in Ω (with decrease in z), and the discontinuity does not form.

An effect of convective accomodation arises at $\partial\rho^*/\partial z<-4(\gamma+\varkappa)/\kappa^{(1)}q$ --Ω increases throughout the entire thickness of the layer within which $\partial\rho^*/\partial z<-4(\gamma+\varkappa)/\kappa^{(1)}q$, resulting in the mixing of this layer and a return of the situation $\partial\rho^*/\partial z>-4(\gamma+\varkappa)/\kappa^{(1)}q$ within it.

4. $\vec{\Omega}=(0,0,\Omega(\lambda,\varphi))$, $\rho^*=\rho^*(\lambda,\varphi,t)$. We write the equation for density corresponding to this case in the form:

$$\frac{\partial\rho^*}{\partial t}+(\vec{v}+\kappa^{(1)}\nabla\times\vec{\Omega})\cdot\nabla\rho^*=\nabla\cdot\left[(\kappa+\kappa^{(2)}\Omega^2)\nabla\rho^*\right]\qquad(7)$$

Equation (7) shows that the action of field $\nabla\times\vec{\Omega}$ on formation of the medium's density structure is similar to the action of the velocity of an incompressible liquid. In particular, field $\nabla\times\vec{\Omega}$ may serve as one of the causes for generation of fronts, and so on.

BIBLIOGRAPHY

1. Nemirovskiy, Yu. V., and Kheynloo, Ya. L., "One Approach to Describing Turbulent Currents," in "Chislennyye metody mekhaniki sploshnykh sred" [Numerical Methods of the Mechanics of Continuous Mediums], Novosibirsk, Vol 8, No 4, 1977, pp 116-134.

A Cascade Model of Turbulent Diffusion

Ya. Kheynloo, A. Toompuu

1) Let a sequence N of filtration operators be given (as defined in (1)), and let q, q_k, $q(k)$ represent, respectively, the variable to be filtered, variable q filtered by a filtration operator with subscript k ($k=1,\ldots,$), and variable q filtered by a succession of filtration operators from 1 to k. For any q, the following expansion is valid.:

$$q = q_{(\kappa)} + \sum_{n=1}^{\kappa} q'_{(n)} \qquad (1)$$

where $q'_{(n)} = q_{(n-1)} - q_{(n)}$ represents pulsation of $q_{(n-1)}$ at the n-th level of description.

Next let q represent the concentration of a passive, conservative substance whose behavior is controlled by the balance equation

$$\left(\frac{\partial}{\partial t} + \vec{v}\cdot\nabla\right) q = \nabla\cdot\vec{j}(0) \qquad (2)$$

($\vec{j}(0)$--vector for diffusive flow of q at the zero level of description). Substituting expansion (1) for q and the similar expansion for $\vec{v}$ in equation (2), after we apply, to the equation obtained in this fashion, the first k filtration operators, and accounting for the rules

$$(q_{(\kappa)}\, p_{(m)})_{(m)} = \begin{cases} q_{(m)}\, p_{(m)}, & \kappa \leq m \\ q_{(\kappa)}\, p_{(m)}, & \kappa \geq m \end{cases}$$

implied by the definition of the filtration operation (1), we find

$$\left(\frac{\partial}{\partial t} + v_{(\kappa)}\cdot\nabla\right) q_{(\kappa)} = \nabla\cdot\sum_{n=0}^{\kappa} \vec{j}(n)_{(\kappa)} \qquad (3)$$

in which

$$\vec{j}(n) = -(v'_{(n)}\, q'_{(n)})_n \qquad (n = 1, \ldots, \kappa)$$

is the vector representing flow of $q_{(n)}$ caused by velocity pulsations at the n-th level of description.

Let $C(k)=(q_{(k)}'^2)_k$ be the deviation of the concentration of this substance at the k-th level of description, and $C(k)=C(k)_{k+1,\ldots,N}$. In accordance with (1), we have

$$(q^2)_{(N)} = (q_{(N)})^2 + \sum_{k=1}^{N} C(k)$$

The equations for $q_{(N)}{}^2$ and $C(k)$ follow from equation (3), and following simple but somewhat cumbersome transformations, they take the form

$$\begin{aligned} &(\frac{\partial}{\partial t} + \vec{v}_{(N)}\cdot\nabla)\, q_{(N)}{}^2 = \nabla\cdot\vec{h}(N+1) - \sum_{n=0}^{N} (N+1,n) \\ &(\frac{\partial}{\partial t} + \vec{v}_{(N)}\cdot\nabla)\, C(k) = \nabla\cdot\vec{h}(k) - \sum_{n=0}^{k-1} (k,n) + \sum_{n=k+1}^{N+1} (n,k) \end{aligned} \qquad (4)$$

In equation (4),

$$\begin{aligned} (N+1,n) &= 2\,\vec{j}^{(n)}{}_{(N)}\cdot\nabla q_{(N)} \\ (k,n) &= 2\,(\vec{j}^{(n)}{}_{(k)}\cdot\nabla q_{(k)}')_{(N)} \end{aligned}$$

are terms describing interaction of fields $q^2_{(N)}$ and $C(k)$, and fields $C(k)$ and $C(h)$;

$$\begin{aligned} \vec{h}(N+1) &= \sum_{h=0}^{N} 2\, q_{(N)}\, \vec{j}^{(h)}{}_{(N)} \\ \vec{h}(k) &= \sum_{n=0}^{k-1} (\vec{j}^{(n)}{}_{(k)}\, q_{(k)}')_{(N)} - \sum_{n=k}^{N} (\vec{v}_{(n)}\,(q_{(n)}'^2)_{(n)}')_{(N)} \end{aligned}$$

are vectors for the flow of variables $q^2_{(N)}$ and $C(k)$.

Note that in the general statement of the problem (for example before the meaning of the filtration operation is made concrete), variables $(N+1,n)$, (k,n), may assume both positive and negative values. However, if we are dealing with a substance being carried by a turbulent flow, and if we select the filtration operations in such a way that the scales of the described movements would increase with growth in [symbol omitted from original], then

$$\begin{aligned} (N+1,n) &\geq 0 \\ (k,n) &\geq 0 \end{aligned} \qquad (5)$$

Inequalities (5) are the mathematical expression of cascade redistribution of nonuniformities in a turbulent flow, and they represent the basic postulate of turbulent diffision models.

2) It would be suitable to simultaneously introduce several filtration operators to describe turbulent diffusion (with the goal of distinguishing processes occurring at different scales) because in a number of cases processes occurring at different scales either differ in their physical origin or differ in a number of important characteristics, and thus they require different closure hypotheses. Let us illustrate this with the example of a model of diffusion in turbulent flows having a rotationally anisotropic eddy structure. The concept of rotational anisotropy of a turbulent flow was introduced in (2) to represent a turbulent current field characterized by relative orientation of eddy motion in the medium. It was also indicated there that presence of oriented eddy motion in a medium results in a certain degree of correlation between the kinematic and geometric characteristics of the field of motion. Presence of this correlation generates a new kinematic characteristic for the medium $\vec{\Omega}$. (See (2) for greater detail on the definition of $\vec{\Omega}$ and on the model of turbulent currents at $\vec{\Omega} \neq 0$ cm). Obviously $\vec{\Omega} \neq 0$ contributes unique features to turbulent diffusion. Inasmuch as, on the other hand, only large-scale eddies make a contribution to the size of $\vec{\Omega}$ (these eddies are precisely what impart orientation to eddy motion in the medium), $\vec{\Omega}$ represents only that part of diffusion in the medium for which large-scale eddies are responsible.

Let us select, as the zero level of description, "black-white" diffusion of molecules of the substance of interest to us (note that in this case $\int^{\vec{r}}(\vec{v}) = 0$ and $q_{v(N)}^2 + \sum_{K=1}^{N} C^{(K)}$ is a variant of any closed volume that does not participate in particle exchange) and, as the first filtration operator, the operation of averaging in relation to a so-called "elementary volume"--one sufficiently large enough for all fluctuations of molecular nature to be filtered out and sufficiently small to permit interpretation of fields $\vec{v}_1$, q_1 as continuous functions of three-dimensional coordinates and time. We select the second filtration (averaging) operator in such a way that fluctuations in fields $\vec{v}_1$, q_1 caused by the motion of fine-scale eddies would be filtered out, and we select the third filtration (averaging) operator in such a way that nonuniformities in fields $\vec{v}_{(2)}$ and $q_{(2)}$ caused by the motion of large-scale eddies would be filtered out. We assume the following in relation to the diffusion terms contained in equations (3), (4):

$$\begin{aligned} -(\vec{v}_1' Q')_1 &= \kappa_M \nabla Q \\ -(\vec{v}_{(2)}' Q')_{(2)} &= \kappa_T \nabla Q \\ -(\vec{v}_{(3)}' Q')_{(3)} &= \mathcal{K}_T \cdot \nabla Q \end{aligned} \qquad (5)$$

In equations (5), Q--arbitrary scalar; k_M, k_T (=const)--coefficients of molecular diffusion and turbulent diffusion (the latter is the product of the motion of fine-scale eddies); $K_T = K_T(\vec{\Omega})$--the tensor of the coefficients of diffusion caused by motion of large-scale eddies.

Expanding K_T into a series in relation to $\vec{\Omega}$ (with regard to the fact that $K_T(\vec{0}) = 0$), and limiting our accuracy to second-order terms, we have

$$\mathcal{K}_T = -\kappa_T^{(1)} E \cdot \vec{\Omega} + \kappa_T^{(2)}(\Omega^2 I - \vec{\Omega}\vec{\Omega}) \qquad (6)$$

(E--Levi-Chivit tensor; I--unit tensor; $k_T^{(1)}$, $k_T^{(2)}$ = const). Given the assumptions (5), (6), we find the following from (3), (4):

$$\frac{D}{Dt} q_{(3)} = \nabla \cdot \vec{h}(q_{(3)}) \qquad (7)$$

$$\frac{D}{Dt} q_{(3)}^2 = \nabla \cdot \vec{h}(3) - 2\kappa_M (\nabla q_{(3)})^2 - 2\kappa_T (\nabla q_{(3)})^2 - 2\kappa_T^{(2)} (\nabla q_{(3)} \times \vec{\Omega})^2$$

$$\frac{D}{Dt} C(1) = \nabla \cdot \vec{h}(3) + 2\kappa_T^{(2)} (\nabla q_{(3)} \times \vec{\Omega})^2 - 2\kappa_T (\nabla q_{(3)}')^2_{(3)} - 2\kappa_M (\nabla q_{(3)})^2_3$$

$$\frac{D}{Dt} C(2) = \nabla \cdot \vec{h}(2) + 2\kappa_T (\nabla q_{(3)})^2 + 2\kappa_T (\nabla q_{(3)}')^2_3 - 2\kappa_M (\nabla q_{(2)}')^2_{2,3}$$

$$\frac{D}{Dt} C(3) = \nabla \cdot \vec{h}(1) + 2\kappa_M (\nabla q_{(3)})^2 + 2\kappa_M (\nabla q_{(3)}')^2_3 + 2\kappa_M (\nabla q_{(2)}')^2_{2,3}$$

where

$$\frac{D}{Dt} = \frac{\partial}{\partial t} + \vec{v}_{(3)} \cdot \nabla$$

$$\vec{h} \begin{pmatrix} q_{(3)} \\ 4 \\ \kappa \end{pmatrix} = \left[(\kappa_M + \kappa_T) I + \mathcal{K}_T \right] \nabla \begin{pmatrix} q_{(3)}^2 \\ (q_{(3)})^2 \\ C(\kappa) \end{pmatrix}$$

Adhering to the notion that turbulence has a cascade nature, we ignore the terms in equations (8) describing molecular "dissipation" of fields $q_{(3)}^2$ and $C(1)$. For the remaining "dissipation" terms, $2\kappa_T (\nabla q_{(3)}')^2_3$ and $2\kappa_M (\nabla q_{(2)}')^2_{2,3}$ we assume:

$$2\kappa_T (\nabla q_{(3)}')^2_3 = \frac{1}{\tau_T} C(3)$$

$$2\kappa_M (\nabla q_{(2)}')^2_{2,3} = \frac{1}{\tau_M} C(2) \qquad (9)$$

Assumptions (9) close system (8). Note that τ_T and τ_M have simple physical meaning. They are equivalent to the typical attenuation times of $C(3)$ and $C(2)$ in a closed volume at $\nabla q_{(3)} = 0$.

BIBLIOGRAPHY

1. Toompuu, A., and Kheynloo, Ya., "A Generalized Representation of a Physical Situation, and Its Application to Hydrodynamic Problems," IZV. AN ESSR, Vol 29, No 1, 1980, pp 22-26.

2. Nemirovskiy, Yu. V., and Kheynloo, Ya. L., "One Approach to Describing Turbulent Currents," in "Chislennyye metody mekhaniki sploshnykh sred" [Numerical Methods of the Mechanics of Continuous Mediums], Novosibirsk, Vol 8, No 4, 1977, pp 116-134.

Investigation of the Finestructure of Hydrophysical Fields by a Remote Acoustic Method

V. P. Shevtsov

The author shares the point of view of those scholars who attach important significance to certain most highly "active" regions of the ocean, from which perturbations propagate over large water areas, in the formation of the finestructure of hydrophysical fields. Such regions include frontal zones, straits, dynamically complex regions, areas of abrupt changes in bottom relief, and so on.

In order to experimentally evaluate the structure-forming effectiveness of such regions and their influence on meso- and microscale variability, we would obviously need to directly inspect the formation of individual perturbations and their transformation over a long period of time. It is extremely difficult to do so by the traditional methods for making measurements in the open ocean from aboard ship. We need a more effective method for performing such studies and reflecting the obtained information, one which should not restrict the maneuverability of the vessel. It is only under these conditions that we can hope to be constantly in touch with the area of perturbations, and thus trace their movements in space and their change in time.

These requirements are fully satisfied by a remote acoustic method, based on vertical sounding of the water column, to which increasingly more attention has been devoted in recent times. Thus in works (1,2,8), the correlation between vertical fluctuations in sound-scattering layers and internal waves was analyzed and the possibility for observing them with the help of [one line omitted from original] was demonstrated.

However, biological accumulations making up sound-scattering layers have the capacity for active movement, and they exhibit three-dimensional nonuniformity. They are weakly associated with the structure of hydrophysical fields, and their behavior is governed mainly by illumination. Moreover sound-scattering layers are located as a rule in a narrow range of depths, and their vertical dimensions are significant. For these reasons active sound-scattering layers cannot serve as a dependable indicator of finestructure throughout the entire water column.

Acoustic nonuniformities associated more closely with microstratification of hydrophysical fields are of interest in relation to the problem at hand. These include passive suspended matter accumulating in layers having a higher density gradient, high frequency fluctuations in the speed of sound, the finestructure of its vertical

gradient, and so on. Estimates show that anisotropic fluctuations in the speed of sound scatter acoustic energy with effectiveness greater by several orders of magnitude than that of a statistically uniform medium (6), and they may be observed by a remote method (3). The possibility for recording sound reflected from a microgradient structure was demonstrated in (4), while that of recording sound reflected from accumulations of various sorts of suspended matter was shown in (5,7).

According to our data, obtained with an echo sounder at 30 kHz in different regions of the Pacific Ocean, the finestructure of hydrophysical fields is completely reflected by the distribution of acoustic irregularities. In most cases it exhibits sufficient contrast, and it may be recorded by reflected scattering. Under favorable conditions it may be observed remotely with exhaustive completeness.

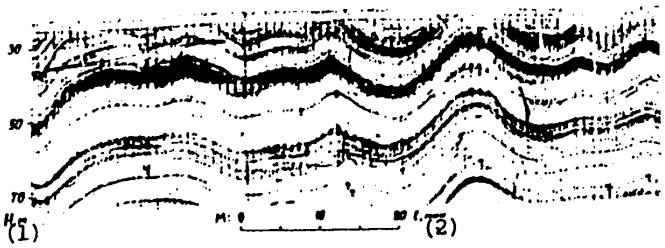

Figure 1. Example of Recordings, Made From a Drifting Platform, of Acoustic Signals Scattered in a 25-75 Meter Layer

Key:
1. Meters
2. Minutes

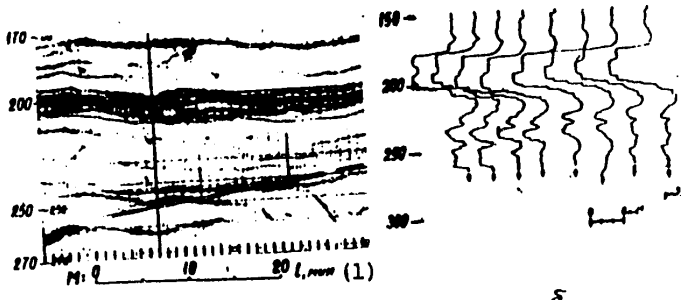

Figure 2. Synchronous Recording of Acoustic Nonuniformities Having a Layered Structure (*a*) and of the Vertical Distribution of the Speed of Sound in a 170-270 Meter Layer (*b*)

Key:
1. Minutes

As an example, Figure 1 shows a fragment of a tape recording of signals scattered in a near-surface layer down to 80 meters. Individual layers, including ones less than a meter thick, with stable boundaries that fluctuate vertically in response to internal waves, are clearly seen. The dark portions of the recording correspond to layers with a greater capacity for sound scattering. They are uniquely associated with layers of abrupt vertical change in hydrophysical parameters (Figure 2).

Obviously we can use the remote method to easily solve the problem of measuring the spatial dimensions of individual finestructure elements. Figure 3 shows a recording obtained aboard a vessel traveling at low speed, reflecting the typical distribution of layers in space. Of interest is the presence of extremely extensive stationary layers exhibiting considerable tilt in the horizontal plane.

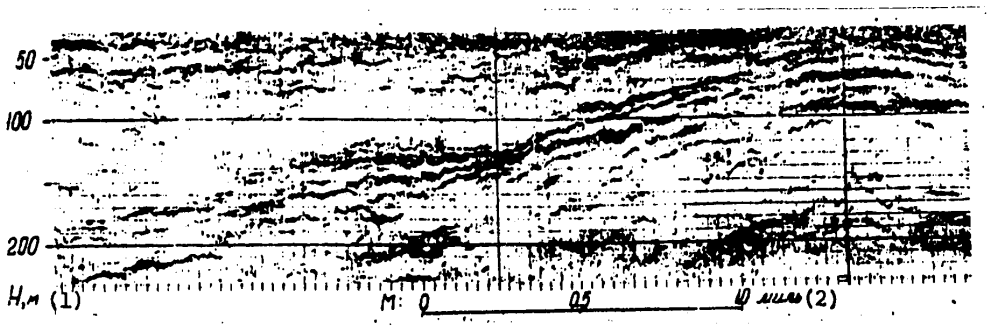

Figure 3. Structure of the Upper Layer Recorded by the Remote Method on a Vessel Traveling at Low Speed

Key:
1. Meters
2. Nautical miles

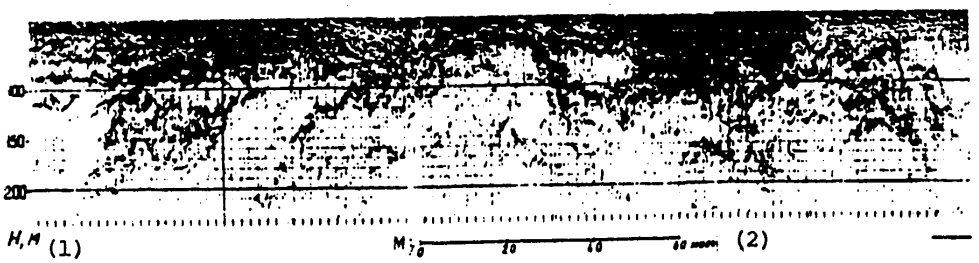

Figure 4. Areas With Developed Microstructure Recorded by the Remote Method on a Straight Tack Aboard a Vessel Traveling at a Speed of 12 Knots

Key:
1. Meters
2. Nautical miles

A number of the Kuril Islands were studied by the remote method. The obtained data show that areas with developed microstratification form. They have horizontal dimensions on the order of 10 km, they exhibit great stability over time, and they move hundreds of kilometers. Figure 4 is a large-scale recording of such areas, made aboard a vessel traveling at full speed. Typically the finestructure of these areas is extremely stable in the face of the constant influence of intensive short-period waves. This is evidence of the weak capacity internal waves have for causing irreversible deformations, and it raises doubts as to their significance to formation of the finestructure of the ocean's hydrophysical fields.

BIBLIOGRAPHY

1. Andreyeva, I. B., and Makshtas, Ya. N., "Fluctuations in the Depth of Sound-Scattering Layers and Internal Waves," OKEANOLOGIYA, No 3, 1976, pp 436-440.

2. Andreyeva, I. B., and Makshtas, Ya. N., "Internal Waves and Sound-Scattering Layers at a Temperature Discontinuity," OKEANOLOGIYA, Vol 17, No 3, 1977, pp 440-444.

3. Korenev, V. G., Lomeyko, A. I., Lyubitskiy, A. A., and Rozenberg, A. D., "Three-Dimensional Scattering of Sound at 25 kHz in the Presence of a Temperature Discontinuity Layer," AKUSTICHESKIY ZHURNAL, Vol 25, No 4, 1979, pp 556-565.

4. Kaye, G. T., and Anderson, V. C., "Scattering From Oceanic Microstructure: Detection With a Large Aperture Array," JASA, Vol 66, No 3, 1979, pp 842-849.

5. Orr, M. H., and Hess, R., "Remote Acoustic Monitoring of Natural Suspensate Distributions, Active Suspensate Resuspension and Slope/Shelf Water Intrusions," J. GEOPHYS. RES., Vol C83, No 8, 1978.

6. Proni, J. R., and Apel, J. R., "On the Use High-Frequency Acoustics for Study of Internal Waves and Microstructure," J. GEOPHYS. RES., Vol 80, 1975, pp 1147-1151.

7. Proni, J. R., Newman, F. C., Rona, D. C., Drake, D. E., Berberian, G. A., Lauter, C. A. Jr., and Sellers, L., "On the Use of Acoustics for Studying Suspended Oceanic Sediment and for Determining the Onset of the Shallow Thermocline," DEEP-SEA RES., Vol 23, No 9, 1976.

8. Proni, J. R., Ostapoff, F., and Sellers, R. L., "Acoustic Observations of High-Frequency, Near-Surface Internal Wave Groups in the Deep Ocean During GATE," DEEP-SEA RES., Vol 25, No 3, 1978, pp 299-307.

The Mechanism Behind Finestructure Generation by Narrow-Spectrum Internal Wave Trains

V. I. Shrira

1. A mathematically grounded hypothesis on the mechanism behind generation of finestructure by internal wave trains was proposed for the first time in (1,2): It was demonstrated that a train of weakly nonlinear short internal waves induces low frequency motion exhibiting fast vertical oscillation; in some cases this motion may be interpreted as the finestructure of hydrophysical fields in the ocean. While it describes a number of significant traits of finestructure well, this hypothesis does nevertheless encounter certain difficulties in explaining the origin of finestructure. Within the framework of this hypothesis: a) generation of finestructure is reversible--that is, finestructure disappears after the wave train passes; b) finestructure created by one wave train exhibits almost regular nature--that is, it is typified by a specific spatial scale; c) finestructure is generated by trains of only relatively short internal waves.

We considered the following fundamental circumstances in our development of the idea that finestructure is low frequency motion induced, in view of nonlinearity, by a train of internal waves: In most real situations, as will be shown below, low frequency motions induced by a wave train are superimposed over the dispersion curves of internal waves--that is, we observe resonance three-wave processes involving two waves from the wave train and a certain low frequency wave. Such processes have been solved for an infinite number of low frequency modes. This means in particular that in the course of its evolution, a wave train generates low frequency waves exhibiting fast vertical oscillations and lagging behind the wave train, so as to form "wakes" after the train passes. We define finestructure as the superimposition of such wakes. This interpretation of finestructure eliminates the difficulties mentioned above, and leads to some new consequences which will be discussed below.

2. The problem of mathematically describing generation of finestructure by internal wave trains may be examined within the framework of the basic equation for internal waves:

$$\partial_{tt}^{1} \Delta w + N^2 \Delta_h w + \Omega^2 \partial_{zz}^2 w = \mathcal{F} \qquad (1)$$

Here w--vertical velocity component, $N^2(z)$--Vyaysyal' frequency, Ω--Coriolis parameter, F--contains nonlinear terms not explicitly expressed through w. Using an asymptotic procedure, we can obtain equations describing joint nonlinear evolution of the wave train and the low frequency waves it induces (3,4). However, in view of the large number of low frequency modes participating in the motion, it is difficult to analyze these equations, even numerically. But if we are not interested in the reverse influence the induced low frequency waves have on evolution of the train, we can reduce the problem to solving a set of linear one-wave equations with the source on the right side, proportional to $\nabla|A|^2$ (where A is the amplitude of the train's complex envelope). The solution to this problem is written as a standard Fourier integral.

The wave vectors of induced low frequency waves are found from the conditions of three-wave synchrony between two waves from a train with basic frequency ω and wave vector $\vec{k}$, and the low frequency wave. In this case the usual condition of synchrony reduces to the following:

$$\vec{V}\cdot\vec{\tilde{c}}/\tilde{c} = \tilde{c}, \qquad (2)$$

where $\vec{V}=\omega\vec{k}$--group velocity of the main wave of the train, $\vec{\tilde{c}}$--phasal velocity of the low frequency mode (throughout the text, the ~ symbol signifies that the variable is associated with low frequency motion). Dependencies $\omega(k)$, $v(k)$, and $\tilde{c}(\tilde{k})$ are found by solving the basic boundary problem:

$$\partial_{zz}^2\varphi+\frac{N^2-\omega^2}{\omega^2-\Omega^2}k^2\varphi=0;\quad \varphi(0)=\varphi(H)=0 \qquad (3)$$

Here H represents ocean depth. It is easy to see that condition (2) is satisfied in relation to all modes of boundary problem (3) for which $\tilde{c}(\tilde{k})\leqslant v(k)$--that is, for sufficiently high modes* (see Figure 1). (However, a finite number of low frequency modes is excited effectively).

Thus the wave vectors of low frequency waves induced by a wave train are found in accordance with condition (2) from the deviation relationship (note that the orders of magnitude of $\tilde{\omega}$ and $\tilde{k}$ are $\Delta\omega$ and $k\Delta\omega/\omega$ correspondingly, where $\Delta\omega$ is the breadth of the train spectrum) and their amplitudes are found from the solution of corresponding one-wave equations with a known right side.

3. Let us discuss the question of interpreting low frequency waves generated by a train as finestructure in greater detail.

Any excited high low-frequency mode creates velocity, density and pressure fields that exhibit fast vertical oscillations. The velocities of particles and deviations in density in low frequency waves are small, while the density gradients (complementary to the Vyaysyal' frequency) may be sizeable, being comparable with the gradients in the main stratification structure. Thus we should refer primarily to the finestructure of the density profile or the Vyaysyal' frequency.

*Condition (2) cannot be met only when the frequency of the main wave is on the order of Ω.

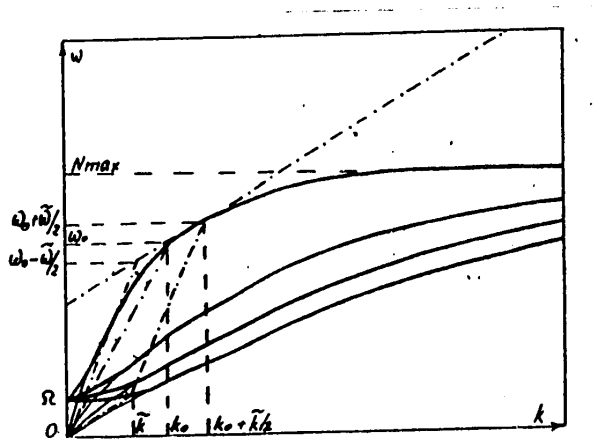

Figure 1. Deviation Curves for the First Four Modes of Internal Waves. Resonance Triad Involving Participation of Two Waves From Vicinity ω_0, k_0 and a Fourth-Mode Low Frequency Wave

One wave train effectively excites a large number of high low-frequency modes having different typical vertical scales h ($h \sim H/S$, where S is the mode number). Inasmuch as low frequency waves remain at a given point following passage of a wave train (their group velocity is lower), superimposition of their wakes should produce a highly disordered finestructure having no specific vertical scale.

The typical scale of horizontal variability in finestructure generated by a single wave train is on the order of the length of the wave train--that is, approximately $(k\Delta\omega/\omega)^{-1}$. The typical scale of temporal variability is on the order of the reciprocal of the train spectrum width--that is, approximately $(\Delta\omega)^{-1}$. The life span of finestructure, interpreted as the typical time of dispersed diffusion of the wake of one wave train, may be assumed to be on the order of $\omega/(\Delta\omega)^2$. That is, the finestructure arising as a consequence is an extremely long-lived formation.

The structure of high low-frequency modes may depend significantly on density nonuniformities of greater scale. In accordance with the properties of boundary problem (3), the zero values of the fundamental functions concentrate together in areas with high density gradients. This means that the vertical scale of finestructure must decrease in areas containing density interstratifications of greater scale, and increase with decrease in N, and with depth in particular. Thus finestructure must manifest itself more intensively in density interstratifications, which is in agreement with observed data.

The maximum vertical scale h of finestructure generated by a given train depends on the minimum number m of the lowest excited mode. (m is found from the solution of boundary problem (3)). Thus for example, in an ocean with a depth of $3 \cdot 10^3$ meters, with an upper uniform layer 10^2 meters thick and a lower layer exponentially stratified with $N = N_0 = 3 \cdot 10^{-3} \text{sec}^{-1}$, a wave train containing a main wave with length λ_0

equal to $2 \cdot 10^3$ meters generates low frequency waves beginning with the 24th mode ($m = 24$); when λ_0 is halved, m increases to 92; when λ_0 is quartered, m increases to $1.4 \cdot 10^3$. Owing to strong dependence upon $m(\lambda_0)$, the amplitudes of low frequency waves and the density gradients they create depend strongly on the length of the main wave λ_0.* For internal waves most typical of the ocean, $\lambda_0 = 5 \cdot 10^2$ meters; in this case the maximum vertical scale of finestructure is $h \sim 2$ meters. The horizontal scale L of finestructure, estimated as $n\lambda_0$ (where n is the number of waves in the train) is on the order of $5 \cdot 10^3$ meters. The ratio h/L is approximately $4 \cdot 10^4$.

The intensity of finestructure depends not only on the amplitude of the train generating it, a_0, but also on the breadth of its spectrum. When a balance exists between nonlinearity and dispersion, the intensity of finestructure is proportional to $a_0^{4/3}$, and not to a_0^2 (as in a nonresonant case)--that is, given the same amplitude for the generating wave, the finestructure is expressed with much greater clarity. In the absence of a balance between nonlinearity and dispersion, the intensity of low frequency waves and, consequently, finestructure is inversely proportional to the breadth of the train spectrum.

Thus this model for finestructure generation (in which finestructure is interpreted as superimposition of the wakes of internal wave trains), being a further development of the model proposed in (1,2), eliminates a number of difficulties encountered with that model, and it is more consistent with the experimental data.

BIBLIOGRAPHY

1. Borisenko, Yu. D., Voronovich, A. G., Leonov, A. I., and Miropol'skiy, Yu. Z., "The Theory of Nonstationary Weakly Linear Internal Waves in a Stratified Liquid," IZV. AN SSSR. FIZIKA ATMOSFERY I OKEANA, Vol 12, No 3, 1976, pp 293-301.

2. Voronovich, A. G., Leonov, A. I., and Miropol'skiy, Yu. Z., "The Theory of Formation of the Finestructure of Hydrophysical Fields in the Ocean," OKEANOLOGIYA, Vol 16, No 5, 1976, pp 750-759.

3. Shrira, V. I., "Resonant Self-Influence of Internal Waves," DAN SSSR, 1980 (in press).

4. Shrira, V. I., "Induced Currents and Resonant Self-Influence of Internal Waves in a Rotating Ocean," OKEANOLOGIYA, 1981 (in press).

*We emphasize that in the presence of a resonant excitation mechanism, in contrast to the situation described in (1,2), finestructure is generated not just by short internal waves alone.

LIST OF AUTHORS

1. A.I. Aytsam (ITEF)
2. V. S. Belyeyav (IOAN)
3. V. A. Bubnov (AO IOAN)
4. Ye. P. Varlatyy (TOI)
5. V. L. Vlasov (IOAN)
6. A. I. Ginzburg (IOAN)
7. V. Z. Dykman (MGI)
8. V. D. Yegorikhin (AO IOAN)
9. A. I. Yermolenko (MGI)
10. O. I. Yefremov (MGI)
11. V. M. Kamenkovich (IOAN)
12. T. R. Kil'matov (TOI)
13. D. A. Kiseleva (MGI)
14. K. V. Konyayev (AI)
15. G. K. Korotayev (MGI)
16. K. N. Korchashkin (IOAN)
17. M. N. Koshlyakov (IOAN)
18. L. K. Kramareva (TOI)
19. T. E. Kullas (ITEF)
20. Ya. Ya. Laanemets (ITEF)
21. V. D. Larichev (IOAN)
22. M. Ya. Kh. Lilover (ITEF)
23. I. D. Lozovatskiy (IOAN)
24. M. M. Lyubimtsev (IOAN)
25. V. A. Moisenko (MGI)
26. V. V. Navrotskiy (TOI)
27. R. V. Ozmidov (IOAN)
28. V. T. Paka (AO IOAN)
29. Yu. Kh. Pavel'son (ITEF)
30. N. A. Panteleyev (MGI)
31. Ye. N. Pelinovskiy (IPF)
32. V. G. Polnikov (MGI)
33. S. N. Protasov (DVGU)
34. I. D. Rostov (TOI)
35. K. K. Rusetskiy (IOAN)
36. K. D. Sabinin (AI)
37. A. G. Sazontov (IPF)
38. D. G. Seidov (IOAN)
39. A. A. Slepyshev (MGI)
40. I. A. Soustova (IPF)
41. Yu. V. Sustavov (LO GOIN)
42. G. G. Sutyrin (IOAN)
43. L. A. Talpsepp (ITEF)
44. R. E. Tamasalu (BaltNIIRKH TO)
45. V. P. Tikhomirov (TOI)
46. A. G. Toompuu (ITEF)
47. K. N. Fedorov (IOAN)
48. B. V. Khar'kov (IOAN)
49. Ya. L. Kheynloo (ITEF)
50. V. P. Shevtsov (TOI)
51. V. I. Shrira (IOAN)
52. Yu. Ya. El'ken (ITEF)

LIST OF ABBREVIATIONS

1. AI - Institute of Acoustics imeni N. N. Andreyev, USSR Academy of Sciences, Moscow
2. AO IOAN - Atlantic Division of the IOAN, Kaliningrad
3. BaltNIIRKH TO - Baltic Scientific Research Institute of Fisheries, Tallinn Division, Tallinn

4. IOAN - Institute of Oceanology imeni P. P. Shirshov, USSR Academy of Sciences, Moscow

5. IPF - Institute of Applied Physics, USSR Academy of Sciences, Gor'kiy

6. ITEF - Institute of Thermophysics and Electrophysics, Estonian SSR Academy of Sciences, Tallinn

7. LO GOIN - State Oceanographic Institute, Leningrad Division, Leningrad

8. MGI - Marine Hydrophysical Institute, Ukrainian SSR Academy of Sciences, Sevastopol'

9. TOI - Pacific Ocean Oceanological Institute, Far East Scientific Center, USSR Academy of Sciences, Vladivostok

11004
CSO: 8144/1441

-END-